Photochemistry of Coumarin Functionalized Silica Nanoparticles and Photochemically Induced Drug Delivery Utilizing *o*-Nitrobenzyl Compounds

Dissertation

zur Erlangung des Doktorgrades

der Naturwissenschaften

(Dr. rer. nat.)

dem

Fachbereich Chemie

der Philipps-Universität Marburg

vorgelegt von

Daniel Kehrlößer

aus

Herschbach

Marburg, Juli 2011

Vom Fachbereich Chemie der Philipps-Universität Marburg
als Dissertation angenommen am: ___.___.2011

Erstgutachter: Prof. Dr. Norbert Hampp
Zweitgutachter: Prof. Dr. Wolfgang Parak
Tag der mündlichen Prüfung (Disputation): 29. Juli 2011

Publications:

The majority of the herein presented work has been previously published:

Daniel Kehrlößer, Norbert Hampp,

"Two-Photon Absorption Triggered Drug Delivery from a Polymer for Intraocular Lenses in Presence of an UV-Absorber",

submitted to the *Journal of Photochemistry and Photobiology A: Chemistry*, **2011.**

Daniel Kehrlößer, Roelf-Peter Baumann, Hee-Cheol Kim, Norbert Hampp,

"Photochemistry of Coumarin-Functionalized SiO_2 Nanoparticles",

Langmuir, 27, **2011**, 4149 – 4155.

Daniel Kehrlößer, Jens Träger, Hee-Cheol Kim, Norbert Hampp,

"Synthesis and Photochemistry of Coumarin Based Self-Assembled Monolayers on Silicon Oxide Surfaces",

Langmuir, 26, **2010**, 3878 – 3882.

Table of Contents

1 Introduction

1.1 Photochemistry

1.1.1 A brief historical overview

Photochemical processes are essential for the life on our planet. The first photochemical process even started billions of years ago. It can be assumed that the atmosphere of the young earth consisted mainly of a mixture of water and carbon dioxide. A lot of photochemical reactions in the atmosphere and later plants using photosynthesis are responsible for conversion of carbon dioxide into oxygen. This oxygen was further converted by the sunlight to ozone protecting the earth from high energy solar irradiation, forming the atmosphere we try to protect today.

First scientific investigations on the interaction of light with matter that are not based on physical phenomena like absorption, reflection or refraction or based on heating by cumulating sunlight, for example for distillation, were reported by Joseph Priestley in 1790. He observed the formation of reddish nitrogen dioxide in the vapor phase above nitric acid, the first laboratory photoreaction in the gas phase.[1] His second contribution to the development of photochemistry were his observations on photosynthesis. In his own words he “fully ascertained the influence of light in the production of dephlogisicated air (oxygen) in water by means of a *green substance*”.[2, 3] During the 19th century more and more photochemical reactions were discribed. Among them, inorganic reactions like the irradiation of iron(III) oxide and oxalic acid in aqueouse solution generating carbon dioxide and iron(II) oxide, being the basis for later developed ferrioxalte actinometrie.[4-6] But also organic reactions like the photochemical induced reargement of santonin, extensivley investigated by Trommsdorff, Sestini and Cannizzaro.[7-10] The photochemical activity of santonin was observed due to the curious effect that its white crystalls turn yellow and burst under irradiation with sunlight. Trommsdorff was actually the first person who used a prism to investigate the wavelength dependency of this reaction, noticing that only the blue and the violet ray induced the reaction and the yellow, green and red caused no change.

In 1881 the young scientist Giacomo Luigi Ciamician, who received his PhD from the University of Gießen and Paul Silber, who was awarded his PhD in Freiburg, joined the group of Cannizzaro at the Istituto Chimico della Regia Università di Roma and contracted one of the most fruitful partnerships in science publishing at least 378 scientific papers.[11] Beeing

focused on pyrrole chemistry in the beginning of their work, Ciamician started his research on photochemical processes in 1885. Silber joined him one year later. Besides the formation of hydroquinone and acetaldehyde from benzoquinone in sunlight,[12] they also isolated aniline acetaldehyde and quinalidne by irradiation of alcoholic nitrobenzene solutions.[13] After these promising first results they stopped reporting on photochemistry for fourteen years respecting the claim of Klinger on the field of research, who had published a paper on phenanthrenequinone[14] a few weeks before Ciamician. At the beginning of the 20th century, Ciamician and Silber started to investigate photochemical processes systematically, with up to then astonishing success that established photochemistry as an independent chemical field. They published 34 papers called "Azione Chimiche della Luce" in the Gazetta Cimica Italiana and "Chemische Lichtwirkung" in "Berichte der deutschen Chemischen Gesellschaft". Among their publications pioneer work on coumarin[15] and *o*-nitrobenzyl-compounds[16], the photoactive compounds that are subject of this thesis. In 1912 Ciamician held a remarkable lecture on "The photochemistry of the future" at the international congress of Applied Chemistry in New York, predicting inventions that should be realized about 80 years later, like solar home heating or photo-electric batteries.[17] In the following century photochemistry developed more and more, supported by the understanding of atomic and molecular interactions and the advances in spectroscopy. Therefore it was possible to achieve a deeper knowledge of topics like fluorescence or singlet and triplet states. With the invention of the laser in 1960[18], complexity of photochemistry increased due to advancing time resolution from nano- over pico- to femto-seconds.[19, 20]

1.1.2 Coumarin

1.1.2.1 *[2π+2π]-Cycloaddition*

[2π+2π]-cycloadditions belong to the group of pericyclic reactions which usually take place in a concerted way. The most prominent reactions in this group are [4π+2π]-cycloadditions, the so-called Diels-Alder reactions.[21-24] Those thermal initiated reactions are relevant in many biological systems for the formation of six membered ring structures[25], besides their widespread use in natural material synthesis[26]. Due to the importance of their work, Otto Diels and Kurt Adler received the Nobel Prize in chemistry in 1950. Contrary to [2π+2π]-cycloadditions that are mostly photochemically induced, form a four-membered cyclobutane ring from two π-bonds under formation of two new σ-bonds. The present understanding of

the mechanisms of pericyclic reactions is due to the work of Woodward, Hoffmann and Fukui in the 1950s to 1960s. They developed a model predicting the stereochemistry of products formed in those reactions by taking the energy and symmetry of every molecular orbital, which is involved in the reaction into account.[27-30] Their work was honored with the Nobel Prize in chemistry for Hoffmann and Fukui in 1981.[31] Unfortunately, Woodward died two years before denying him his second Nobel Prize in chemistry after 1965.

According to the Woodward Hoffmann rules, the reaction takes always place between the highest occupied molecular orbital (HOMO) of one educt with the lowest unoccupied molecular orbital (LUMO) of another educt. (Figure 1.1) However, a further restriction for a binding interaction is that it is symmetry allowed, meaning the ellipsoids of the orbitals approaching have the same sign. In case of a [2π+2π]-cycloaddition, interaction between HOMO and LUMO seem to be symmetry forbidden, if one regards the reaction as thermally induced.

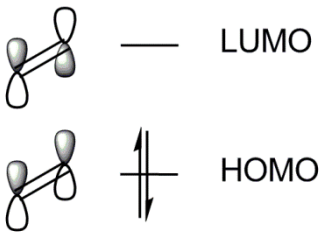

Figure 1.1: Molecule Orbital Symmetry of reacting alkenes in a [2π+2π]-cycloaddition.

A suprafacial approach of the educts, meaning the same side of the interacting π–bonds results in antibonding interactions. A binding interaction would be possible if the educts approach in an antarafacial way, but this is impossible due to geometric reasons. (Figure 1.2)

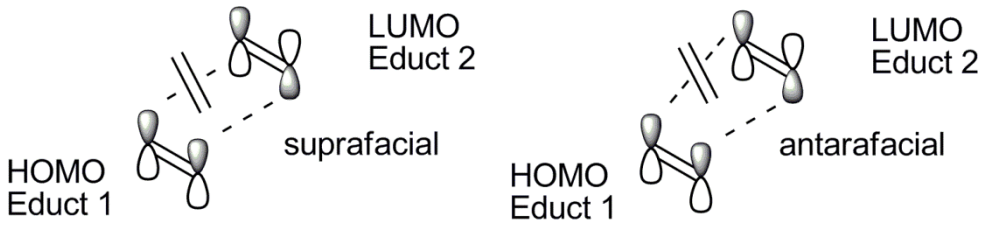

Figure 1.2: supra and antarafacial approach of alkene in a thermal [2π+2π]-cycloaddition.

However, the situation changes for a photochemically induced [2π+2π]-cycloaddition. If one of the educts is able to absorb a photon of the energy equivalent to the gap between HOMO

and LUMO, an electron can be promoted from the HOMO to the LUMO, forming two single occupied molecular orbitals (SOMO) (Figure 1.3)

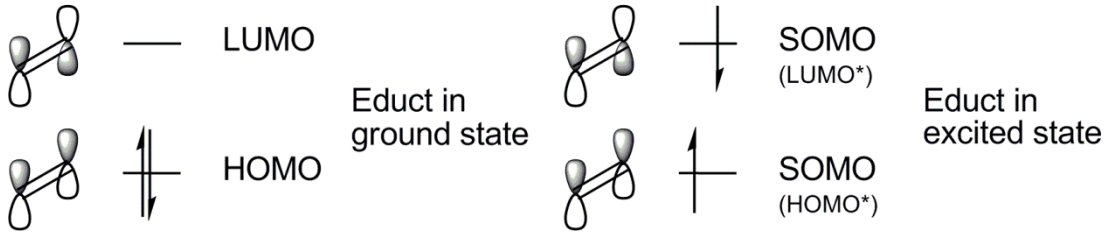

Figure 1.3: HOMO and LUMO in photochemical ground and excited state.

Two binding interactions are possible considering the approach of an educt in the ground state to an educt in the excited state. On the one hand the HOMO of the ground state molecule could bind to the SOMO, resulting from the former HOMO of the excited molecule. On the other hand the LUMO of the educt in the ground state could interact with the SOMO, resulting from the former LUMO of the excited molecule to form two new σ-bonds. (Figure 1.4)

Figure 1.4: Molecule orbital interactions in a photochemical induced [2π+2π]-cycloaddition.

A [2π+2π]-cycloaddition that follows this concerted mechanism is stereoselective. Nevertheless it was found that in most cases [2π+2π]-cycloadditions are not stereoselective, which can be explained by formation of a triplet 1,4-biradical intermediate. (Scheme 1.1)

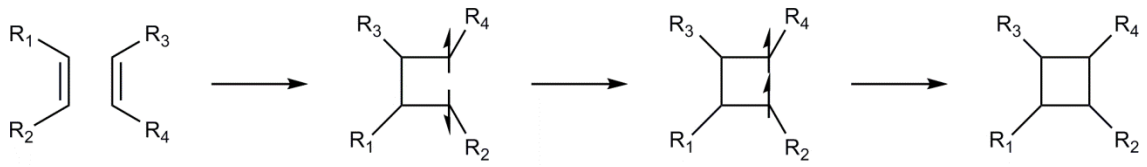

Scheme 1.1: 1,4-Biradical Mechanism of [2π+2π]-cycloaddition.

The stereochemistry of the products formed following this reaction pathway is no longer stereospecific and the thermodynamically most stable will be formed taking into account the number and steric demand of the possible substituents.

The formation of an excited triplet state requires a so called intersystem crossing, meaning spin twist of an electron excited into a higher vibrational state of the first excited electronic singlet state, during non-irradiative dissipation into the vibrational ground state of the excited electronic state. In general this is found for molecules with a strong angular momentum, coupling through spin-orbit interaction. An increase in reaction rate can be achieved either by promoting alkenes, which usually exhibit low intersystem crossing probabilities into a triplet state, or by utilizing triplet sensitizers like acetophenone or benzophenone. Those distinguish themselves by high intersystem crossing quantum yield and pass their triplet energy to the reactants via collisions.[32-34]

1.1.2.2 *[2π+2π]-Cycloaddition of Coumarin*

As already mentioned dimerization of coumarin induced by a [2π+2π]-cycloaddition is known since 1902, when Ciamician and Silber conducted their chemical experiments on the roof of the Università di Bologna.[15] But their discovery was not the first photochemically induced dimerization to be observed. Already in 1859, Fritzsche discovered the photochemical dimerization of anthracene known today as an [4π+4π]-cycloaddition.[35] The first [2π+2π]-cycloaddition was the dimerization of thymoquinone in 1871, observed by Liebermann in the solid state.[36]

Since these early days in photochemistry, an enormous number of studies was published, especially on the unique photochemical behavior of coumarin and its 7-alkoxy-derivatives. Photochemical excitation of coumarin is achieved by UV-light of a wavelength longer than 300 nm resulting in [2π+2π]-cycloaddition as shown in Scheme 1.2.

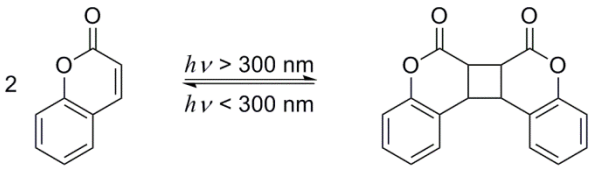

Scheme 1.2: Photochemical dimerization of coumarin.

The selective formation of any one of the four possible stereoisomers is dependent upon the solvent and the use of different triplet sensitizers. In nonpolar solvents without a triplet sensitizer, the excited singlet state is only poorly stabilized, resulting in almost no conversion. Using triplet sensitizers a stable triplet state of coumarin is promoted, resulting in formation of the *anti-head-to-head-dimer* as major product, due to the fact that it is favored during formation of the 1,4-biradical over the *anti-head-to-tail-dimer*.[37] In polar solvents coumarin is promoted into a solvent stabilized excited singlet state followed by concerted formation of the *syn-head-to-head-dimer.*[38] The addition of boron trifluoride as Lewis acid results in formation of the *anti-head-to-head-dimer*[39] (Scheme 1.3). This applies only to non-functionalized coumarin. Formation of isomers of coumarin derivatives can be influenced by steric and electronic effects of possible substituents.

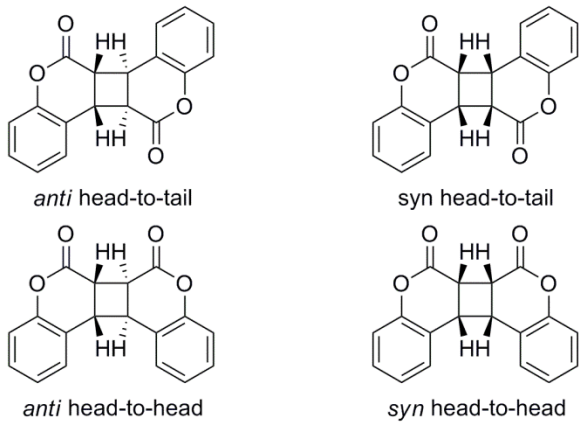

Scheme 1.3: Stereoisomers of coumarin.

The [2π+2π]-cycloreversion of coumarin with light of a wavelength shorter than 300 nm is known since the work of Schlenck and Krauch in 1966.[32, 33] The photochemistry of coumarin is therefore completely reversible, as long as the lactone ring in the dimer is not cleaved, being the assumption for symmetrical cleavage regenerating the monomeric coumarin. The equilibrium between monomer and dimer can be adjusted by the wavelength of the irradiated light. During dimerization the conjugated π-system in the molecule is shortened. This and the ring strain of the formed cyclobutane ring results in a higher cleavage probability of the lactone ring by nucleophiles like hydroxide ions, amines or primary alcohols, reducing the ring strain. Lactone ring opening results in the possibility of an unsymmetrical photo cleavage and loss of reversibility.[40-43]

1.1.2.3 *UV-Vis and Fluorescence Excitation of Coumarin*

The conjugated π-system of the coumarin, consisting of the phenyl ring connected via an additional double bond to the carbonyl function, enables excitation of two characteristic electronic transitions when irradiated with UV-light. Between 310 nm and 340 nm, depending on the configuration of possible substituents,[44] a (n—>π*)-like transition is observed related to the carbonyl function. At higher energies between 250 nm and 300 nm, there is a (π—>π*)-transition which corresponds to the conjugated π-system. Irradiation with UV-light of a wavelength longer than 300 nm mainly results in a decrease of the absorption between 310 nm and 340 nm, because the length of the conjugated π-system is reduced during the induced [2π+2π]-cycloaddition. (Scheme 1.4)

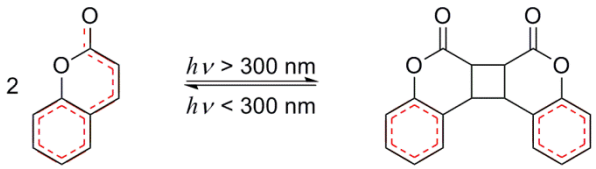

Scheme 1.4: Conjugated π-system in coumarin monomer and dimer.

Fluorescence of unsubstituted coumarin cannot be observed at room temperature due to the short lifetime of the excited state. Investigation at 77 K showed an emission at 384 nm using an excitation wavelength of 313 nm arising from (π—>π*)-transition.[45] The lifetime of the excited state of coumarins which are alkyloxy or hydroxy substituted in the 7-postion is increased, enabling fluorescence detection at room temperature. At an excitation of 320 nm emission maxima between 380 nm and 450 nm can be observed.[46]

1.1.2.4 *Applications of Coumarin in Material Science*

Besides theoretical studies on the photochemical behavior of coumarin, there are a lot of studies utilizing the reversibility of coumarin dimerization in material science applications. Coumarin has been incorporated into different polymers. For example polyvinyl acetate was used as polymer matrix to stabilize coumarin in thin films.[47] Other polymers or copolymers containing coumarin in the side chain allow photochemical induced crosslinking[48-50] that may be used to adjust the refractive index of the material.[51-53] Polymers with coumarin dimers in the main chain are known as well.[54, 55] Another interesting approach is the synthesis of gold and silicon oxide based self-assembled monolayers (SAM).[43, 56, 57] Prior to

the work presented in this thesis, coumarin has also been used by different other groups to apply its unique photochemical properties to silica based nanoparticles. In 2000 Graf et al. described the functionalization of silica nanoparticles with coumarin for the first time. In this study coumarin 343 was attached to the particles to investigate the formation of particle clusters due to photochemical dimerization.[58] The probably most prominent study was published by Mal et al. in 2003. They combined the photochemical properties of coumarin with silicon based nanotechnology by modifying the mesoporous silica cavity MCM-41 with coumarin. The coumarin moieties worked like a gate that could be closed or opened by photochemical dimerization or cleavage respectively. They were able to control the uptake, storage, and release of organic molecules in MCM-41 by photo-controlled dimerization and cleavage.[59] In the same year Fujiwara et al. investigated the formation of polymeric organic-inorganic hybrid materials by photo-dimerization. Intermolecular dimerization of concentrated solutions of the Pentacyclo[9.5.1.1^{3,9}.1^{5,15}.1^{7,13}]octasiloxan, bearing eight coumarin groups, were compared to the intramolecular dimerization of the same siloxan in diluted solutions.[60] Three years later Zhao et al. synthesized photo-deformable spherical hybrid nanoparticles consisting of coumarin dimers. These particles 'melted away' when irradiated with hard UV-light.[61] Just recently Ha et al. came up with biocompatible fluorescent silica nanoparticles utilizing the fluorescence of coumarin derivatives that may be used for in vivo imaging.[62]

1.1.3 *ortho*-Nitrobenzyl Compounds

1.1.3.1 *Mechanism of the Photoreaction*

Since the discovery of the photo activity of ortho-nitrobenzyl compounds (*o*-NBnCs) by Ciamician and Silber in the beginning of the twentieth century[16] a lot of research on the mechanism of the reaction was conducted. Especially since *o*-NBnCs were introduced as photochemical protecting groups in the 1960s.[63-65] The general mechanism assumes that the reaction proceeds either through a singlet or a triplet channel. Femtosecond spectroscopy techniques (transient absorption and femtosecond Raman spectroscopy) revealed the detailed excitation process at 258 nm for *o*-nitro-benzyl acetate[66] and were additionally supported by spectroscopy and quantum chemistry.[67, 68] Photochemical excitation into an upper singlet state of ππ* character feeds a lower singlet of nπ* character within approx. 0.05 ps. From this point on two different reaction pathways are observed.

Within 1 ps the nπ* singlet state decays either under direct benzylic H-atom transfer into the so called *aci*-nitro form or undergoes inter-system crossing (ISC) during 8 ps of vibrational cooling into an excited triplet state from which unreactive decay within 560 ps or formation of a biradical due to H-atom transfer followed by formation of the *aci*-nitro form is possible. (Figure 1.5)

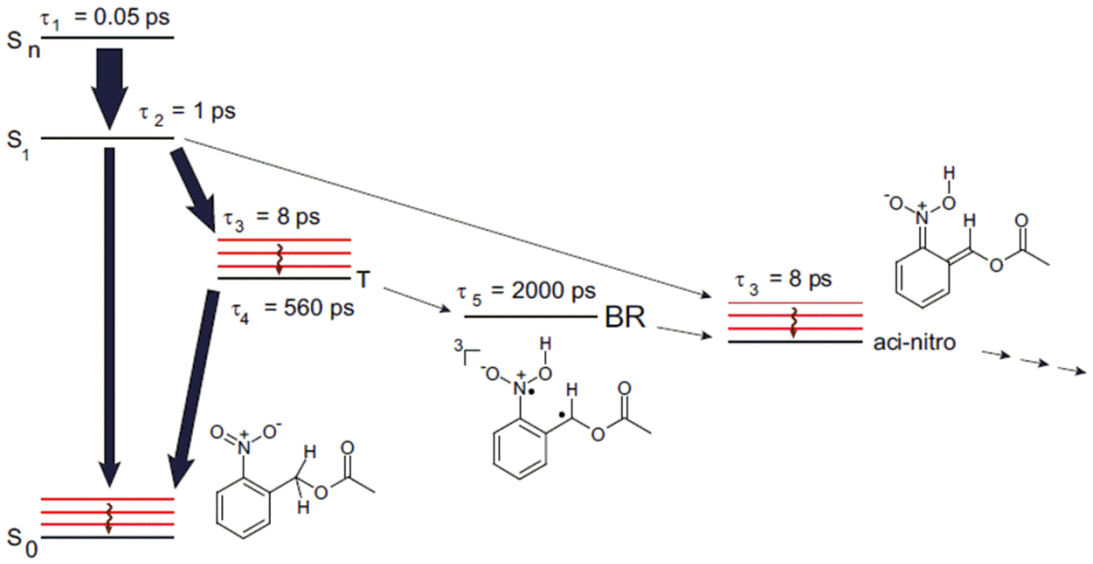

Figure 1.5: Kinetic scheme of the photo-reaction of oNBAc. The time constants mark lifetimes of the respective species except for τ_3 which represent a cooling process. The thicknesses of the arrows represent ratios of rate constants as far as applicable. Adopted from Schmierer et. al.[66]

The resulting *aci*-nitro form undergoes tautomerization and forms two distinguished stereoisomers **$HA_{E/Z}$** concerning the formed benzylic/quinoid group which can be distinguished spectroscopically.[69] In the next step rearrangement into a cyclic benzisoxazoline **HB** occurs.

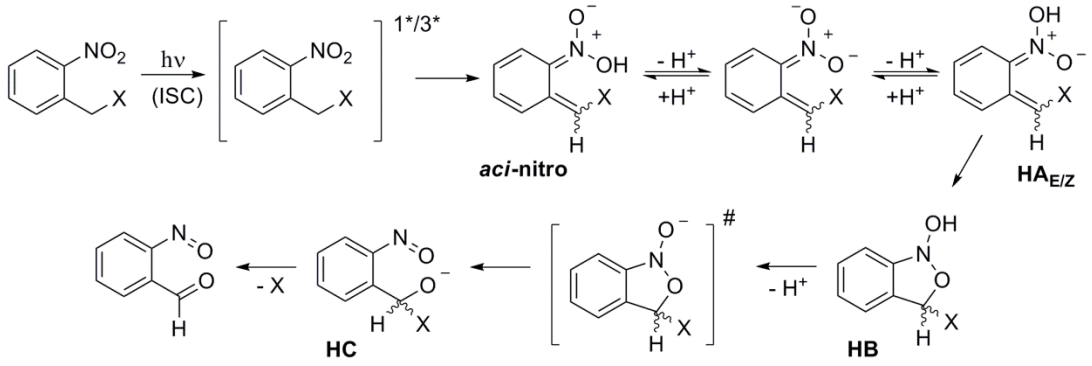

Scheme 1.5: Mechanism of o-NBnC photo cleavage.

Deprotonation leads via an intermediate state to formation of the hemiacylal **HC**, which finally releases protected/caged X under generation of the nitroso-benzaldehyde.[70] (Scheme 1.5) The key step during the photo reaction is the H-atom transfer to form the *aci*-nitro species. For *o*-nitro-benzyl acetate a quantum yield of 0.11 was determined which equals the overall "deprotection yield".

1.1.3.2 *Improvement of Reactivity of o-NBnCs*

Besides the mechanistic studies a lot of research deals with further improvement of *o*-NBnCs concerning properties like hydrophilicity, absorption maximum and quantum yield. Therefore different substituents were introduced to improve properties. (Figure 1.6) Substitution in 4,5 position (R_1/R_2 in Figure 1.6) with electron donating groups like methoxy / methylendioxy moieties results in bathochromic shift of the absorption maximum from 260 nm up to 350 nm which is necessary if used in biological applications with DNA bases or amino acids.[70-72] Substitution with a carboxyl group increases the hydrophilicity of the compounds, another feature favored in biological applications.[73, 74] Introduction of another nitro group in 6-position (R_3 in Figure 1.6) increases quantum yield due to higher probability of H-atom transfer into an *aci*-nitro form.

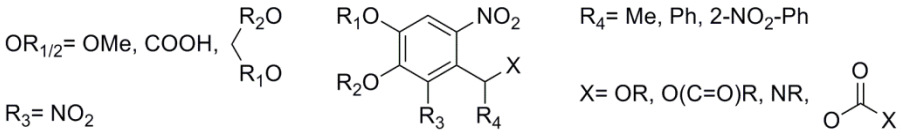

Figure 1.6: Possible substituents to improve photochemical properties of *o*-NBnCs.

Substitution of a benzyl proton (R_4 in Figure 1.6) with a methyl or phenyl group accelerates the photo reaction because of steric effects. Acceleration besides higher quantum yield can be provided by an *o*-nitro-phenyl group as substituent.[70] The leaving group (X in Figure 1.6) can be modified by insertion of an additional carboxyl group which decarboxylates during the cleavage process. Exploiting this entropic effect results in an increased rate of cleavage.[65]

1.1.3.3 *Applications of o-NBnCs in Material Science*

Besides their use as photo cleavable protecting groups in organic chemistry, *o*-NBnCs are of great significance mainly for biophysical and biochemical investigations in material science today.[75] Taking into account the variety and great number of applications only a few examples from the last decade concerning bio-inorganic chemistry, polymer chemistry and material science focused on nanoparticle functionalization and drug delivery are mentioned here.

In 2009 Bandara et al. reported the synthesis and photochemistry of an *o*-nitro-benzyl based Zn^{2+} complex. Incorporation of an *o*-nitro-benzyl moiety into the ligand backbone, resulted in the possibility of light induced ion release. The free Zn^{2+} ion is of great importance for neurological processes, making the designed complex interesting for many biological investigations.[76] Jiang et al. utilized *o*-NBnCs in the synthesis of amphiphilic block copolymers, which were employed for encapsulation of Nile Red in micellar structures that released their load upon irradiation.[77] In the Landfester group this approach was further improved generating photo-sensitive microgels, containing two different *o*-nitro-benzyl based crosslinkers enabling swelling and degradation of the particles energy and wavelength controlled.[78] An analytical approach combing the properties of o-NBnCs with nanoparticles, was presented in 2003 by Diaspro et al., who investigated the two-photon induced properties of 2-nitrobenzaldehyde as a caged proton compound utilizing fluorescent labeled nanocapsules as a new sensor[79]. An even more complex system of gold nanoparticle capped mesoporous silica nanospheres was published by Vivero-Escoto et al. Gold nanoparticles were functionalized with thioundecyltetraethyleneglycoester-o-nitrobenzyl-ethyldimethyl ammonium bromide which leads to a positive surface charge of the gold particles, resulting in incorporation into the drug loaded negatively charged MCM-41 capping the pores and caging the drug. Irradiation released thioundecyltetra-ethyleneglycolcarboxylate generating a negatively charged gold nanoparticle surface. The resulting charge repulsion between gold and MCM-41, causes gold nanoparticle dissociation and thereby drug release.[80] A similar system was presented by Park et al., who functionalized mesoporous silica particles with an *o*-nitro-benzyl ester bearing an alkyne function, loaded the particles and capped the pores with cycodextrins via click chemistry. Photochemical cleavage of the *o*-nitro-benzyl moiety removed the cyclodextrins and released the drug load.[81, 82] Recently Banerjee et al. reported a multifunctional magnetic

nanocarrier. Energy up-conversions of the irradiated near infrared light, enables the release of a drug conjugated via an *o*-nitro-benzyl moiety.[83] In 2009 Agasti et al. reported the photochemical drug release of 5FU from gold nanoparticles utilizing a nitro-benzyl moiety, similar to the synthesized monomer in this work.[84]

1.1.4 Two-Photon Absorption

Two-photon absorption (TPA) is a nonlinear process in which two-photons induce an electronic transition that would normally be induced by a single photon of half of the wavelength or respectively double the energy. The first who described this phenomenon theoretically was Maria Göppert-Mayer in 1931 (Nobel Prize in physics, 1963). Her PhD-Thesis, supervised by Max Born (Nobel Prize in physics, 1954), was titled "Über Elementarakte mit zwei Quantensprüngen" and described the simultaneous absorption of two-photons.[85] In view of fact that there was no light source of sufficient intensity, her considerations were regarded as intellectual curiosity. Initially the discovery of the first pulse laser in 1960 by Maiman[18] provided light at an intensity that enabled TPA. Not surprisingly one year and a month later, Kaiser and Garrett confirmed Göppert-Mayer's theory using Maimans Laser at 694.3 nm to excite $CaF_2:Eu^{2+}$ crystals to emit a bright blue fluorescence at 425 nm.[86]

A Transition during TPA proceeds via a virtual state of extreme short life times between 10^{-17} s and 10^{-15} s. Only when a second photon is absorbed before the virtual state is deactivated, excitation of the molecule into a real excited state is possible. (Figure 1.7) This explains the necessity of a high photon density which is only achieved with short pulsed lasers. Using monochromatic light, results in absorption of two-photons of the same wavelength. Such a TPA process is called degenerated. Due to conservation of angular momentum there are different selection rules for SPA and TPA processes. Considering SPA of a centrosymmetric molecule, a transition is only allowed if there is a change in parity. In contrast, TPA processes are only allowed for transitions between states of the same parity. This makes TPA very useful in spectroscopy to reach excited states only weak populated by SPA.

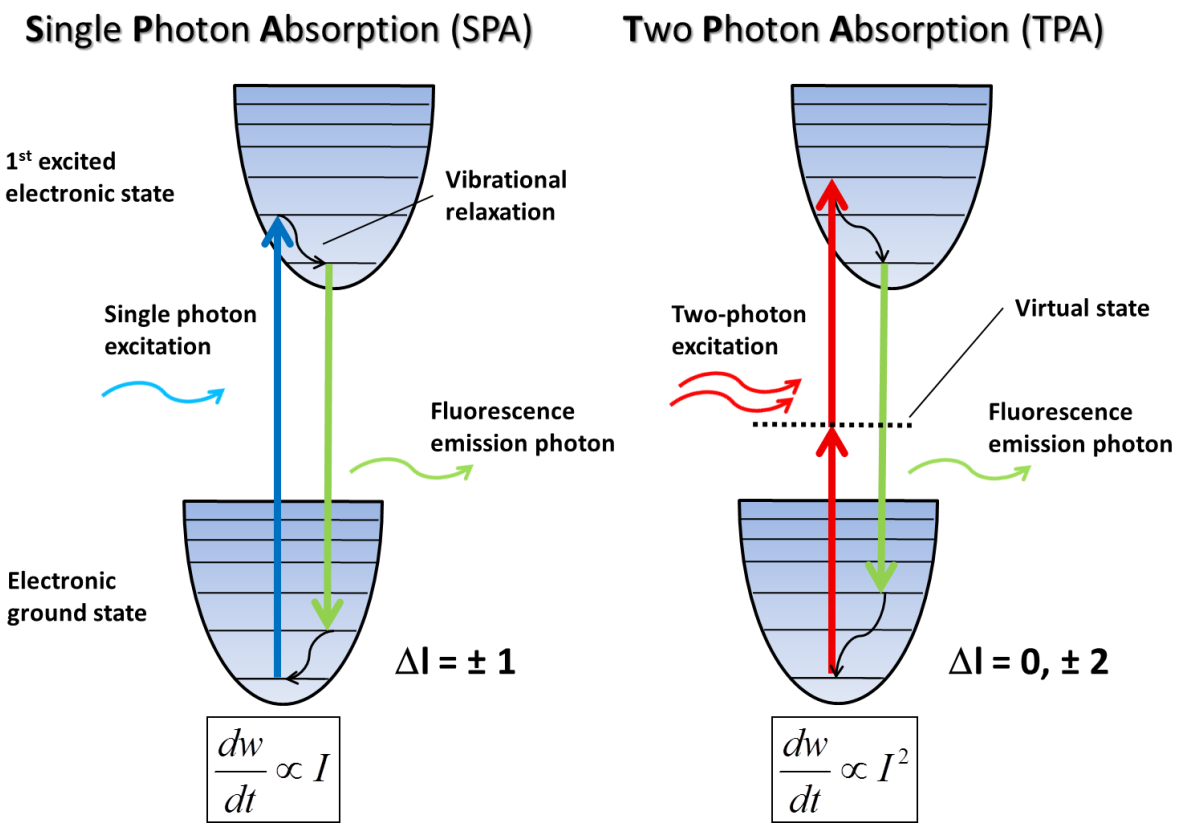

Figure 1.7: Schematic sketch of SPA and TPA.

Another essential difference between SPA and TPA is the correlation between absorption rate and light intensity. In case of degenerated TPA, a nonlinear dependency between absorbed energy over time and the intensity of the monochromatic light occurs, being described mathematically as follows:[87]

$$\frac{dW}{dt} = \frac{8\pi\omega}{n^2c^2} \cdot I^2 \cdot \mathrm{Im}\left(\chi^{(3)}\right) \tag{1.1}$$

Equation 1.1: with W: absorbed energy; t: time; ω: radiation frequency; n: refractive index; c: speed of light; I: irradiation intensity; $\mathrm{Im}(\chi^{(3)})$; imaginary part of 3rd order susceptibility tensor

Equation 1.1 shows that the rate of absorption of energy is quadratically dependent on the laser intensity. If a focused laser beam is used, this enables a very high resolution in space for two-photon excitation, being a significant advantage for fluorescence microscopy. Figure 1.8 shows how the high resolution can be achieved. In a TPA process only in the focal spot is the intensity high enough to excite fluorescence (right picture) while for single photon absorption all flourophores in the laser beam are excited (left picture). Besides the higher resolution bleaching of the flourophores is reduced.

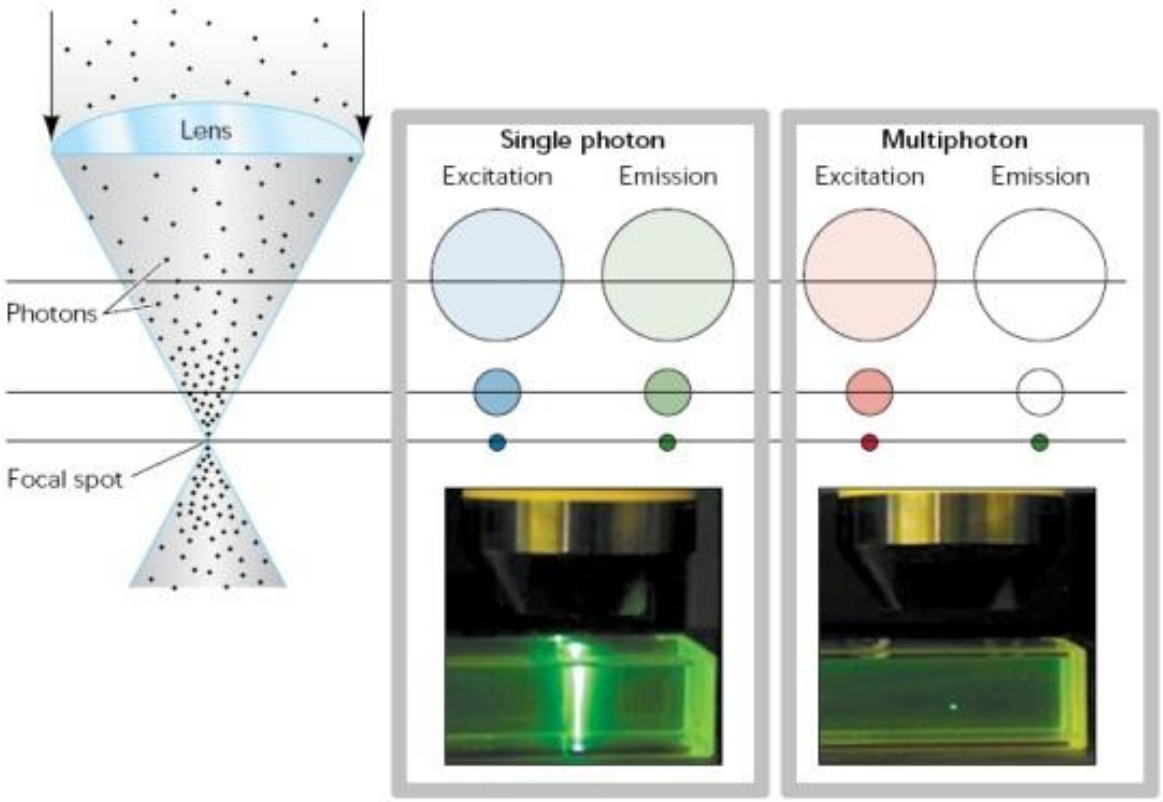

Figure 1.8: Two-photon Fluorescence Microscopy. Adapted from Cahalan et al.[88]

To compare the ability of different molecules to undergo a TPA process, two-photon cross section (σ_{TPA}) is defined. The number of absorbed photons per time depends on the number of absorbing molecules per volume the photon density squared and the two-photon cross section.

$$\frac{dn}{dt} = \sigma_{TPA} \cdot N \cdot F^2 \tag{1.2}$$

Equation 1.2: with n: amount of substance; N: number of absorbing molecules; F: photon density.

The photon density is defined by:

$$F = \frac{I}{h\nu} \tag{1.3}$$

Equation 1.3: h: Planck's constant; v: frequency of light.

The common unit of the two-photon cross section is GM (Goeppert-Mayer 1 GM = 10^{-50} $cm^4 \cdot s$).

To prove that a photochemical process is TPA induced, the time dependent reaction rate can be derived from Equation 1.1 to:

$$\frac{dc}{dt} = \underbrace{\sigma_{TPA} \cdot c_0 \cdot \Phi_{TPA}}_{k} \cdot I^2 \tag{1.4}$$

Equation 1.4: c: concentration; c_0: initial concentration; ΦTPA: two-photon quantum yield.

$$v_0 = k \cdot I^2 \tag{1.5}$$

Equation 1.5: v_0: initial velocity; k: rate constant.

Reformulation in logarithmic form:

$$\ln v_0 = \ln k + 2 \ln I \tag{1.6}$$

Equation 1.6: logarithmic initial velocity vs. logarithmic rate constant and intensity.

This means in case of a TPA process a double logarithmic plot of the initial velocity over the intensity should result in a linear dependency with a slope of two.[87]

Besides the already mentioned two-photon fluorescence spectroscopy[89] TPA is used for several other applications, like two-photon initiated polymerization. This application uses the high special resolution to initiate polymerization in three dimensional arrays to create micro and nano devices.[90-92] A medical application of TPA is the so called photodynamic therapy where near infrared light, which is able to penetrate tissue, is used to generate singlet oxygen as therapeutically active species from a photosensitizing agent, with a high spacial resolution in vivo.[93, 94]

1.2 Silica Nanoparticles

1.2.1 Synthesis and Functionalization of Silica Nanoparticles

Talking about silica nanoparticles, it is necessary to differentiate between classical silica nanoparticles and mesoporous silica nanospheres. The latter have been developed in the early 1990s as non spherical polydisperse microparticles with highly ordered well-defined pores of 1 nm to 10 nm.[95, 96] This well ordered porous structure leads to further investigations concerning the control of size and size distribution. The perhaps most prominent structure is MCM-41 prepared from tetraethyl orthosilicate (TEOS) with cetyltrimethylammonium bromide as structure directing agent. Today mesoporous silica nanospheres are tunable in particle size, pore size and surface functionalization[97] enabling many different applications as in drug and gene delivery[80, 98-100], biosensors[101] and sample separation.[102]

Classical silica nanoparticles are synthesized mainly by five different methods. In 1968, Stöber et al. described the "Controlled Growth of Monodiperse Silica Spheres in the Micron Size Range"[103] based on the so called sol gel process.[104, 105] Synthesis in microemulsion[106] as well as acidic hydrolysis of sodium silicate[107] are two other methods based on the same process. A third possibility also based on the sol gel chemistry is the amino acid catalyzed synthesis of silica nanoparticles in a two phase system.[108] A solvent free method is the flame aerosol process.[109]

All particles synthesized for this thesis were either prepared by Stöber synthesis or in an amino acid catalyzed process. Formation of particles proceeds in both cases in three steps similar to the sol gel process:

Hydrolysis	$Si(OEt)_4 + 4\ H_2O$	$\longrightarrow\ Si(OH)_4 + 4\ EtOH$
Condensation	$n\ Si(OH)_4$	$\longrightarrow\ [SiO_x(OH)_{4-2x}]_n + xn\ H_2O$
Dehydration	$[SiO_x(OH)_{4-2x}]_n$	$\longrightarrow\ (SiO_2)_n + n\ (4-2x)/2\ H_2O$

Scheme 1.6: Stöber synthesis / sol gel process.

The Stöber synthesis is based on an ammonium catalyzed hydrolysis of TEOS in an aqueous alcoholic solution. The resulting particle size depends on the hydrolysis rate of TEOS gaining smaller particles by increasing the rate. Variation of different reaction parameters results in almost monodispers particles from a few nanometers up to 1.5 µm. The influence of the

ammonia and water concentration in the system was already determined by Stöber et al. (Figure 1.9) Increasing the monomer concentration results in an increase of the particle size but at the cost of an increasing size distribution.[110]

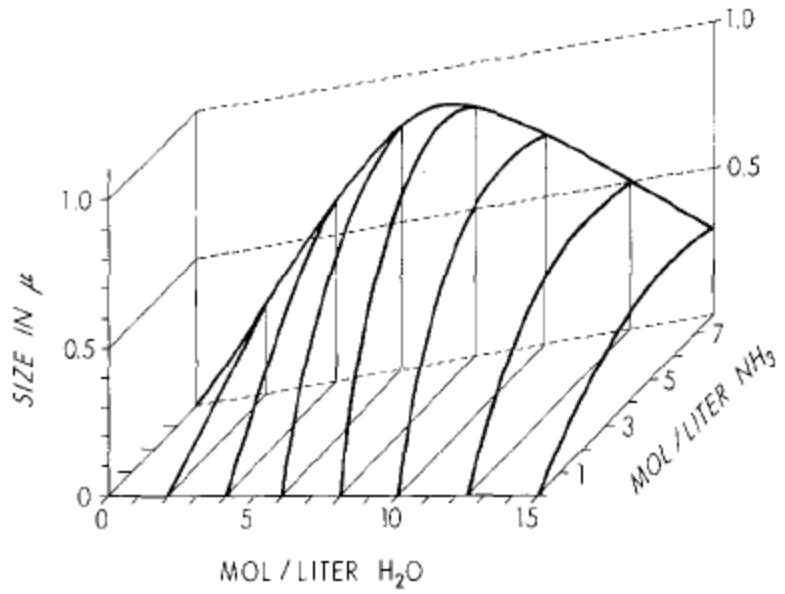

Figure 1.9: Particle size dependency from water and ammonia concentration. Adapted from Stöber et al.[103]

The use of more reactive tetramethyl orthosilicate instead of TEOS results in smaller particle sizes. Slower hydrolyzed monomers with longer alkyl chains than TEOS cause larger particles. Changing temperature means changing the hydrolysis rate and therefore influencing particle size.[111] Solvent polarity also effects the size of the particles, due to the fact that more polar solvents like methanol increase hydrolysis, while more nonpolar solvents like isopropyl alcohol decrease the hydrolysis rate.[103]

However, all these findings were empirical and the exact formation mechanism of particles from hydrolysis over particle nucleation to particle growth was and possibly still is being discussed. The first kinetic description of particle growth was the model by LaMer and Dinegar.[112] In the initial phase of the reaction the concentration of the monomer, in case of silica silanol ($Si(OH)_4$) formed during hydrolysis, is increasing until a critical concentration (supersaturation) is reached. The resulting nucleation decreases the concentration of monomer, resulting in particle growth without further nucleation, due to the fact that the probability of a monomer to react with the large number of seeds is much more likely than further nucleation. From this point on the reaction should be diffusion controlled and progress until equilibrium in concentrations is reached. At first glance the model fits the experimental results of monodispers particles whose size should depend primarily on the

number of formed seeds. This is covered by the dependencies from the reaction parameters that were described above. E.g. a slow nucleation rate (low number of seeds) results in a lot of remaining monomer, leading to growth of larger particles.

However, the model did not fit particle properties like porosity and low density of smaller particles or an increasing density gradient from the core to the particle shell.[113] Further investigation of the early processes of particle formation and growth, utilizing many different techniques such as dynamic light scattering[114, 115], ^{1}H, ^{13}C and ^{29}Si-nuclear magnetic resonance spectroscopy (NMR)[116] and cryo-transmission electron microscopy (TEM),[117] suggested a different continues nucleation/aggregation mechanism. Hydrolyzed or partially hydrolyzed TEOS still starts nucleation after reaching a supersaturation, but the initially formed small mass fractal particles aggregate to bigger particles and further nucleation proceeds for quite a long time. The monodispersity of the resulting dispersion is explained by the fact that once particles reach a certain electrostatic stabilized size, the formed react diffusion controlled with the stabilized particles by increasing density and smoothing of the surface, without further aggregation with each other. This mechanism was proven by Small-Angle X-ray Scattering (SAXS)[118] supported with synchrotron irradiation[119] identifying initial particles of ~ 3 nm in diameter. The existence of even smaller nuclei could be revealed by time resolved fluorescence anisotropy.[120, 121]

Functionalization of particles received in Stöber synthesis is possible using silicates bearing one under the reaction conditions unreactive organic residue and three hydrolysable residues like alkoxy- or chloro-groups. Two different approaches are possible, copolymerization with TEOS, during particle formation or surface modification by adding the functionalization reagent after completing the initial particle formation. Functionalization is even necessary to transfer particles into other solvents than alcohol or water, due to the fact that unmodified Stöber particles are electrostatically stabilized by dissociated silanol groups on the surface or by absorption of hydroxyl ions. Dilution with nonpolar solvents or neutralization with acid or by evaporation of ammonia, results in irreversible aggregation and flocculation of the particles. Surface functionalization is described by hydrolysis of the functionalization agent, followed by polymerization to oligomers which are rapidly absorbed on the particle surface under condensation. In general, only one bond of the functionalization agent is bound to the particle. The remaining silanol groups are present either in condensed form in the polymeric network around the particle or in free form.[122]

Purification of functionalized particles can easily be achieved by repeated centrifugation and redispersion. However, it is important to avoid irreversible particle aggregation by condensation of unreacted silanol groups. Stability of the functionalized particles depends on the solubility of the functionalization agent in the desired solvent.[123]

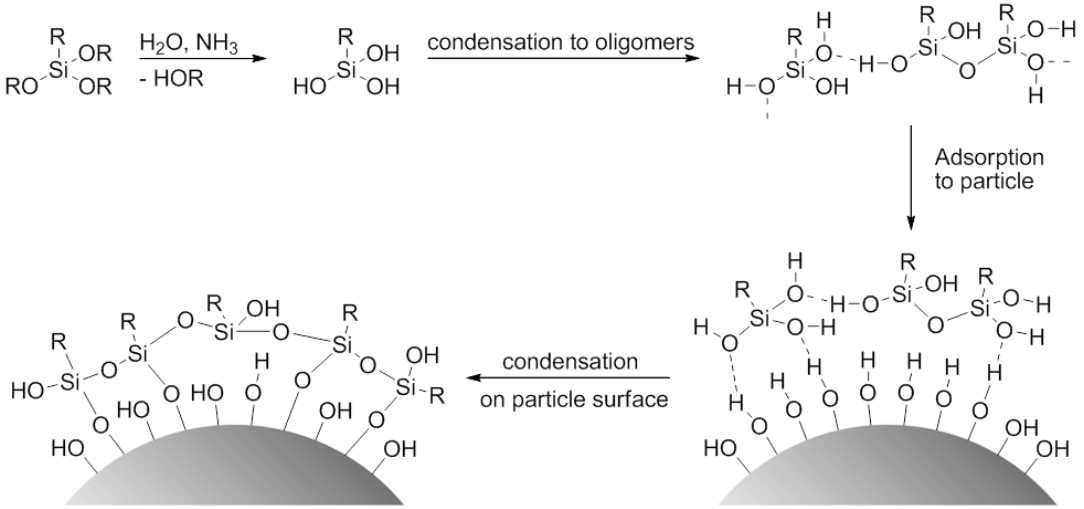

Scheme 1.7: Functionalization of Stöber particles.

The amino acid catalyzed synthesis is a quite new approach by Yokoi et al.[108] of obtaining silica nanoparticles in aqueous solution without any other solvent, which is especially valuable for biological applications. Typical particle synthesis is conducted in a two phase system consisting of an aqueous lysine or arginine solution and TEOS. Particle size can be tuned between 8 nm and 35 nm, by varying reaction parameters such as stirring conditions and molar composition of the reactants.

The mechanism of particle formation is not clarified in every detail. Contrary to the Stöber synthesis, the hydrolysis of TEOS is very slow, which can be mainly attributed to the two phase system enabling hydrolysis only at the interface. Additionally, the pH value of the solution is only within the rage of 9-10, resulting in a further decrease of hydrolysis rate compared to the values of 11-12 during Stöber synthesis. Observation of the particle formation by means of field emission scanning electron microscopy (FE-SEM), SAXS and NMR measurements, reveals the formation of 4 nm particles within half an hour, followed by continuous diffusion control growth of particles, until a homogenous dispersion due to complete TEOS hydrolysis is formed.[124] Unlike in Stöber synthesis there is no evidence for a continuous nucleation/aggregation mechanism. After formation of primary particles, only diffusion controlled growth is observed without formation of new particles, enabling size

control by stepwise addition of TEOS using already formed particles as seeds.[125] Further modification of the reaction parameters led to preparation of anisotropic silica nanoparticles by controlled assembling of preformed seeds.[126]

The amino acid concentration controls the pH value of the water phase and therefore the hydrolysis rate. Decreasing the concentration of amino acid results in a lower hydrolysis rate of TEOS, decreasing the amount of silicate supplied to the water phase. Therefore, the number of primary particles is decreased, increasing the final size of the particles due to the increased amount of TEOS remaining for diffusion controlled growth. As revealed by thermo gravimetric analysis and NMR, half of the amount of amino acid in the finally formed particle dispersion is absorbed on the particle surface, considering electrostatic interactions between the negatively charged particle surface and the pH-value of the system, protonated amino acid.[124]

A second effect of the amino acid is buffering of the formed particle dispersions during evaporation of the solvent. In contrast to particle dispersion received by Stöber synthesis, during which ammonia is evaporated much faster than water, resulting in a change of the ζ-potential of the dispersion during solvent evaporation, amino acid catalyzed formed particles are regularly arranged into a cubic closed-packed structure (ccp) upon solvent evaporation.[108, 124, 125]

Functionalization of silica nanoparticles synthesized by this new method is also easily accomplished. After formation of particles of a desired size, their surface can be functionalized by addition of the same functionalization agents that are used in Stöber synthesis, diluted in cyclohexane or a similar nonpolar solvent. Restrictions for the functionalization may occur due to the solubility properties of the functional groups in an aqueous dispersion.[125]

1.2.2 Applications of Silica Nanoparticles in Material Science

Industrial production of silica nanoparticles in a range between 10 nm and 100 nm is mainly conducted in the flame aerosol process by pyrolysis of tetrachloro silane or hexamethyl disiloxan in a methane-oxygen atmosphere. They are most commonly used as composite material in polymers. Homogenous dispersions of silica nanoparticles in polymers can improve thermal, electrical and mechanical properties of the material. For example polymeric coatings like car finish can be improved in their scratching resistance using silica

nanoparticles as a composite material. Another application is to increase the refractive index of transparent polymers by adding a certain amount of silica nanoparticles.[127]
To improve the dispersibility extensive researches on functionalization of silica nanoparticles with polymerizable organic molecules were performed. Enabling the whole variety of known polymerization reactions, ranging from radical emulsion and suspension polymerization, to atom radical transfer polymerization (ATRP) and radical addition fragmentation chain transfer (RAFT) polymerization up to living anionic and cationic as well as ring opening metathesis polymerizations.[128-130]

Silica nanoparticles are also of great importance to cosmetics and pharmaceutical industry. They are used as additive in lotions, creams and tablets to improve the distributions of active pharmaceutical ingredients, for example. Other industrial applications are known from fields like paper industry[131] or the display industry, which applies silica particles help to improve anti-reflective coatings.[132]

Besides these industrial applications, silica nanoparticles have a great impact on material science and are of great interest in many different fields of research. The major fields are biomedical applications, like drug delivery or as gene transfection carriers, especially in form of mesoporous nanospheres.[98, 133, 134]
Classical silica nanoparticles are mainly used in bioanalytical applications. Surface functionalization of silica nanoparticles with fluorescent dyes or incorporation of the dyes into the particles, improved the sensitivity of detection and made the active dye much more photostable.[135-137] Analytical applications are the use of nanoparticle-based pseudostationary phases in capillary electrochromatography[138, 139] or the modification of AFM tips with a single 10 nm to 40 nm gold particle or carbon nanotubes, which can indent and penetrate the membranes of living cells.[140]

Besides all these concepts, silica nanoparticles are often used to modify metallic nanoparticles in core shell approaches, combining the biocompatible features of silica with the magnetic properties of certain metallic nanoparticles, for example.[141, 142]

1.3 Purpose and Motivation

One of the major goals in science is to cure diseases. Therefore, medicine utilizes drugs besides surgical approaches which are mainly developed by pharmacists and chemists. Especially in the last century with the rapid growing knowledge in chemistry, providing the ability of characterizing molecules gained from nature or synthesizing identified drugs, distinguished progress in treatment was achieved by taking advantage of simple organic molecules to heal many lethal or painful diseases. Some prominent examples might be acetylsalicylic acid which was developed by Eichengrün in 1897 and the discovery of the antibacterial effect of penicillin by Fleming in 1928.[143]

Today there are millions of different drugs, aiming at all kinds of diseases but one of the major problems is efficient drug targeting, particularly when dealing with aggressive drugs with multiple side effects. The common ways of drug administration are oral application or injection, either intravenous or intramuscular. This exposes almost the entire body to the drug. The vast majority of the active drug is thereby more or less efficiently metabolized and eliminated.

Therefore, pharmaceutical research is improving the so called drug targeting devices. It concerns the drug delivery system, transporting the unreactive drug to the desired part of the body, e.g. a tumor. Once the desired position is reached, the drug is released either by a special biochemical recognition mechanism activating the drug release or via an external pulse, e. g. infrared-irradiation.

Another approach is to develop polymeric implant materials, containing drugs which are either delivered in a sustained release mechanism or inactive and bound until released due to an external pulse.

Prior to this work, different studies on photochemical activated drug delivery from intra-ocular lenses were published utilizing coumarin and tetralone as photo linkers. The implantation of intraocular lenses is the standard treatment for cataract. Cataract is one of the major age related diseases. The clouding of the natural eye lens along the visual axis is, according to the world health organization, the reason for 48% of blindness in the world, especially in developing countries, where surgical treatment is inadequate.[144] Although cataract surgery is very successful in restoring sight, there are typical postoperative complications, e. g. the posterior capsule opacification. This so called secondary cataract is caused by proliferation and migration of retained lens epithelial cells into the visual axis.

Aiming at the treatment of secondary cataract, different copolymers and polymer composites have been developed, using photoactive linker structures to immobilize drugs that be released on demand by photochemical stimulation. Due to the fact that the cornea is absorbing UV-light, two-photon activated photo cleavage was used. All cases were successful and improved step by step. The latest studies even proved the developed system *in vivo* in animal experiments.[53, 145-151]

To improve prior work, the purpose of this thesis is to investigate the combination of silica nanoparticles, well-known as biocompatible composite material for polymers and coumarin as potential photoactive linker. In addition, two different kinds of silica nanoparticles were synthesized and functionalized with coumarin. (Scheme 1.1) Investigations concerning their photochemical properties were used to reveal their potential as photoactive linker in a drug delivery approach.

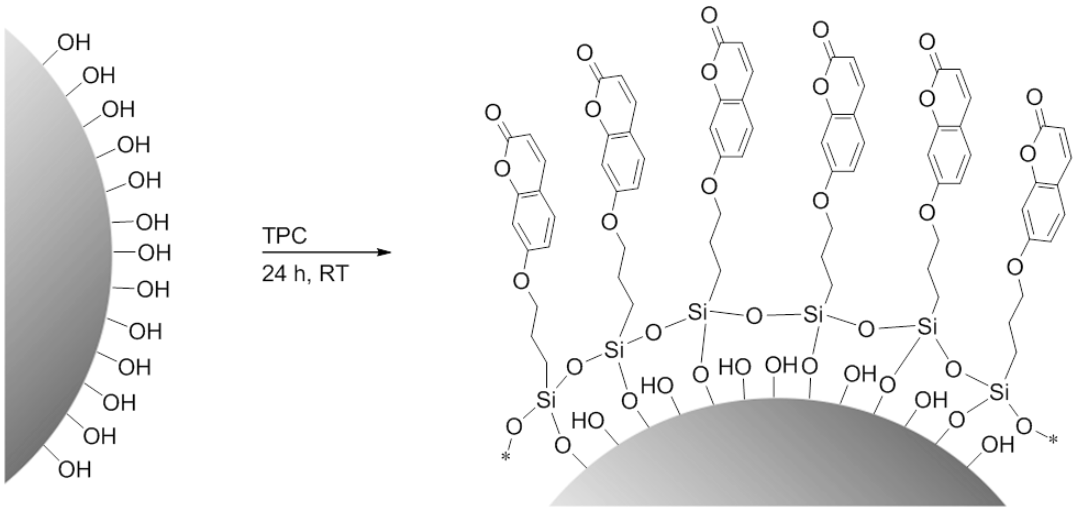

Scheme 1.8: Coumarin functionalization of silica nanoparticles.

One disadvantage of the prior work is that the drug is loaded by photochemical dimerization of coumarin with 2-N-heptanoyl-5-fluorouracil. Formation of the desired hetero-dimer is much less likely than formation of coumarin homo-dimers, resulting in low yields. A second disadvantage is that once a dimer by [2π+2π] cycloaddition is formed, standard purification by column chromatography is no longer possible. All further steps require reversed phase preparative High Performance Liquid Chromatography (prep. HPLC). To overcome those disadvantages it is the purpose of this thesis to develop a new photochemical drug delivery approach based on *o*-NBnCs, not involving photochemistry during synthesis.

2 Experimental Section

2.1 Methods

2.1.1 Physical Data

2.1.1.1 *Nuclear Magnetic Resonance Spectroscopy (NMR)*

All NMR-spectra were recorded on AV-300 (300 MHz ^{1}H, 282 MHz ^{19}F, 75 MHz ^{13}C, Bruker) or AV-500 (500 MHz ^{1}H, 125 MHz ^{13}C, Bruker) spectrometer, at room temperature either in deuterochloroform ($CDCl_3$) or in dimethylsulfoxid d_6 (DMSO) as solvent. Chemical shifts (δ) were given in parts per million (ppm) and calibrated using the residual solvent signal (^{1}H: δ_{CDCl_3} =7.26 ppm, δ_{DMSO} =2.50 ppm; ^{13}C: δ_{CDCl_3} =77.0 ppm, δ_{DMSO} =39.52 ppm) as internal standard. Dissolved multiplets were analyzed by multiplicity with coupling constants given in Hz.

2.1.1.2 *Ultra Violet -Visible Spectroscopy (UV-Vis)*

All UV-Vis-spectra were recorded on a Lambda 35 spectrometer (Perkin Elmer) between 200 nm – 600 nm with 480 nm·min^{-1} in steps of 1.0 nm. Measurements in solution were performed in quartz cuvettes (QS, Hellma; UQ, Portman Instruments) with 10 mm path length in the given solvents. All samples had absorptions of less than 2.5 at the observed wavelength to ensure a linear operation of the spectrometer.

2.1.1.3 *Fluorescence Spectroscopy*

Fluorescence spectroscopy was performed on a Shimadzu RF-1502 spectrometer at room temperature. The excitation wavelength of the measured emission spectra was 320 nm. Liquid samples were measured in a four window quartz cuvette (QS, Hellma).

2.1.1.4 *Mass Spectrometry*

All given mass-spectra (MS) using electron impact ionization (EI) were recorded either in high resolution (HRMS) on a MAT 95s (Finnigan) mass spectrometer or for low resolution on a QP505A (Shimadzu) spectrometer, with ionization energy of 70 eV. Mass-spectra utilizing electrospray ionization (ESI) were recorded on LCQ-Duo (Thermo) spectrometer.

2.1.1.5 *Thermo Gravimetric Analysis (TGA)*

Thermo gravimetric analysis was performed on a TGA/SDTA 851^e System (Mettler Toledo) in an open corundum crucible between 25 °C and 1000 °C in nitrogen atmosphere with a heating rate of 10 K·min^{-1}.

2.1.1.6 *Dynamic Light Scattering (DLS) and ζ-Potential Measurements*

Dynamic light scattering measurements and ζ-potential were accomplished with a Delsa Nano C (Beckmann Coulter).

DLS is a powerful method to determine the size of particles dispersed in solution ranging from 1 nm up to a few µm. The method is based on Brownian motion of the particles, which was named after the English botanist Robert Brown, who observed the random motion of flower pollens in water in 1827. In the early 20th century, Einstein and Smoluchowski[152, 153] described this random motion by the diffusion rate of particles, which is determined by their size. If particle dispersion is irradiated with light, the particles cause dynamic light scattering. These changes in the intensity of the scattered light can be analyzed at a given detecting angle by autocorrelation. The autocorrelation function gained is used afterwards to derive the particle size using the cumulant method, the CONTIN algorithm or other mathematical models.

In the used setup, backscattering at a detecting angle of 165° was analyzed. Dispersions of nanoparticles diluted in the given solvents were irradiated in a temperature controlled glass cuvette, with 10 mm path length. The presented data was derived either by the cumulant method or by CONTIN algorithm.

ζ-potential is the electric potential arising at the slipping plane within the interfacial double layer of a colloidal particle in a liquid system. (Figure 2.1)

The ζ-potential determines if a colloidal dispersion of particles is charge stabilized. Values above 30 mV or below -30 mV should stabilize an aqueous colloidal dispersion. To determine the ζ-potential, electrophoretic light scattering is utilized. By applying a defined electrical field to the particle dispersion, it is possible to measure the flow profile of the particles, which depends on the ζ-potential.

In the setup used, dispersions of nanoparticles diluted in the given solvents were measured in a standard glass flow cell.

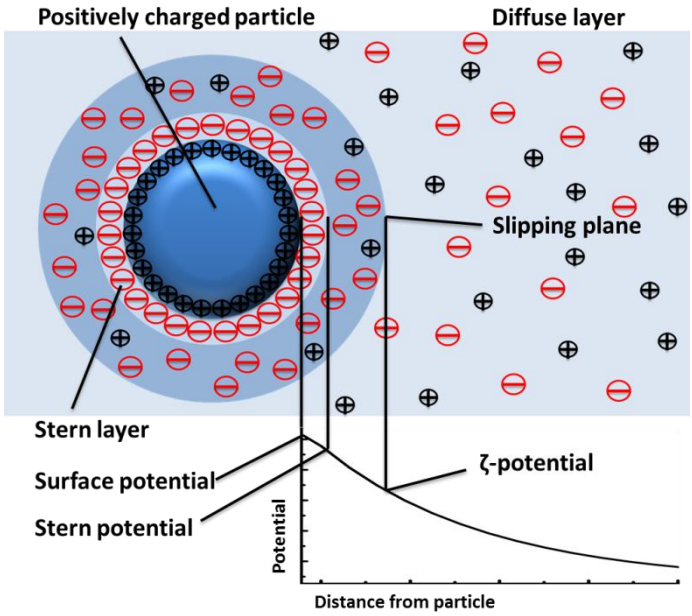

Figure 2.1: ζ-Potential of a positively charged particle

2.1.2 Microscopy

2.1.2.1 *Single Electron Scanning Microscopy (SEM)*

Field-emission Scanning-Electron-Microscope (SEM) imaging was performed on a JSM-7500F (Jeol) with a YAG-BSE detector (Autrata). Accelerating voltages between 5 kV and 10 kV were used. Samples were prepared by evaporation of 20 µl of a 0.01 $mg \cdot ml^{-1}$ dispersion of the respective particles, ambient temperature and pressure on isolating silicon wafers as substrates. Samples were sputtered with platinum and transferred via an ALTO-2500 LN_2-Cryo-Transfersystem (Gatan) and measured in high vacuum.

2.1.2.2 *Atomic Force and Electrostatic Force Microscopy (AFM/EFM)*

Particle imaging was realized using an atomic force microscope Nanoscope IV (Veeco Metrology). All measurements were carried out in tapping mode (TM-AFM) with pyramidal, oxide-sharpened Si_3N_4 tips in air at ambient conditions. For EFM measurements SCM-PIT tips (Sb_n:Si, k = 1-5 N/m, f_0 = 70-83 kHz, 0.01-0.025 $Ohm \cdot cm^{-1}$, Veeco, Metrology) were used.

EFM allows determination of a sample's surface potential in two steps. First, one line of the sample is scanned in regular TM-AFM tapping mode to gain the height profile. In the second step the same line is scanned again by moving the tip, referring to the previously scanned height profile in a defined distance along the sample. Thereby, the electrostatic signal is

gained, due to the fact that differently charged areas on the surface exert different electrostatic forces to the tip. This can be detected by cantilever deflection or the inhibition thereof. In this so called lift mode (Veeco Metrology) no bias was employed to either tip or surface.

Samples were prepared by evaporation of about 20 µl of a diluted mixture of functionalized and non-functionalized particles in ethanol, on a freshly oxidized silicon wafer.

2.1.3 Chromatography

2.1.3.1 *Thin Layer Chromatography (TLC)*

Classical silica TLC plates (Merck) based on silica gel 60 on aluminum sheets with fluorescence indicator F_{254} as stationary phase, were used with given solvent combination as mobile phase. Detection of sample separation was accomplished by UV light (254 nm) and oxidation by `Seebach Regent´ solution.

2.1.3.2 *Column Chromatography*

For classical column chromatography Silica gel 60 (Machery Nagel) was used. All product separations were performed at room temperature and room pressure up to a slight excess pressure with freshly distilled solvents.

2.1.3.3 *High Performance Liquid Chromatography (HPLC)*

Analytical HPLC was performed on a Dionex Ultimate 3000. Separation of sample components was utilized by reversed phase chromatography using a Nucleosil RP18 (3 µm Bischoff) with a mixture of acetonitrile (ACN) (Rotisolv HPLC grade; Roth) and deionized water (millipore quality, acidified with 300 $\mu l \cdot l^{-1}$ phosphoric acid) and a Nulceosil RP 18 (5 µm Bischoff), eluted with methanol (HPLC grade; Fisher Scientific) and deionized water. Solvent ratio was mostly kept isocratic with ratios between 80 % ACN (methanol) / 20 % water and 40 % ACN (methanol) / 60 % water. In some cases gradient methods were used to accelerate sample elution. The flow rate was adjusted between 0.45 $ml \cdot min^{-1}$ and 0.9 $ml \cdot min^{-1}$, depending on the solvent ratio to avoid a pump pressure higher than 200 bar. Peak detection was enabled by diode array detector (DAD), recording absorption spectra at different wavelengths to identify separated substances by their UV-Vis spectra. To quantify

sample composition, calibration standards were used to calculate substance concentrations by integration over their respective peak area.

2.1.4 Light Sources

2.1.4.1 *UV-Lamps*

In photo cleavage experiments, light of 254 nm, 266 nm and 280 nm was used. Light source for 254 nm was a 9 W low-pressure mercury-vapor lamp (Philips). The light was monochromatized by a suitable interference filter. Irradiation at 266 nm and 280 nm was applied, using excitation light of a Shimadzu RF-1502 spectrometer, equipped with a 508 W Xenon arc lamp and a grating monochromator at these wavelengths. The light energy was determined by using azobenzene as an actinometer, following Gauglitz and Hubig[154].

2.1.4.2 *Lasers*

Two different laser systems served as light sources for single- and two-photon absorption experiments. All experiments at 355 nm were accomplished with an AVIA 355-7 (Coherent Inc.), a diode-pumped, q-switched, frequency-tripled neodymium doped yttrium aluminium garnet (Nd:YAG) laser with a pulse length of 25 ns. In the described experiments, the laser was operated at a repetition rate of 10 kHz and an average pulse energy of 260 µJ. The beam diameter was adjusted by different optical setups between 1 cm and 1.5 cm. Irradiation at 532 nm was carried out with an Infinity 40-100 (Coherent Inc.), a q-switched Nd:YAG laser with a pulse length of 3 ns and a repetition rate of 40 Hz. The beam has a flat top profile and the diameter was adjusted to 5.5 mm.

The energy at the location of the sample was measured using a Fieldmaster GS (Coherent) set to the appropriate wavelength and equipped with a power meter head Model 80 (Coherent).

2.2 Materials

All chemicals used were purchased from Sigma Aldrich, Acros Scientific, Merck, ABCR, Flurochem or TCI Europe and if not mentioned otherwise, used as received. Anhydrous solvents were also purchased from Sigma Aldrich or Acros Scientific and used with the specified moisture. All other solvents were purchased from the chemical stock of the faculty

of chemistry department of the Philipps-University of Marburg and purified by distillation under reduced pressure prior to use.

2.3 Synthetic Procedures

All reactions were carried out under Schlenk conditions with Argon 5.0 (Air Liquid) as protecting gas.

2.3.1 Synthesis of *ortho*-Nitrobenzyl Compounds

2.3.1.1 *Synthesis of 3-Hydroxy-4-methoxy-2,6-dinitrobenzaldehyde* ***(1)***[84]

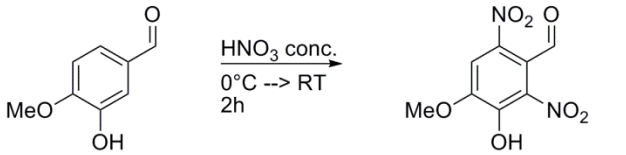

Molecular Weight: 152.15 Molecular Weight: 242.14

	eq.	n / mmol	M / g·mol^{-1}	M / g	V / ml
Isovanilin	1.0	30	152.05	4.56	
Nitric acid (68 %, 15 M)					10
Water					4

Isovanilin was suspended in a 250 ml round bottom flask in 4 ml of water and chilled to 0°C with an ice bath. Concentrated nitric acid was added dropwise afterwards to the suspension under stirring conditions. During the addition period, the beige suspension turned to a dark yellow, generating brown NO_x-gases. After complete addition of the nitric acid, the mixture was stirred for 2 h at room temperature (RT). The reaction mixture was then transferred into 50 ml of ice cold water. After filtration, the bright yellow solid was collected and recrystallized from water (approx. 500 ml) to obtain 4.4 g (18 mmol, 62%) of compound **(1)** as yellow needles.

^{1}H-NMR (300 MHz, $CDCl_3$): δ/ppm = 10.46 (s, 1H, C*H*O), 7.85 (s, 1H, $C_{ar}H$), 4.10 (s, 3H, OCH_3).

MS (ESI): *m/z* (%): 244 (7) [M + 2 H^+], 243 (100) [M + H^+], 180 (2).

2.3.1.2 *Synthesis of 3-Hydroxy-4-methoxy-2,6-dinitrobenzylalcohol* ***(2)***[84]

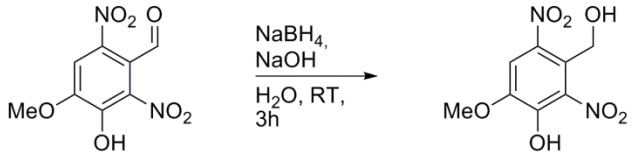

Molecular Weight: 242.14 Molecular Weight: 244.16

	eq.	n / mmol	M / g·mol^{-1}	M / g	V / ml
3-Hydroxy-4-methoxy-2,6-dinitrobenzaldehyde	1.00	17.00	242.02	4.11	
Sodium hydroxide	1.00	17.00	39.99	0.68	
Sodium borohydride	0.75	12.75	38.03	0.49	
Water					50

The benzaldehyde was suspended in 50 ml of water in a 250 ml round bottom flask and sodium hydroxide was added under stirring conditions. Within 10 min, all remaining solid was dissolved and the yellow solution turned red. After addition of sodium borohydride the solution was stirred for additional three hours. Acidification with 2 M hydrochloric acid resulted in precipitation of a yellow solid. The suspension was extracted three times with ethyl acetate. The combined organic layers were extracted twice with water and once with brine. After drying over sodium sulfate, removal of ethyl acetate under reduced pressure afforded 3.9 g (15.9 mmol, 94%) of compound **(2)** as brown solid, pure enough for the next step.

^{1}H-NMR (300 MHz, $CDCl_3$): δ/ppm = 7.69 (s, 1H, $C_{ar}H$), 4.76 (s, 2H, $C_{ar}CH_2OH$), 4.07 (s, 3H, OCH_3).

MS (EI): *m/z* (%): 244 (9), 209 (26), 192 (43), 179 (12), 166 (37), 149 (23), 138 (33), 122 (37), 107 (37), 93 (32), 79 (72), 69 (85), 53 (100).

2.3.1.3 *Synthesis of 5-Iodo-1-tert-butyldimethylsilyloxypentane*[155]

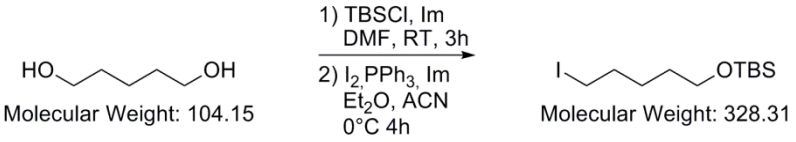

	eq.	n / mmol	M / g·mol^{-1}	M / g	V / ml
***tert*-Butyldimethylsilyl Chloride**	1.0	30	150.72	4.52	
1,5-Pentanediol (ρ = 0.994 g·ml^{-1})	9.0	270	104.15	28.12	28.29
Imidazole	2.2	66	68.08	4.49	
Triphenylphosphine	1.2	36	262.29	9.44	
Imidazole	3.0	90	68.08	6.13	
Iodine	1.2	36	253.81	9.14	
Dichloromethane					5
DMF					26
Diethyl ether					75
ACN					25

To a stirred solution of 1,5-pentanediol and 2.2 eq. imidazole a solution of *tert*-butyldimethylsilily chloride (TBSCl) in dichloromethane (DCM) was added dropwise. After two hours of stirring at RT the solutions was diluted with 150 ml of water and extracted three times with diethyl ether. The combined organic layers were washed with water and brine, dried over anhydrous sodium sulfate and concentrated to yield the alcohol as colorless oil.

The alcohol was dissolved in 75 ml diethyl ether and 25 ml ACN with triphenylphosphine and 3 eq. of imidazole and chilled to 0°C. To the resulting suspension iodine was added portionwise, until the color of the suspension changed from white to red. After additional stirring for 30 minutes at 0°C, the reaction was quenched with aqueous sodium thiosulfate. The organic layer was separated, dried over anhydrous sodium sulfate and concentrated. The resulting crude product was purified further by column chromatography (500 g silica; eluent: pentene / ethyl acetate 20:1), yielding 7.6 g (23.2 mmol, 77%) of the desired product as colorless oil.

^{1}H-NMR (300 MHz, $CDCl_3$): δ/ppm = 3.61 (t, 2H, $^{3}J_{CH2-CH2}$ = 6.2 Hz, C*H*$_2$OTBS), 3.19 (t, 2H, $^{3}J_{CH2-CH2}$ = 7.1 Hz, C*H*$_2$I) , 1.85 (p, 2H, $^{3}J_{CH2-CH2}$ = 7.1 Hz, *CH*$_2$CH$_2$I) , 1.58 – 1.39 (m, 4H, C*H*$_2$C*H*$_2$CH$_2$OTBS), 0.89 (s, 9H, (C*H*$_3$)$_3$CSi), 0.05 (s, 6H, (C*H*$_2$)$_2$Si).

^{13}C-NMR (75 MHz, $CDCl_3$): δ/ppm = 62.81, 33.33, 31.67, 26.91, 25.94, 6.90, -5.29.

MS (ESI): *m/z* (%): 464 (9) [Diether + 2Na$^+$], 351 (100) [M + Na$^+$].

2.3.1.4 *Synthesis of 3-(5-(Tert-butyldimethylsilyloxy)pentyloxy)-4-methoxy-2,6-dinitro-benzylalcohol* ***(3a)***

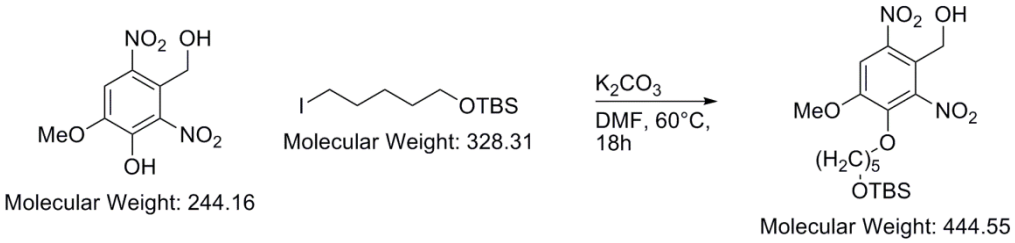

	eq.	n / mmol	M / g·mol^{-1}	M / g	V / ml
3-Hydroxy-4-methoxy-2,6-dinitrobenzylalcohol	1.0	5.0	244.03	1.22	
5-Iodo-1-*tert*-butyldimethylsilyloxypentane	1.0	5.0	328.31	1.64	
Potassium carbonate	1.5	7.5	137,91	1.03	
DMF					50

The benzyl alcohol was suspended with potassium carbonate in 50 ml DMF in 250 ml round bottom flask and stirred for 10 min at RT until color changed from orange to red. After addition of the iodine, the resulting solution was stirred for 72 h at 60°C. The suspension was chilled to room temperature and filtrated. The resulting clear red solution was diluted with 150 ml of water and extracted with ethyl acetate (three times). The combined organic layers were washed with brine and dried over anhydrous sodium sulfate. Removal of the solvent under reduced pressure, afforded the crude product as red oil. Further purification by column chromatography (200 g silica; eluent: pentene / ethyl acetate 4:1) yielded 1.26 g (2.9 mmol; 57 %) of the desired product as yellow solid.

^{1}H-NMR (300 MHz, $CDCl_3$): δ/ppm = 7.70 (s, 1H, $C_{ar}H$), 4.70 (d, 2H, ^{3}J = 7.3 Hz, $C_{ar}CH_2OH$), 4.25 (t, 2H, ^{3}J = 6.6 Hz, $C_{ar}OCH_2CH_2$), 3.99 (s, 3H, OCH_3), 3.62 (t, 2H, ^{3}J = 6.3 Hz, CH_2OTBS), 1.79 – 1.69 (m, 2H, CH_2 aliphatic), 1.61 – 1.51 (m, 4H, CH_2 aliphatic), 0.89 (s, 9H, $SiC(CH_3)_3$), 0.05 (s, 6H, $Si(CH_3)_2$).

^{13}C-NMR (75 MHz, $CDCl_3$): δ/ppm = 152.46, 144.62, 121.27, 110.28, 75.48, 62.92, 57.07, 56.84, 32.32, 29.61, 25.94, 25.62, 21.83, 18.33, 1.00, -5.31.

UV/Vis: (ACN): λ_{max}/nm (normalized absorption) = 197 (1), 218 (0.50), 326 (0.14)

$\varepsilon_{326\ nm}$ = 4,547 l·mol^{-1}·cm^{-1} ± 113 l·mol^{-1}·cm^{-1}

HRMS (ESI): *m/z* = 445.2008 [M + H^{+}] Δmmu = 0.7

2.3.1.5 *Synthesis of 3-(Allyoxy)-4-methoxy-2,6-dinitrobenzylalcohol* ***(3b)***

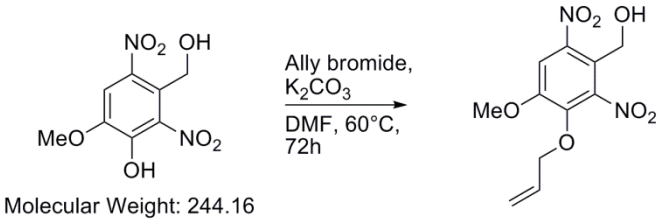

	eq.	n / mmol	M / g·mol^{-1}	M / g	V / ml
3-Hydroxy-4-methoxy-2,6-dinitrobenzylalcohol	1.0	18	244.03	4.39	
Allyl bromide (ρ = 1.398 g·ml^{-1})	1.5	27	119.96	3.24	2.32
Potassium carbonate	3.0	54	137.91	7.45	
N,N-Dimethylfromamid (DMF)					50

The benzyl alcohol was suspended with potassium carbonate in 50 ml DMF in 250 ml round bottom flask and stirred for 10 min at RT, until a color change from orange to red occurred. After addition of allyl bromide the resulting solution was stirred for 72 h at 60°C. The suspension was chilled to room temperature and filtrated. The resulting clear red solution was diluted with 150 ml of water and extracted with ethyl acetate (three times). The combined organic layers were washed with brine and dried over anhydrous sodium sulfate. Removal of the solvent under reduced pressure afforded the crude product as red oil.

Further purification by column chromatography (500 g silica; eluent: pentene / ethyl acetate 3:1) yielded 2.5 g (8.8 mmol; 49 %) of the desired product as yellow solid.

^{1}H-NMR (300 MHz, $CDCl_3$): δ/ppm = 7.70 (s, 1H, $C_{ar}H$), 5.97 (tdd, 1H, $^3J_{CH\text{-}CH2}$ = 6.2 Hz, $^3J_{CH\text{-}CH,\ cis}$ = 10.3 Hz, $^3J_{CH\text{-}CH,\ trans}$ = 17.1 Hz, CH_2=CH) , 5.34 (dd, 1H, ^2J = 1.4 Hz, $^3J_{CH\text{-}CH,\ trans}$ = 17.1 Hz, CH_2=CH) , 4.93 (dd, 1H, ^2J = 1.4 Hz, $^3J_{CH\text{-}CH,\ cis}$ = 10.2, $^4J_{H\text{-}C=C\text{-}C\text{-}H}$ 1.1 Hz, CH_2=CHCH_2), 4.78 (dt, 2H, $^3J_{CH\text{-}CH2}$ = 6.2 Hz, $^4J_{H\text{-}C=C\text{-}C\text{-}H}$ 1.1 Hz, CH_2=CHCH_2), 4.70 (d, 2H, $^3J_{CH2\text{-}OH}$= 7.4 Hz, $C_{ar}CH_2OH$), 4.01 (s, 3H, OCH_3), 2.72 (t, 1H, $^3J_{CH2\text{-}OH}$= 7.4 Hz, $C_{ar}CH_2OH$).

2.3.1.6 *Synthesis of 1-N-Benzoyl-5-fluorouracil* ***(Bz5FU)***[156]

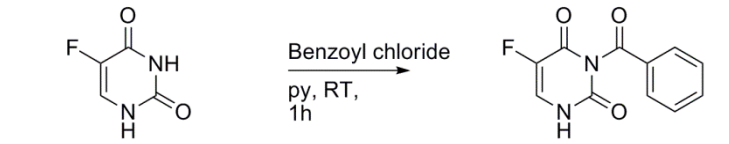

Molecular Weight: 130.08 Molecular Weight: 234.18

	eq.	n / mmol	M / g·mol^{-1}	M / g	V / ml
5-Fluorouracil	1	10	130.08	1.30	
Benzoyl chloride (ρ = 1.211 g·ml^{-1})	3	30	140.57	4.22	3.43
Pyridine					30

5FU was diluted in 24 ml of pyridine and added dropwise utilizing an additional funnel to a solution of benzoyl chloride in 6 ml of pyridine. After stirring one hour at RT, the reaction mixture is quenched with 50 ml of ice water and extracted three times with toluene. The combined organic layers were dried over anhydrous sodium sulfate and concentrated. The crude product was recrystallized from chloroform yielding 2.08 g (8.9 mmol, 89 %) of the desired product as white crystals.

^{1}H-NMR (300 MHz, DMSO): δ/ppm = 11.56 (s, 1H, NH), 8.09 (d, 1H, $^3J_{CH\text{-}CF}$ = 6.1 Hz, CH=CF), 8.05 (d, 2H, ^3J = 7.4 Hz, CH_{ar}), 7.81 (t, 1H, ^3J = 7.4 Hz, CH_{ar}), 7.61 (t, 2H, ^3J = 7.8 Hz, CH_{ar}).

^{19}F-NMR (282 MHz, DMSO): δ/ppm = -170.8.

^{13}C-NMR (75 MHz, DMSO): δ/ppm = 148.48, 135.60, 130.80, 130.41, 129.40, 129.13, 128.44, 127.67, 127.25,

MS (ESI): *m/z* (%): 382 (7) [M + 5FU + H_3O^+], 339 (7) [M + Bz^+], 295 (10) [M + 2H_3O^+ + Na^+], 235 (19) [M + H^+], 105 (100) [Bz^+].

2.3.1.7 *Synthesis of 3-N-(3-(5-(Tert-butyldimethylsilyloxy)pentyloxy)-4-methoxy-2,6-di-nitrobenzyl)-1-N-benzoyl-5-fluorouracil* ***(4a)***

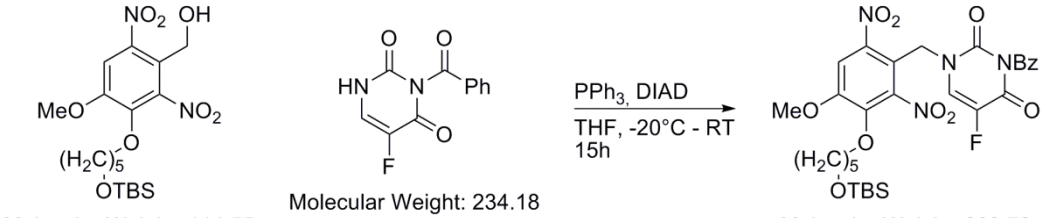

	eq.	n / mmol	M / g·mol^{-1}	M / g	V / ml
3-(5-(*tert*-Butyldimethylsilyloxy)-pentyloxy)-4-methoxy-2,6-dinitro-benzylalcohol	1.0	3.10	444.55	1.38	
1-N-Benzoyl-5-fluorouracil	1.1	3.41	234.18	0.80	
Triphenylphosphine	2.0	6.20	262.29	1.63	
Diisopropyl azodicarboxylate (DIAD) (ρ = 1.03 g·ml^{-1})	2.0	6.20	202.21	1.25	1.22
Tetrahydrofuran (THF)					30

At 0 °C 2 eq. DIAD were added slowly to a suspension of 2 eq. triphenylphosphine in 20 ml anhydrous THF and stirred for additional 30 minutes. 12 ml (1.2 eq.) of this preformed beige complex suspension were added slowly to a suspension of 1-N-Benzoyl-5-fluorouracil and the benzyl alcohol in 10 ml anhydrous THF at -20 °C. The reaction mixture was stirred for 15 h and allowed to warm to RT. After evaporation of the solvent, the crude reaction mixture was purified by column chromatography on silica gel with pentane and *tert*-butylmethyl ether (1:1) as eluent, yielding 1.65 g (2.5 mmol, 80 %) of the desired product as pale yellow solid.

^{1}H-NMR (300 MHz, $CDCl_3$): δ/ppm = 7.95 (d, 2H, ^{3}J = 7.3 Hz, Bz: C_qCHCH) 7.70 – 7.65 (m, 2H, $C_{ar}HCNO_2$, Bz: C_q-CH-C*H*), 7.52 (t, 2H, ^{3}J = 7.3 Hz, Bz: CHCHC*H*), 7.28-7.26 (m, C*H*=CF, solvent signal), 5.07 (s, 2H, $C_{ar}CH_2N$), 4.29 (t, 2H, ^{3}J = 6.6 Hz, $C_{ar}OCH_2CH_2$), 4.02 (s, 3H, OCH_3), 3.63 (t, 2H, ^{3}J = 6.3 Hz, CH_2OTBS), 1.81 – 1.72 (m, 2H, CH_2 aliphatic), 1.61 – 1.51 (m, 4H, CH_2 aliphatic), 0.90 (s, 9H, $SiC(CH_3)_3$), 0.06 (s, 6H, $Si(CH_3)_2$).

^{19}F-NMR (282 MHz, $CDCl_3$): δ/ppm = -163.4.

^{13}C-NMR (75 MHz, $CDCl_3$): δ/ppm = 166.62, 153.57, 148.13, 144.86, 144.26, 138.53, 135.45, 130.75, 130.51, 129.25, 127.22, 126.77, 113.87, 110.58, 75.79, 62.88, 57.02, 44.24, 32.31, 32.10, 29.61, 28.60, 25.94, 22.78, 21.88, 18.34, 1.00, -5.30.

UV/Vis: (ACN): λ_{max}/nm (normalized absorption) = 197 (1), 252 (0.48), 280 (0.26), 325 (0.07)

$\varepsilon_{252\ nm}$ = 27,479 l·mol^{-1}·cm^{-1} ± 205 l·mol^{-1}·cm^{-1}

MS (ESI): *m*/*z* (%): 684 (23) [M + Na^+ + H^+], 684 (68) [M + Na^+], 679 (100) [M + H_3O^+], 561 (31) [M + H^+], 558 (4), 105 (26).

HRMS (ESI): *m*/*z* = 683.2155 [M + Na^+] Δmmu = -0.1

2.3.1.8 *Synthesis of 3-N-(3-(5-Hydroxypentyloxy)-4-methoxy-2,6-dinitrobenzyl)-5-fluoro-uracil* ***(5)***

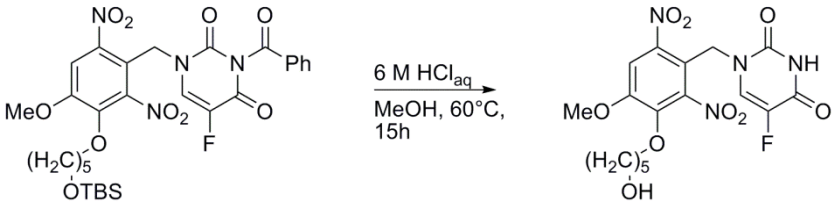

Molecular Weight: 660.72 Molecular Weight: 442.35

	eq.	n / mmol	M / g·mol^{-1}	M / g	V / ml
3-N-(3-(5-(*tert*-Butyldimethylsilyl-oxy)pentyloxy)-4-methoxy-2,6-di-nitrobenzyl)-1-N-benzoyl-5-fluoro-uracil	1	2.3	60.72	1.52	
Hydrochloric acid (35 wt.%)					10
Methanol					10

To 3.1 mmol of **4a** dissolved in 10 ml methanol, 10 ml of concentrated hydrochloric acid were added. The resulting solution was stirred at 60 °C for 15 h. After cooling to RT the reaction mixture was diluted with 50 ml of deionized water and extracted thrice with chloroform. The combined organic layers were dried over anhydrous sodium sulfate and the solvent was evaporated under reduced pressure. The sustained crude product was purified by column chromatography on silica gel with chloroform and methanol (15:1) as eluent yielding 840 mg (1.90 mmol, 83 %) of the desired product as white solid.

^{1}H-NMR (300 MHz, $CDCl_3$): δ/ppm = 8.64 (s, 1H, NH), 7.69 (s, 1H, $C_{ar}HCNO_2$), 7.19 (d, 1H, ^{3}J = 5.68 Hz, C*H*=CF), 5.04 (s, 2H, $C_{ar}CH_2N$), 4.29 (t, 2H, ^{3}J = 6.4 Hz, $HOCH_2$), 4.02 (s, 3H, OCH_3), 3.67 (t, 2H, ^{3}J = 6.3 Hz, CH_2OC_{ar}), 1.81 – 1.72 (m, 2H, CH_2 aliphatic), 1.61 – 1.51 (m, 4H, CH_2 aliphatic).

^{19}F-NMR (282 MHz, $CDCl_3$): δ/ppm = -166.45.

^{13}C-NMR (75 MHz, $CDCl_3$): δ/ppm = 152.67, 149.00, 144.11, 143.92, 138.36, 133.48, 127.24, 126.80, 114.10, 110.10, 74.99, 61.29, 56.56, 43.32, 31.72, 29.05, 21.30,

MS (ESI): *m/z* (%): 461 (5) [M + H_3O^+], 460 (27), 443 (100) [M + H^+], 321 (2), 159 (4), 119 (5), 77 (2).

HRMS (ESI): *m/z* = 465.1026 [M + Na^+] Δmmu = -0.2

2.3.1.9 *Synthesis of 3-N-(3-(5-methacryloxypentyloxy)-4-methoxy-2,6-dinitrobenzyl)-5-fluorouracil* ***(6)***

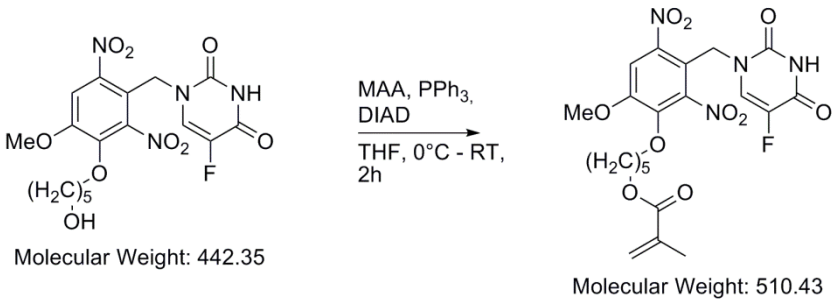

Molecular Weight: 442.35

Molecular Weight: 510.43

	eq.	n / mmol	M / g·mol^{-1}	M / g	V / ml
3-N-(3-(5-Hydroxypentyloxy)-4-methoxy-2,6-dinitrobenzyl)-5-fluoro-uracil	1.0	2.0	442.35	0.89	
Methacrylic acid (ρ = 1.015 g·ml^{-1})	1.2	2.4	86.09	0.21	0.20
Triphenylphosphine	2.0	4.0	262.29	1.05	
DIAD (ρ = 1.03 g·ml^{-1})	2.0	4.0	202.21	0.80	0.79
THF					30

At 0 °C 2 eq. DIAD were added slowly to a suspension of 2 eq. of triphenylphosphine in 20 ml anhydrous THF and stirred for additional 30 minutes. 12 ml (1.2 eq.) of the preformed beige complex suspension were added slowly to a suspension of methacrylic acid and **5** in anhydrous THF at -20 °C. The reaction mixture was stirred for 3h and allowed to warm to RT. After evaporation of the solvent, the crude reaction mixture was purified by column chromatography on silica gel with pentane and ethyl acetate (3:2) as eluent resulting in 561 mg (1.10 mmol, 55 % yield) of the desired product as white solid.

^{1}H-NMR (300 MHz, $CDCl_3$): δ/ppm = 7.70 (s, 1H, $C_{ar}H$), 7.18 (d, 1H, J = 5.7 Hz, C*H*=CF), 6.11 (m, 1H, CH_2=C_q), 5.56 (p, 1H, J = 1.5Hz CH_2=C_q), 5.04 (s, 2H, $C_{ar}CH_2N$), 4.28 (t, 2H, ^{3}J = 6.4 Hz, $C_{ar}OCH_2CH_2$), 4.16 (t, 2H, ^{3}J = 6.5 Hz, CH_2O(C=O)), 4.02 (s, 3H, OCH_3), 1.94 (m, 3H, CH_2=C_qCH_3), 1.82 – 1.68 (m, 4H, CH_2 aliphatic), 1.53 – 1.46 (m, 2H, CH_2 aliphatic).

^{19}F-NMR (282 MHz, $CDCl_3$): δ/ppm = -164.8.

^{13}C-NMR (75 MHz, $CDCl_3$): δ/ppm = 153.49, 148.95, 146.82, 144.60, 144.45, 138.86, 136.41, 129.53, 128.33, 127.65, 127.20, 125.33, 113.96, 110.51, 75.42, 64.35, 57.03, 43.97, 29.41, 28.20, 22.09, 18.28.

UV/Vis: (ACN): λ_{max}/nm (normalized absorption) = 198 (1), 268 (0.33), 325 (0.09)

$\varepsilon_{268\ nm}$ = 14,265 l·mol^{-1}·cm^{-1} ± 87 l·mol^{-1}·cm^{-1}

MS (ESI): *m*/*z* (%): 533 (8) [M + Na^+], 529 (66) [M + H_3O^+], 511 (100) [M + H^+], 425 (4).

HRMS (ESI): *m*/*z* = 533.1287 [M + Na^+] Δmmu = -0.3

2.3.1.10 *Synthesis of 3-N-(3-Allyloxy-4-methoxy-2,6-dinitrobenzyl)-1-N-Benzoyl-5-fluoro-uracil* ***(4b)***

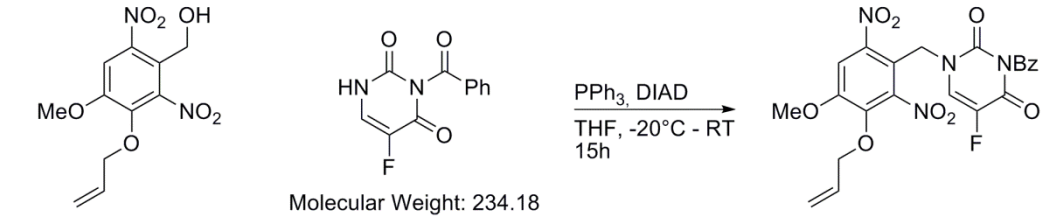

	eq.	n / mmol	M / g·mol^{-1}	M / g	V / ml
3-Allyloxy-4-methoxy-2,6-dinitrobenzylalcohol	1.0	3.30	284.22	0.94	
1-N-Benzoyl-5-fluorouracil	1.2	4.95	234.18	0.93	
Triphenylphosphine	2.0	6.60	262.29	1.73	
DIAD (ρ = 1.03 g·ml^{-1})	2.0	6.60	202.21	1.34	1.3
THF					50

At 0 °C 2 eq. DIAD were added slowly to a suspension of 2 eq. triphenylphosphine in 20 ml anhydrous THF and stirred for additional 30 minutes. 12 ml (1.2 eq.) of this preformed beige complex suspension was added slowly to a suspension of 1-N-Benzoyl-5-fluorouracil and the benzyl alcohol in 10 ml anhydrous THF at -20 °C. The reaction mixture was stirred for 15 h and allowed to warm to RT. Addition of 150 ml diethyl ether and cooling to -15 °C results in precipitation of the desired product as small white crystals yielding 1.18 g (2.3 mmol, 71.5%).

^{1}H-NMR (300 MHz, DMSO): δ/ppm = 8.27 (d, 1H, J = 6.9 Hz, CH=CF), 7.99-7.95 (m, 3H, C_{ar}*H*CNO_2, Bz: C_{ar}*H*), 7.82 (t, 1H, J = 7.4 Hz, Bz: C_{ar}*H*), 7.62 (t, 2H, J = 7.8 Hz Bz: C_{ar}*H*), 5.92 (tdd, 1H, $^{3}J_{CH\text{-}CH2}$ = 6.0 Hz, $^{3}J_{CH\text{-}CH,cis}$ = 10.4 Hz, $^{3}J_{CH\text{-}CH,\ trans}$ = 17.1 Hz, CH_2=*CH*), 5.37 – 5.24 (2H, m, *C*H_2=CH), 5.10 (s, 2H, C_{ar}*C*H_2N), 4.75 (d, 2H, ^{3}J = 6.0 Hz, CH_2=CHCH_2), 4.00 (s, 3H, OCH_3).

^{19}F-NMR (282 MHz, DMSO): δ/ppm = -168.67

^{13}C-NMR (75 MHz, DMSO): δ/ppm = 167.43, 156.02, 155.65, 152.51, 147.80, 144.84, 142.44, 140.35, 137.27, 135.97, 132.30, 131.14, 130.68, 130.35, 130.30, 129.48, 119.54, 113.95, 111.48, 74.85, 57.34, 44.63.

HRMS (ESI): *m/z* = 523.0868 [M + Na^+] Δmmu = -0.4

2.3.1.11 *Synthesis of 3-N-(3-Allyloxy-4-methoxy-2,6-dinitrobenzyl)-5-fluorouracil* ***(7)***

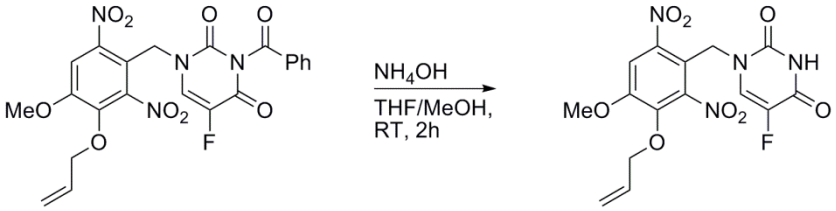

Molecular Weight: 500.39 Molecular Weight: 396.28

	eq.	n / mmol	M / g·mol^{-1}	M / g	V / ml
3-N-(3-Allyloxy-4-methoxy-2,6-di-nitrobenzyl)-1-N-Benzoyl-5-fluoro-uracil	1	2	500.39	1.00	
Ammonium hydroxide (25 wt.%)					4
THF					16
Methanol					13

To a Suspension of **4b** in 16 ml of THF and 13 ml of methanol, 4 ml of ammonium hydroxide were added slowly and stirred for two hours at RT. The resulting red solution was acidified with 50 ml of a 2 M hydrochloric acid and extracted thrice with ethyl acetate. The combined organic layers were washed with brine, dried over anhydrous sodium sulfate and concentrated. The obtained crude product was further purified by column chromatography (120 g silica; eluent: pentene/ethyl acetate 1:1), yielding 729 mg (1.8 mmol, 92%) of the desired product as white solid.

^{1}H-NMR (300 MHz, $CDCl_3$): δ/ppm = 8.17 (s, 1H, NH), 7.70 (s, 1H, $C_{ar}HCNO_2$), 7.17 (d, 1H, ^3J = 5.68 Hz, C*H*=CF), 5.97 (tdd, 1H, $^3J_{CH\text{-}CH2}$ = 6.2 Hz, $^3J_{CH\text{-}CH,cis}$ = 10.3 Hz, $^3J_{CH\text{-}CH,\ trans}$ = 17.1 Hz, CH_2=*CH*), 5.38 – 5.29 (2H, m, CH_2=CH), 5.04 (s, 2H, $C_{ar}CH_2N$), 4.79 (d, 2H, ^3J = 6.2 Hz, CH_2=CHCH_2), 4.04 (s, 3H, OCH_3).

^{19}F-NMR (282 MHz, $CDCl_3$): δ/ppm = -166.66.

^{13}C-NMR (75 MHz, $CDCl_3$): δ/ppm = 152.42, 148.84, 145.79, 144.28, 142.89, 141.23, 138.10, 131.23, 127.28, 119.17, 113.94, 109.96, 74.77, 56.44, 43.15.

HRMS (ESI): *m/z* = 397.0788 [M + H^+] Δmmu = -0.2

2.3.1.12 *Synthesis of 3-N-(3(3-Triethoxy)-propyloxy-4-methoxy-2,6-dinitrobenzyl)-5-fluorouracil* ***(8)***

Molecular Weight: 396.28

Molecular Weight: 560.56

	eq.	n / mmol	M / g·mol^{-1}	M / g	V / ml
3-N-(3-Allyloxy-4-methoxy-2,6-dinitrobenzyl)-5-fluorouracil	1.000	1.260	396.28	1.001	
Triethoxysilane (ρ = 0.89 g·ml^{-1})	3.000	3.780	164.28	0.621	0.698
Karstedt's catalyst solution (0.086 M)	0.008	0.009	381.48	0.004	0.095
THF					10

To a solution of **7** in 10 ml THF the catalyst was added first, followed by slow addition of triethoxysilane. The reaction mixture was stirred for 15 h at RT. Removal of the excess amount of silane under reduced pressure, yielded the desired product in fair purity in almost quantitative yield.

^{1}H-NMR (300 MHz, $CDCl_3$): δ/ppm = 8.32 (s, 1H, NH), 7.70 (s, 1H, $C_{ar}HCNO_2$), 7.19 (d, 1H, ^{3}J = 5.78 Hz, C*H*=CF), 5.05 (s, 2H, $C_{ar}CH_2N$), 4.02 (s, 3H, OCH_3), 3.91 - 3.79 (m, 8H, $Si(OCH_2CH_3)_3$, $C_{ar}OCH_2$), 1.27 – 1.17 (m, 13H, $(CH_2)_2Si(OCH_2CH_3)_3$).

^{19}F-NMR (282 MHz, DMSO): δ/ppm = -169.55

^{13}C-NMR (75 MHz, DMSO): δ/ppm = 157.40, 157.05, 149.25, 148.38, 144.36, 140.53, 139.91, 137.89, 129.70, 128.12, 127.38, 116.09, 109.86, 57.12, 55.99, 44.24, 18.47,

MS (ESI): *m*/*z* (%): 579 (48) [M + H_3O^+], 561 (45) [M + H^+], 516 (100) [M - OEt + H^+], 341 (2), 199 (43), 176 (16), 83 (13).

HRMS (ESI): *m*/*z* = 583.1479 [M + Na^+] ∆mmu = 0.1

2.3.2 Synthesis of Coumarin Compounds

2.3.2.1 *Synthesis of 7-Allyloxycoumarin*[157, 158]

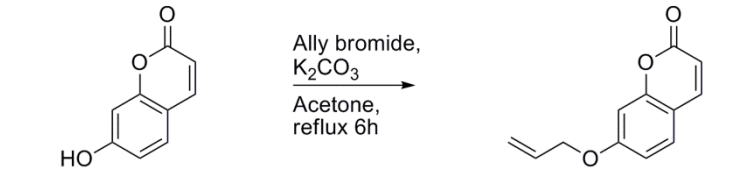

Molecular Weight: 162.14 Molecular Weight: 202.21

	eq.	n / mol	M / g·mol^{-1}	M / g	V / ml
7-Hydroxycoumarin	1.0	0.10	162.14	16.21	
Allyl bromide (ρ = 1.398 g·ml^{-1})	1.3	0.13	119.96	15.73	11.25
Potassium carbonate	1.5	0.15	137.91	20.73	
Acetone					400

To a suspension of 7-hydroxycoumarin and potassium carbonate in acetone, allyl bromide was added dropwise. Subsequently, the reaction mixture was refluxed for four hours. After cooling to RT, all solids were filtered off and the remaining solution was concentrated. The resulting crude product was recrystallized from methanol yielding 17.9 g (89 %, 0.089 mol) of the desired product as pale yellow needles.

^{1}H-NMR (300 MHz, $CDCl_3$): δ/ppm = 7.64 (d, 1H, ^{3}J = 9.5 Hz, (C=O)C_{ar}*H*C_{ar}H), 7.37 (d, 1H, ^{3}J = 8.5 Hz, $C_{q,ar}C_{ar}HC_{ar}$*H*$C_{q,ar}$), 6.86 (dd, 1H, ^{5}J = 2.4 Hz, ^{3}J = 8.5 Hz, $C_{q,ar}C_{ar}$*H*$C_{ar}HC_{q,ar}$), 6.83 (d, 1H, ^{5}J = 2.4 Hz, $C_{q,ar}C_{ar}$*H*$C_{q,ar}$), 6.26 (d, 1H, ^{3}J = 9.5 Hz, (C=O)$C_{ar}HC_{ar}$*H*), 6.05 (tdd, 1H, $^{3}J_{CH\text{-}CH2}$ = 5.3 Hz, $^{3}J_{CH\text{-}CH,\ cis}$ = 10.6 Hz, $^{3}J_{CH\text{-}CH,\ trans}$ = 17.2 Hz, CH_2=*CH*), 5.44 (ddd, 1H, J = 1.5 Hz, J = 3.0 Hz, $^{3}J_{CH\text{-}CH,trans}$ = 17.2 Hz, *CH_2*=CH) , 5.34 (ddd, 1H, J = 1.3 Hz, J = 2.6 Hz, $^{3}J_{CH\text{-}CH,\ cis}$ = 10.6 Hz, *CH_2*=CH), 4.60 (dt, 2H, J = 1.5 Hz, ^{3}J = 5.3 Hz, *CH_2*O).

^{13}C-NMR (75 MHz, $CDCl_3$): δ/ppm = 161.70, 161.07, 155.75, 143.31, 132.09, 128.70, 118.44, 113.10, 113.01, 112.58, 101.68, 69.20.

HRMS (EI): *m/z* = 202.0633 Δmmu = -0.3

2.3.2.2 *Synthesis of 7-(3-Triethoxy)-propyloxycoumarin* ***(TPC)*** [59]

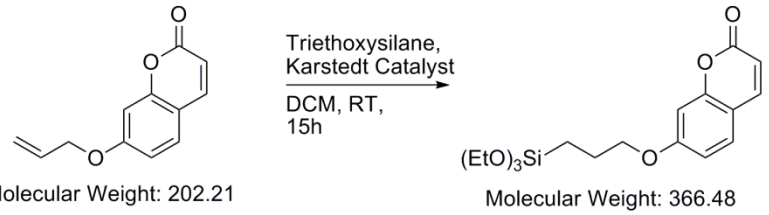

Molecular Weight: 202.21

Molecular Weight: 366.48

	eq.	n / mmol	M / g·mol^{-1}	M / g	V / ml
7-Allyloxycoumarin	1.000	25.000	202.06	5.05	
Triethoxysilane (ρ = 0.89 g·ml^{-1})	3.000	75.000	164.28	20.54	14.92
Karstedt's catalyst solution (0.086 M)	0.005	0.125	381.48	0.05	1.25
DCM					5

To a solution of 7-allyloxycoumarin in 5 ml DCM at 0 °C the catalyst was added first, followed by dropwise addition of triethoxysilane. The reaction mixture was stirred for 15 h at RT. Removal of the excess amount of silane under reduced pressure, yielded the crude product which was further purified, utilizing column chromatography (300 g silica, eluent: pentene / ethyl acetate 3:1) yielding 5.53 g (60%, 15 mmol) of the desired product as pale yellow liquid.

^{1}H-NMR (300 MHz, $CDCl_3$): δ/ppm = 7.64 (d, 1H, ^{3}J = 9.5 Hz, (C=O)C_{ar}*H*C_{ar}H), 7.36 (d, 1H, ^{3}J = 8.5 Hz, $C_{q,ar}C_{ar}HC_{ar}$*H*$C_{q,ar}$), 6.83 (dd, 1H, ^{5}J = 2.4 Hz, ^{3}J = 8.5 Hz, $C_{q,ar}C_{ar}$*H*$C_{ar}HC_{q,ar}$), 6.80 (d, 1H, ^{5}J = 2.4 Hz, $C_{q,ar}C_{ar}$*H*$C_{q,ar}$), 6.24 (d, 1H, ^{3}J = 9.5 Hz, (C=O)$C_{ar}HC_{ar}$*H*), 4.00 (t, 2H, ^{3}J = 6.6 Hz, C*H*$_2$OC_{ar}), 3.84 (q, 6H, ^{3}J = 7.0 Hz, Si(OC*H*$_2$CH$_3$)$_3$), 1.99 – 1.89 (m, 2H, CH_2 aliphatic), 1.23 (t, 9H, ^{3}J = 7.0 Hz, Si(OCH$_2$C*H*$_3$)$_3$), 0.80 – 0.75 (m, 2H, CH_2 aliphatic).

^{13}C-NMR (75 MHz, $CDCl_3$): δ/ppm = 162.32, 161.15, 155.84, 143.35, 128.61, 112.84, 112.79, 112.29, 101.30, 70.35, 58.37, 22.52, 18.21, 6.41,

UV/Vis: (ACN): λ_{max}/nm (Absorption) = 201 (1.00), 216 (0.30), 295 (0.20), 321 (0.33)

$\varepsilon_{321\ nm}$ = 16,047 l·mol^{-1}·cm^{-1} ± 142 l·mol^{-1}·cm^{-1}

HRMS (EI): *m/z* = 366.1500 Δmmu = -0.1

2.3.3 Synthesis of Functionalized Silica Nanoparticles

2.3.3.1 *Synthesis of 7-(3-triethoxysilylpropyloxy)coumarin functionalized silica nanoparticles*[159]

Two different 7-(3-triethoxysilylpropyloxy)coumarin functionalized silica nanoparticles were synthesized, following two different protocols.

The synthesis generating particles of a diameter of 45 nm (TPC-NP) follows mainly the modified Stöber synthesis for organo silica spheres, reported by van Blaaderen et al.[103, 123] In the first step 3.64 ml ammonium hydroxide solution were added to a solution of 3.58 ml TEOS in 93 ml ethanol and stirred for 20 h. Then 700 mg 7-(3-triethoxysilyl-propyloxy)coumarin were added to 25 ml of this solution and stirred again for 20 h. Afterwards, the surface functionalized particles were sedimented, using screwed 50 ml FEP oak ridge tubes in a Sorvall Super T21 (Thermo Fisher Scientific), equipped with a SL50T rotor running at 18,000 rpm (38,724 rcf) at 4°C. The supernatant was discarded and the particles were dispersed in methanol. For further purification, this process was repeated 10 times until the supernatant was coumarin free. After evaporation of the solvent, the nanoparticles were dried in vacuum.

The synthesis generating particles of a diameter of 19/15 nm (TPC-Ly-NP-1/2), is mainly predicated on the protocol published by Yokoi et al.[108, 124]. In the first step 1.1 ml of TEOS were added to 14.6 ml of a 6.9 mM solution of Lysin in deionized water stirred at 550 rpm. The resulting two phase system was heated to 60 °C for 24 h, until all TEOS reacted. In the second step the so formed silica particles were functionalized by adding a 0.12 M solution of TPC in cyclohexane, heating and stirring under the former conditions for 24h or 48 h respectively. Functionalization was monitored by DLS. After cooling to RT, the particle containing aqueous phase, was separated from cyclohexane and washed thrice with ethyl acetate. The resulting particles were kept in solution and only small amounts were evaporated to determine concentration and weight loss.

2.3.3.2 *Synthesis of 3-N-(3(3-Triethoxy)-propyloxy-4-methoxy-2,6-dinitrobenzyl)-5-fluorouracil functionalized silica nanoparticles*

The synthesis of drug loaded nanoparticles 40 nm in diameter (*o*-NBnC-NP) was analog to the synthesis described in 2.3.3.1 for TPC-NPs. In the first step 1.8 ml ammonium hydroxide

solution were added to a solution of 1.8 ml tetraethyl orthosilicate (TEOS) in 46 ml ethanol and stirred for 20 h. Afterwards 300 mg of **8** solved in 1 ml ethanol were added to 25 ml of this solution and again stirred for 20 h. Later, the surface functionalized particles were sedimented analog to TPC-NPs. The supernatant was discarded and the particles were dispersed in methanol. For further purification this process was repeated 5 times, until the supernatant was colorless and the UV-Vis spectra showed no unbound **8**. After evaporation of the solvent the nanoparticles were dried in vacuum.

2.3.4 Polymerization Procedure

All studied drug loaded polymer plates were photo-polymerized in bulk polymerization. The basic copolymer was composed of 86.5% of hydroxyethyl methacrylate (HEMA), 12.0% of methyl methacrylate (MMA), 1.0% of ethylene glycol dimethacrylate (EGDMA) as cross linker and 0.25% of champherquinone and 0.25% ethyl 4-dimethylamino benzoate as photo initiator. For drug load 4.0% of (**6**) and in some cases 1% of 4-2-(acryloxyethoxy)-2-hydroxybenzophenone (UV-416) (Melrob Europe) as UV-absorber were copolymerized with the basic monomer composition.

Therefore, 1 – 5 ml of the monomer mixtures were degassed for 5 min by sonification and then filled into the polymerization chamber, consisting of a vertical assembly of two glass plates of about 8 cm x 8 cm x 0.4 cm. Depending on the desired size of the polymer plate, a one or two millimeter thick silicon gasket was placed between the glass plates, to form the polymerization volume of the desired size. To avoid adhesion of the polymer plate to the glass plates a polyethylene terephthalate foil was used as spacer between the glass plates and the silicon gasket. The polymerization was initiated by a 7 cm x 7 cm array, consisting of 7 x 7 465 nm ±25 nm LEDs (Kingbright, L-7113-PBC-Z). Each LED providing 120 mW at a forward current of 20 µA with a viewing angle of 16°. The array was placed about 20 cm in front of the polymerization chamber with an additional 8 cm x 8 cm x 0.4 cm translucent glass in between for better light diffusion. Illumination was conducted in three cycles, after filling the monomer mixture into the polymerization chamber. First 10 min at half power, after a break of 30 min an additional hour at half power, followed by 18 h at maximum power. The resulting polymer plates were extracted with deionized water to remove all remaining initiator and unreacted monomer.

3 Results and Discussion

3.1 Coumarin functionalized Silica Nanoparticles

As described in 2.3.3.1, two different coumarin functionalized silica nanoparticles could be synthesized. The larger particles (TPC-NP) of approx. 45 nm in diameter, forming a stable dispersion in acetonitrile were synthesized following the original Stöber synthesis, slightly modified by van Blaadern et al. [103, 123] Particles of approx. 19 nm in diameter (TPC-Ly-NP-1) and 15 nm respectively (TPC-Ly-NP-2), forming a stable dispersion in water, were synthesized according to the protocol of Yokoi et al.[108, 124] In all cases 7-(3-triethoxysilylpropyloxy)coumarin was utilized for functionalization. In the next paragraphs, both kinds of particles are characterized, starting with their morphology and degree of functionalization followed by their photochemical properties.

3.1.1 Morphology and Degree of Functionalization

Characterization of the particle morphology could be realized by SEM – images of the silica nanoparticles dried from diluted particle dispersions on a silicon wafer.

Figure 3.1 a shows the non-functionalized nanoparticles, resulting from Stöber synthesis. They are slightly agglomerated spherical particles with a diameter of about 40 nm. In Figure 3.1 b, c, and d, TPC-NPs are shown at different magnifications. The TPC functionalization slightly enhances the tendency of the particles to agglomerate (b), but they still have a spherical shape. Their diameter is now about 45 nm. Figure 3.1 c and d show a TPC-modified nanoparticle cluster, as well as a single particle. Figure 3.1 e shows TPC-NPs that have been irradiated with light of 355 nm, which causes dimerization of the coumarin functionalities. No changes in shape and no striking changes in size, compared to the non-irradiated particles, are observed. This is in accordance with the expectations, as dimerization of two coumarin groups, both anchored adjacently on the same nanoparticle surface, is much more probable, than a dimerization between coumarin groups on two different nanoparticles. Figure 3.1 f shows such a nanoparticle-dimer.

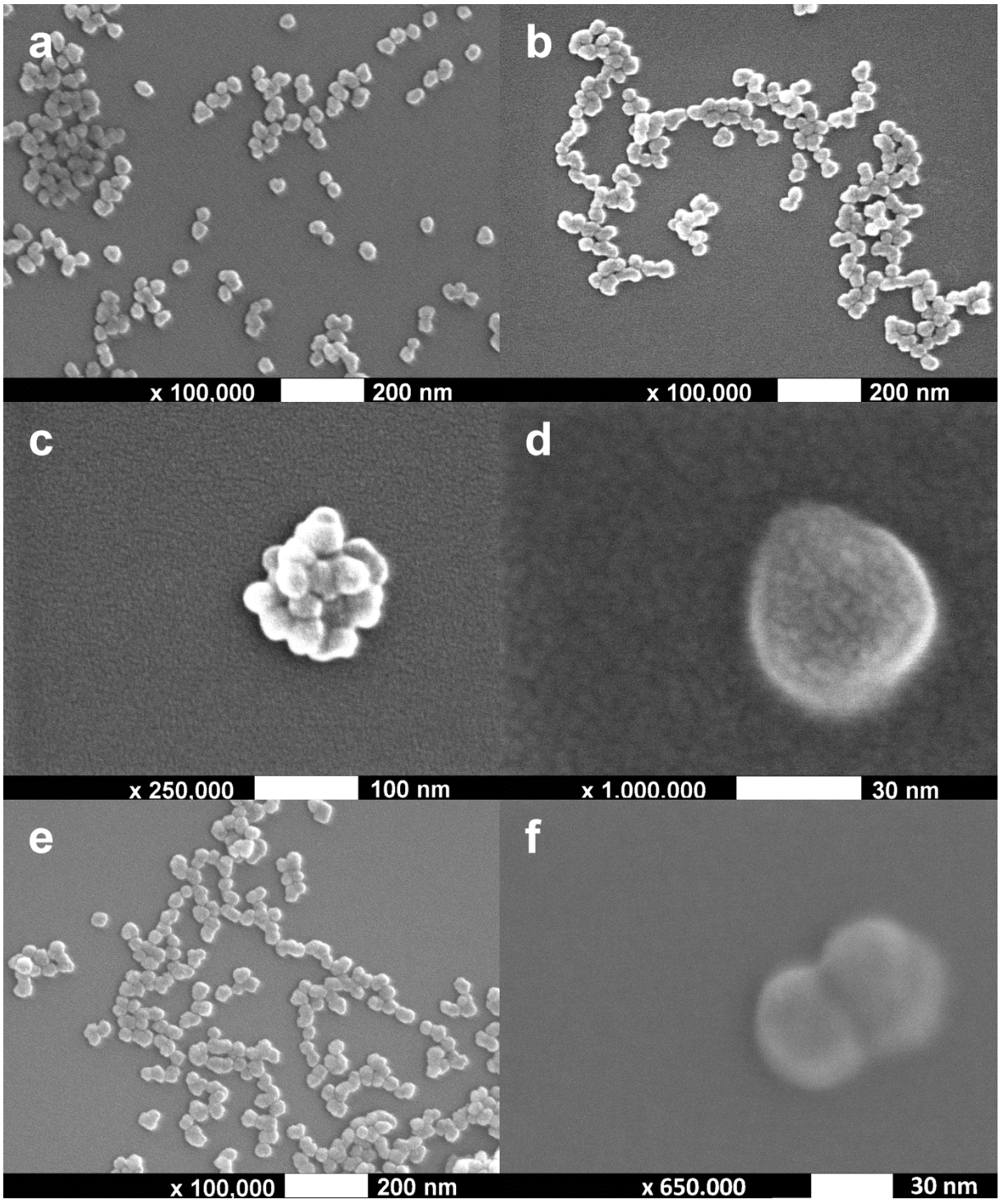

Figure 3.1: SEM images of silica nanoparticles on silicon wafer. a: non-functionalized Stöber particles; b, c, d: TPC-NPs at different magnifications; e, f: photochemically dimerized TPC-NPs.[159]

The measured diameters of the non-functionalized Stöber particles and the TPC-NPs, agree well with the results from the DLS measurements, where an average diameter of 39.3 nm ± 9.6 with a polydispersity index of 0.036 for the non-functionalized Stöber particles and 45.6 nm ± 15.0 nm with a polydispersity of 0.181 for TPC-NPs was derived. (Figure 3.2)

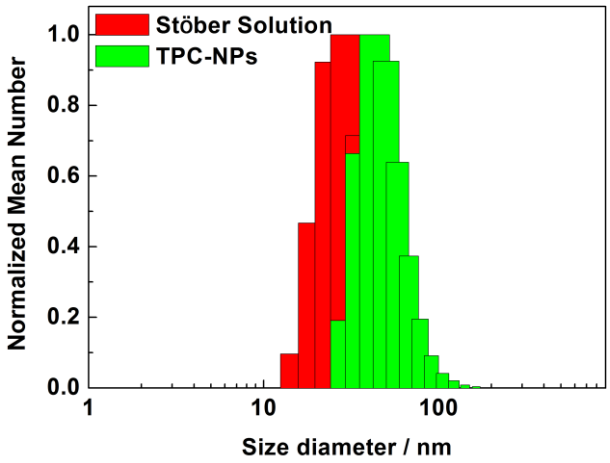

Figure 3.2: Normalized mean number derived from DLS measurements of non-functionalized Stöber particles and TPC-NPs dispersed in ethanol and acetonitrile respectively.

The length of one fully extended TPC-molecule is 1.35 nm. This should result in an increase in diameter of 2.7 nm, i.e. from 39.3 nm to 42 nm. However, both SEM and DLS measurements indicate an increase in diameter of about twice as much, which could possibly be explained by the formation of some type of a 'bilayer' of TPC on the nanoparticle surface. After a one-time exposure to light, the statistic contribution of such nanoparticle clusters is not sufficient to change the average diameter of the nanoparticles significantly. The average diameter determined by DLS measurement remains about 45 nm with a similar polydispersity index, as before.[159]

Further investigations of the particle morphology and functionalization were done, utilizing AFM and EFM. Therefore, a few microliters of a diluted mixture of dispersed non-functionalized Stöber particles and TPC-NPs were applied with a pipette on a freshly oxidized silicon wafer, used as substrate for AFM/EFM measurements. Figure 3.3 a shows the height image of 2 µm x 2 µm of the silicon wafer. The particles seem to be more agglomerated than in the SEM pictures, which probably is due to the higher surface potential of the oxidized Si-wafers compared to the untreated Si-wafers used for SEM imaging. As far as the resolution of the image reveals, the size and shape of the particles corresponds well with the values that could be determined by SEM and DLS measurements. The growth of approximately 5 % in diameter from the non-functionalized Stöber particles to the TPC-NPs, resulting from the TPC-functionalization of the particles, is not enough to be reliably resolved in the AFM images.

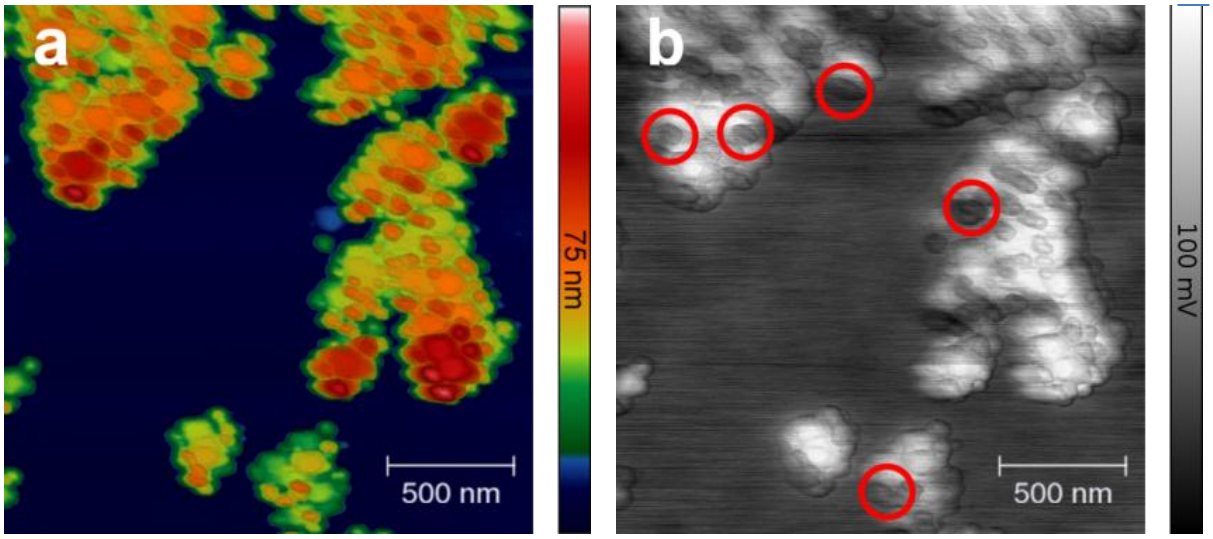

Figure 3.3: a: AFM height profile of a mixture of non-functionalized Stöber particles and TPC-NPs on a freshly oxidized silicon wafer surface; b: potential image (EFM) of a."

Figure 3.3 b shows the same 2 µm x 2 µm of the silicon wafer as Figure 3.3 a, but as an EFM-image reflecting the surface potential. For this measurement, Veeco's lift-mode without any bias to tip or surface was employed. As one can see, two different species emerge. Considering that the silicon oxide surface of a freshly oxidized silicon wafer is terminated with hydroxyl groups, the particles that are charged like the surface (selected examples highlighted in red) should be the non-functionalized silica nanoparticles, due to the fact that they are terminated with hydroxyl groups as well, resulting in the same surface potential. The second species, differing by approximately 75 mV in charge, can therefore be identified as TPC-NPs, due to the fact that TPC-functionalization leads to "end capping" of the highly negatively charged hydroxyl groups, resulting in a significant change of the surface potential of the particles. Areas with intermediate charge occur due to stacking of the two different species. Because the silicon wafer is an insulator, no absolute values concerning the sign of the charge could be determined by the applied EFM method. However, it is clearly shown, that functionalization leads to a significant change in surface potential on the single nanoparticle level. Further confirmation of the results could be achieved by ζ–potential measurements of the bulk material. The ζ–potential of the non-functionalized Stöber particles was -69.64 mV, the value for the TPC-NPs was -49.64 mV, corresponding well with the trend of the prior EFM measurements. As shown in Figure 2.1 the ζ–potential is measured at the slipping plane between the electric double layer and the diffuse layer. The particles potential is, as shown, decreasing with distance from particle explaining the lower ζ–potential difference compared to the potential difference determined in EFM

measurements corresponding to the actual surface potential. This was the first time that EFM was used to differentiate on a single particle level between functionalized and non-functionalized silica nanoparticles.[159] Only in 2004 Melin et al. reported on charge-injection experiments performed on silica nanoparticles[160] and Pacifica et al. described EFM imaging of different silica coated metal nanoparticles.[161]

To quantify the degree of functionalization, TGA measurements were performed. Between 100 °C and 800 °C, the sample showed a weight loss of 11.8%. Assuming that at these temperatures only the organic functionalization is affected and the amorphous silica core is not, it is possible to determine the molar concentration of coumarin per particle mass. With an average of 4.5 silanol groups per square nanometer[107], 22,620 potential binding sites are calculated for a particle of 40 nm in diameter. Taking the molar mass of 7-propanyloxycoumarin corresponding to the affected organic rest, a concentration of 0.57 µmol·mg^{-1} is calculated equaling 23002 TPC-molecules, assuming a particle of 40 nm in diameter and a density of 2.0 g·cm^{-3}. Due to the mechanism, only 1.5 of three ethoxy-groups of the functionalizing molecule react with the surface, resulting in formation of a double layer. This assumption is well supported by the congruent SEM and DLS measurements.

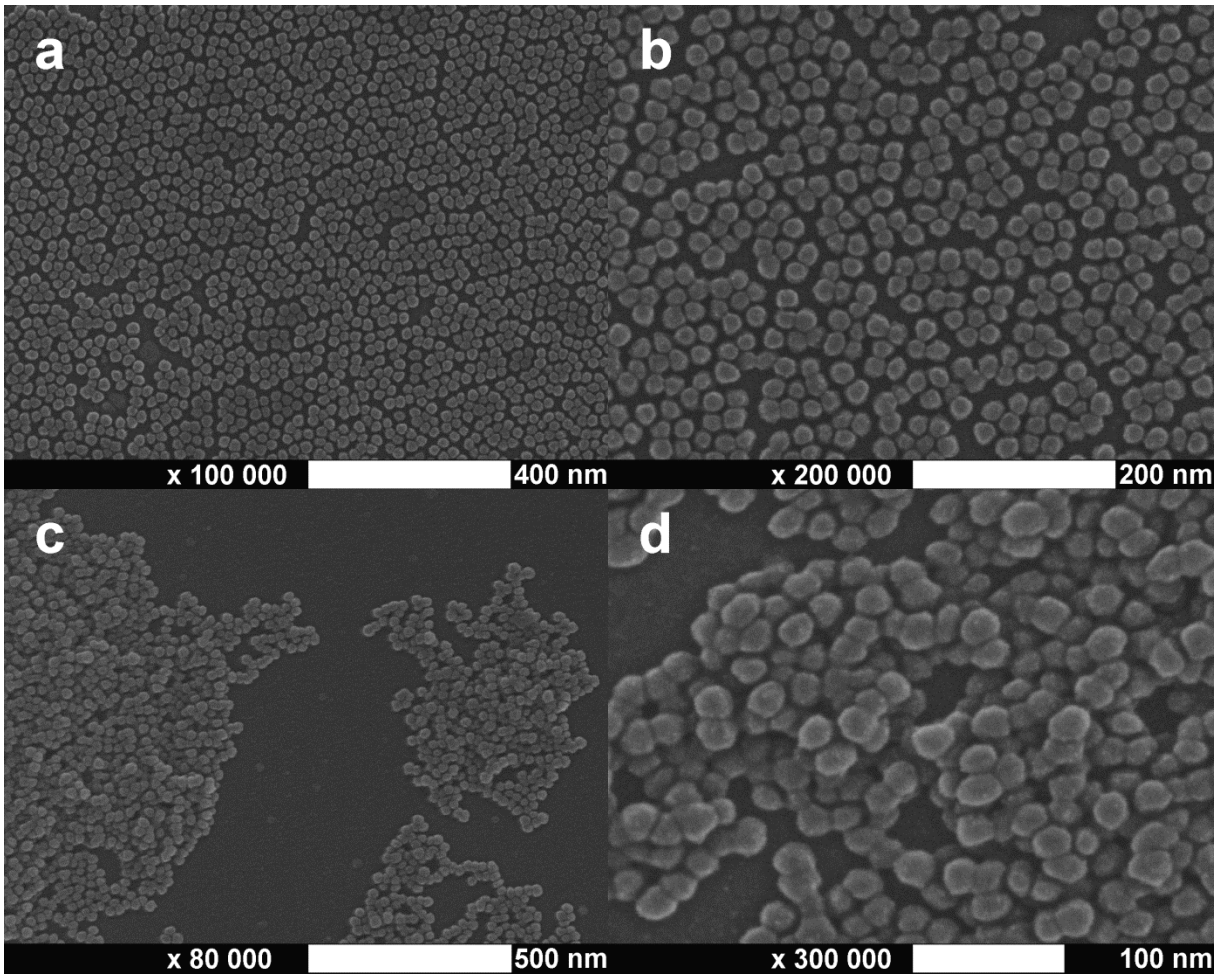

Figure 3.4 SEM images of silica nanoparticles on silicon wafer. a and b: non-functionalized lysine stabilized particles; c and d: TPC-Ly-NP-1 at different magnifications.

Figure 3.4 a & b show SEM-pictures of non-functionalized lysine stabilized silica nanoparticles at different magnifications. Graphical analysis of these pictures revealed that the mostly monodispers and spherical nanoparticles have a mean diameter of about 18 nm. This is in good agreement with the DLS measurements which derive a diameter of 16.5 nm ±7 nm. (Figure 3.5) The difference of 1.5 nm is due to the platinum shell of the particles, which had to be implemented to make the sample conductive. The particles were dried from aqueous solutions and tend to arrange themselves in a hexagonal structure as described in literature.[108] Figure 3.4 c & d show TPC-Ly-NP-1 at different magnifications. Functionalization obviously changes the affinity of the particles towards each other. The particles now tend to agglomerate when dried on the substrate and no structural self-organization can be monitored. The diameter of the TPC-Ly-NP-1 that could be obtained from the SEM-images is about 22 nm. In consideration of the platinum coating of the

particles this is again in good agreement with the DLS measurements that derived a mean diameter of 19.7 nm ±6 nm. (Figure 3.5).

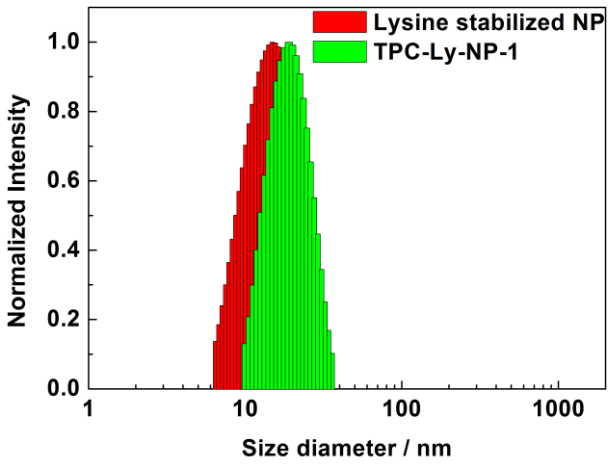

Figure 3.5: Normalized mean intensity derived from DLS measurements of non-functionalized lysine stabilized particles and TPC-Ly-NP-1 dispersed in water.

These results indicate the formation of a monolayer of TPC on the particle surface due to the fact that one fully extended TPC-molecule is 1.35 nm. This should result in an increase in diameter of 2.7 nm.

This is further supported by TGA-measurements of TPC-Ly-NP-1 between 100 °C and 800 °C. A weight loss of 3.0% was monitored, which is in good agreement with 0.14 µmol·mg^{-1} or 440 coumarin groups per particle. Compared to 3849 silanol groups on the surface of a 16.5 nm particle formation of an incomplete monolayer is probable.

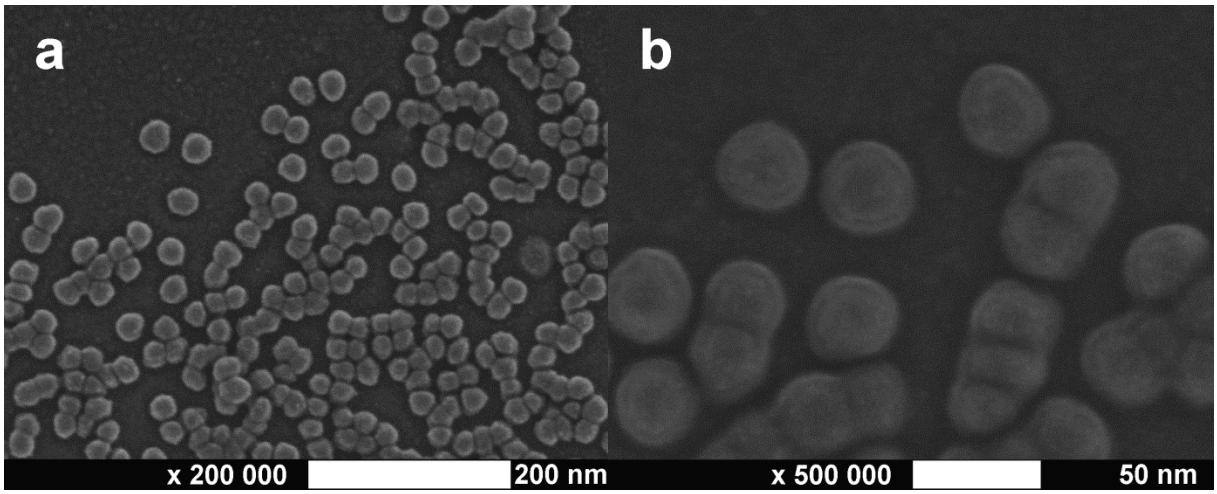

Figure 3.6: SEM images of photochemically dimerized TPC-Ly-NP-1 at different magnifications.

As already seen for the TPC-NPs photochemical dimerization of the coumarin groups has no significant influence on the particle morphology. Figure 3.6 a shows TPC-Ly-NP-1 after

exposure to laser light of 355 nm. Compared to the irradiated particles the majority of the SEM-images taken as well as DLS measurements showed no change in morphology. However with enough patience it was again possible to find some bigger particles that seem to be dimerized on the inter particle level. (Figure 3.6 b)

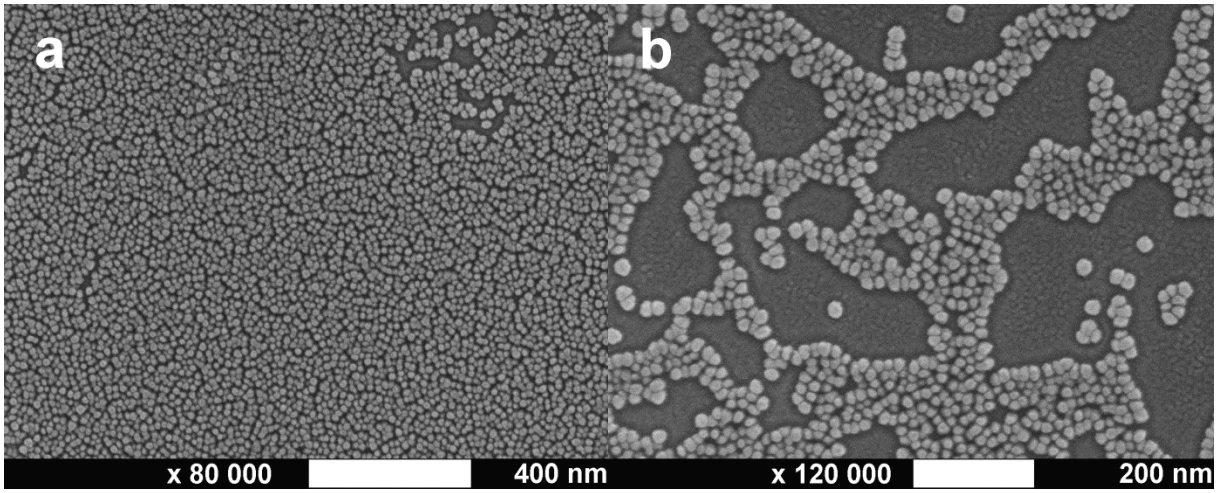

Figure 3.7: SEM images of non-functionalized lysine stabilized silica nanoparticles on silicon wafer.

Due to the low degree of functionalization a second synthesis of TPC-Ly-NP was performed. Although the reaction conditions for the non-functionalized lysine stabilized particles remained unchanged the resulting particles reached only a slightly smaller mean diameter of about 14 nm according to the SEM images (Figure 3.7a) and 12.4 nm ±6.1 nm derived from the DLS measurements. (Figure 3.8) The particles also seem to be a little more polydisperse (Figure 3.7 b) resulting in less tendency to arrange themselves in a hexagonal assembly.

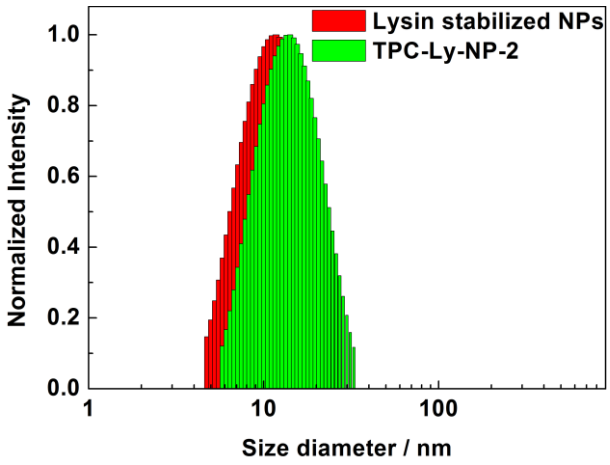

Figure 3.8: Normalized mean intensity derived from DLS measurements of non-functionalized lysine stabilized particles and TPC-Ly-NP-2 dispersed in water.

To increase the coumarin functionalization the reaction time was doubled from 24 hours to 48 hours. The resulting TPC-Ly-NP-2 are shown in Figure 3.9 a. Their mean diameter is about 17 nm referring to the SEM-images and 15.5 nm ±6.5 nm derived from the DLS-measurements. (Figure 3.8)

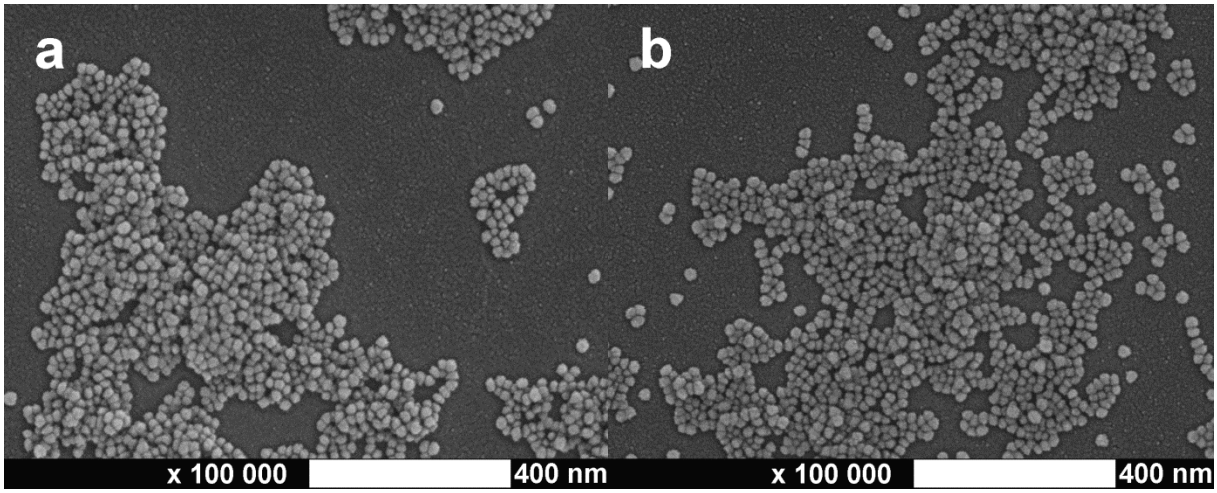

Figure 3.9: SEM images of a: TPC-Ly-NP-2 and b: photochemically dimerized TPC-Ly-NP-2.

Again the growth in diameter indicates the formation of a monolayer of TPC on the particles surface. Due to the longer reaction time the weight loss between 100 °C and 800 °C during TGA measurement could be increased up to 5.5% corresponding to 0.26 µmol·mg^{-1} 610 coumarin moieties per particle. Compared to 3396 silanol groups on the surface of a 15.5 nm particle, again only an incomplete monolayer is formed although the coverage could be increased from 13% for TPC-Ly-NP-1 to 18% for TPC-Ly-NP-2. The absolute concentration, due to the smaller diameter, is increased by almost 60%. As already seen for former TPC functionalized nanoparticles photochemical dimerization of the coumarin groups has no greater influence on the particle morphology. Figure 3.9 b shows TPC-Ly-NP-2 after exposure to laser light of 355 nm. Compared to the non-irradiated particles, the SEM-images taken as well as DLS measurements performed, showed no difference.

3.1.2 Photochemistry of Coumarin Functionalized Nanoparticles

As described in 1.1.2.3 coumarin shows two typical absorption bands. One between 310 nm and 340 nm due to a (n—>π*)-like transition caused by the carbonyl function and one (π—>π*)-transition between 250 nm and 300 nm which corresponds to the conjugated π-system. Those bands are also found in the absorption spectra of dispersions of coumarin functionalized silica nanoparticles as shown in Figure 3.10. Due to the fact, that the functionalization is implemented with a 7-alkoxy derivate of coumarin fluorescence of the particles at 390 nm could be monitored as well, when excited at 320 nm.

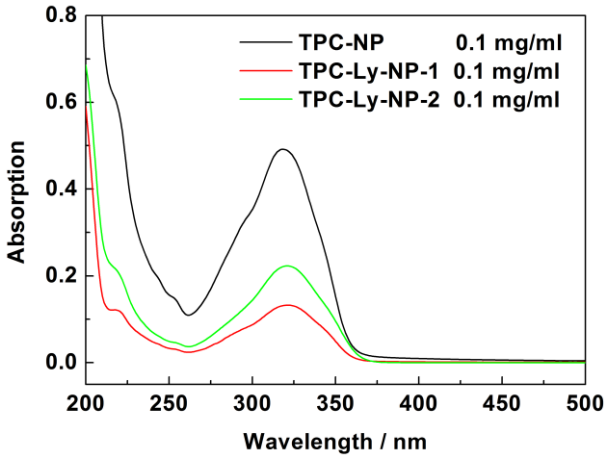

Figure 3.10: Absorption spectra of TPC functionalized silica nanoparticles.

Figure 3.10 shows the absorption spectra of all three synthesized silica nanoparticles at a concentration of 0.1 mg·ml^{-1}. Considering the coumarin concentration on the silica nanoparticle surface of 0.57 µmol·mg^{-1}, determined by TGA measurements, it is possible to derive a molar extinction coefficient for TPC-NP dispersed in acetonitrile of $\varepsilon_{320\,nm}$ = 8,802 l·mol^{-1}·cm^{-1} + 126 l·mol^{-1}·cm^{-1}. Compared to the molar extinction coefficient of TPC of $\varepsilon_{320\,nm}$ = 16,047 l·mol^{-1}·cm^{-1} + 142 l·mol^{-1}·cm^{-1} TPC-NP seem to have only half the absorption strength. This finding is not surprising, as in a nanoparticle dispersion always half of the surface bound molecules are in the 'shadow' of the nanoparticle and thus not measurable for the spectrometer, which results in an ostensibly lower absorption and the observed decrease of the apparent molar extinction coefficient.[159]

The extinction coefficient of the particles should be independent of the particle diameter. In order to prove this, theoretical absorptions values for TPC-Ly-NP-1 and TPC-Ly-NP-2 were

derived from coumarin concentrations measured by TGA and compared to experimentally obtained values:

	TGA / µmol·mg^{-1}	theo. Abs. 320 nm (0.1 mg·ml^{-1})	measured Abs. 320 nm 0.1 mg·ml^{-1}	Error
TPC-Ly-NP-1	0.14	0.123	0.133	7.3%
TPC-Ly-NP-2	0.26	0.229	0.223	2.6%

Table 3.1: Comparison between theoretical and measured absorption of TPC-Ly-NP-1 and TPC-Ly-NP-2.

As expected, the absorption of the coumarin groups attached to the nanoparticles is independent from the particle size and can be used to determine the degree of functionalization. All further photochemical investigations were carried out with TPC-NP and TPC-Ly-NP-2 due to the bigger difference in size and the higher degree of functionalization.

As described in 1.1.2.2 coumarin undergoes [2π+2π] cycloaddition when irradiated with light of a wavelength longer than 300 nm and [2π+2π] cycloreversion under irradiation with light of a wavelength shorter than 300 nm. To investigate the photochemical properties of TPC-NP and TPC-Ly-NP-2 diluted dispersion of those particles were irradiated with laser light of 355 nm to induce [2π+2π] cycloaddition and 254 nm, 266 nm and 280 nm to induce [2π+2π] cycloreversion. In case of TPC-NP the reaction was monitored by absorption and fluorescence spectroscopy. All further investigations concerning photochemical dimerization and cleavage were just monitored by absorption spectroscopy, due to the fact that fluorescence spectroscopy used 320 nm as excitation wavelength, already influencing the photochemical reaction while collecting spectroscopic data.

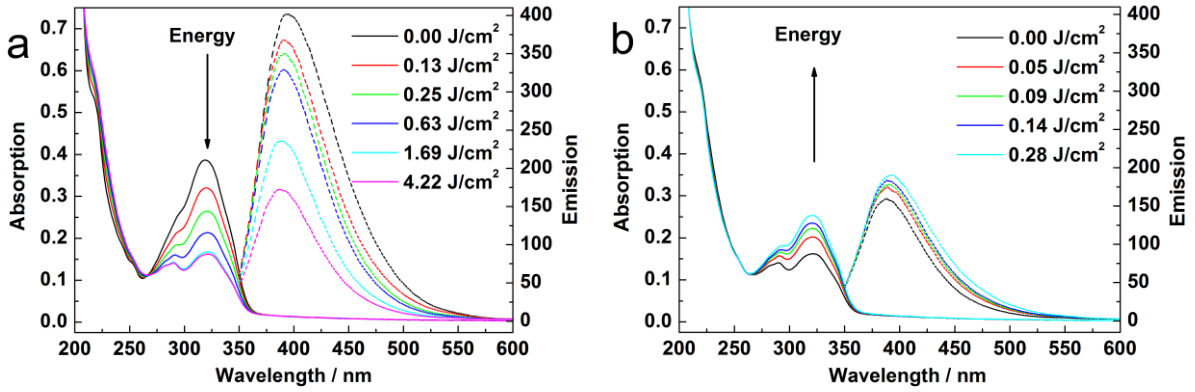

Figure 3.11: Absorption and fluorescence spectra of TPC-NPs dispersed in acetonitrile. A: photo-dimerization after consecutive irradiations with 355 nm light with the total energies given, and b: photo-cleavage after consecutive light exposures to 280 nm with the total energies given.[159]

Figure 3.11 shows the absorption and emission spectra of TPC-NPs while irradiated with 355 nm and 280 nm respectively. In case of photo dimerization at 355 nm the absorption band at 320 nm and the emission band at 390 nm decreases with increasing energy input, indicating [2π+2π] cycloaddition and thereby shortening of the conjugated π-system. Irradiation at 280 nm induces [2π+2π] cycloreversion resulting in an increase of the absorption band at 320 nm and as well of the emission band at 390 nm, due to the restoration of the extended conjugated π-system

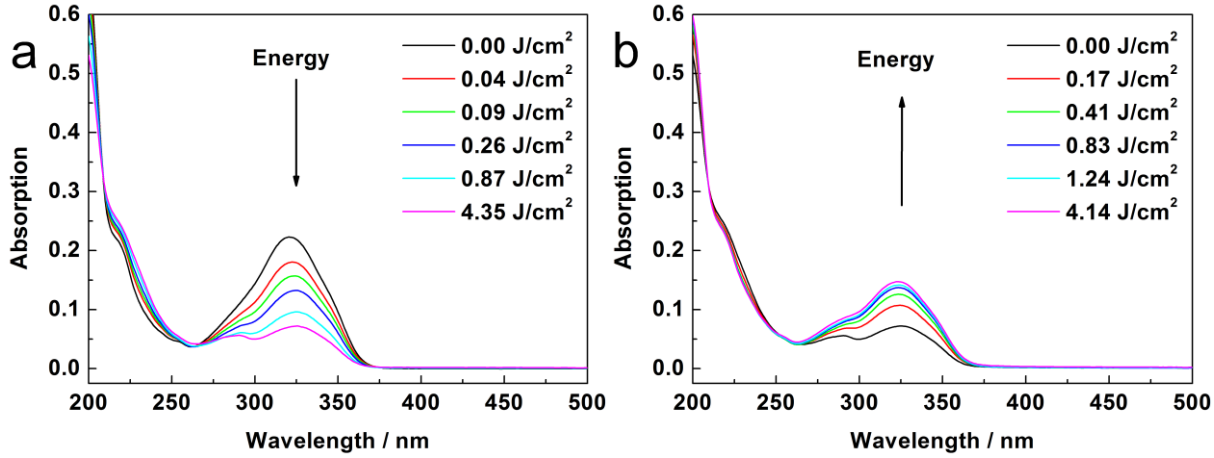

Figure 3.12: Absorption and fluorescence spectra of TPC-Ly-NP-2 dispersed in water. a: photo-dimerization after consecutive irradiations with 355 nm light with the total energies given, and b: photo-cleavage after consecutive light exposures to 280 nm with the total energies given.

Figure 3.12 shows the same for TPC-Ly-NP-2. In solution the absorption band at 320 nm disappears completely when all coumarins are dimerized. This cannot be observed for the nanoparticles, because of statistical reasons. Dimerization of neighboring molecules leads to

33.75% of isolated molecules on the surface with no remaining reactant in range. The only possibility would be dimerization with another isolated molecule on a different particle, but this is hindered by steric constraints.

To quantify the efficiency of the photochemical cleavage the single photon quantum yield ϕ_{cleave} can be attained by equation

$$\Phi_{cleave} = \frac{n_{dimer}}{n_{photon}} = \frac{n_{dimer}}{E_{abs}} \cdot \frac{E_{abs}}{n_{photon}} \quad (3.1)$$

Equation 3.1: n_{dimer}: number of cleaved coumarin dimers; n_{photon}: number of photons absorbed by coumarin dimers; E_{abs}: absorbed energy.

The quantum yield for the single photon cleavage reaction is limited due to deactivating processes like fluorescence or dissipation. Because of the low concentration of coumarin in the nanoparticle dispersion not all irradiated energy is absorbed. The actual energy absorbed ($P_{abs,280nm}$) was calculated to be $2.01 \cdot 10^{-4}$ W·cm^{-2} by

$$P_{abs,280nm} = P_{280nm} \cdot (1 - 10^{-A_{0,280nm}}) \quad (3.2)$$

Equation 3.2: P_{280nm}: irradiated energy; $A_{0,280nm}$: absorption at the beginning of the irradiation.

The number of cleaved coumarin dimers per absorbed energy can be calculated by

$$\frac{n_{dimer}}{E_{abs}} = \frac{c_{dimer}}{E_{abs}} \cdot V \cdot N_A \quad (3.3)$$

Equation 3.3: c_{dimer}: concentration of cleaved dimers; V: volume (2 ml); N_A: Avogadro constant.

Plotting the concentration of cleaved dimers versus the actual energy absorbed results in a linear increase with $c_{dimer} \cdot E_{abs}^{-1}$ as the slope of the linear fitting of the data points. The coefficient of determination for the linear fitting was 0.998 in both cases. (Figure 3.13 b & d)

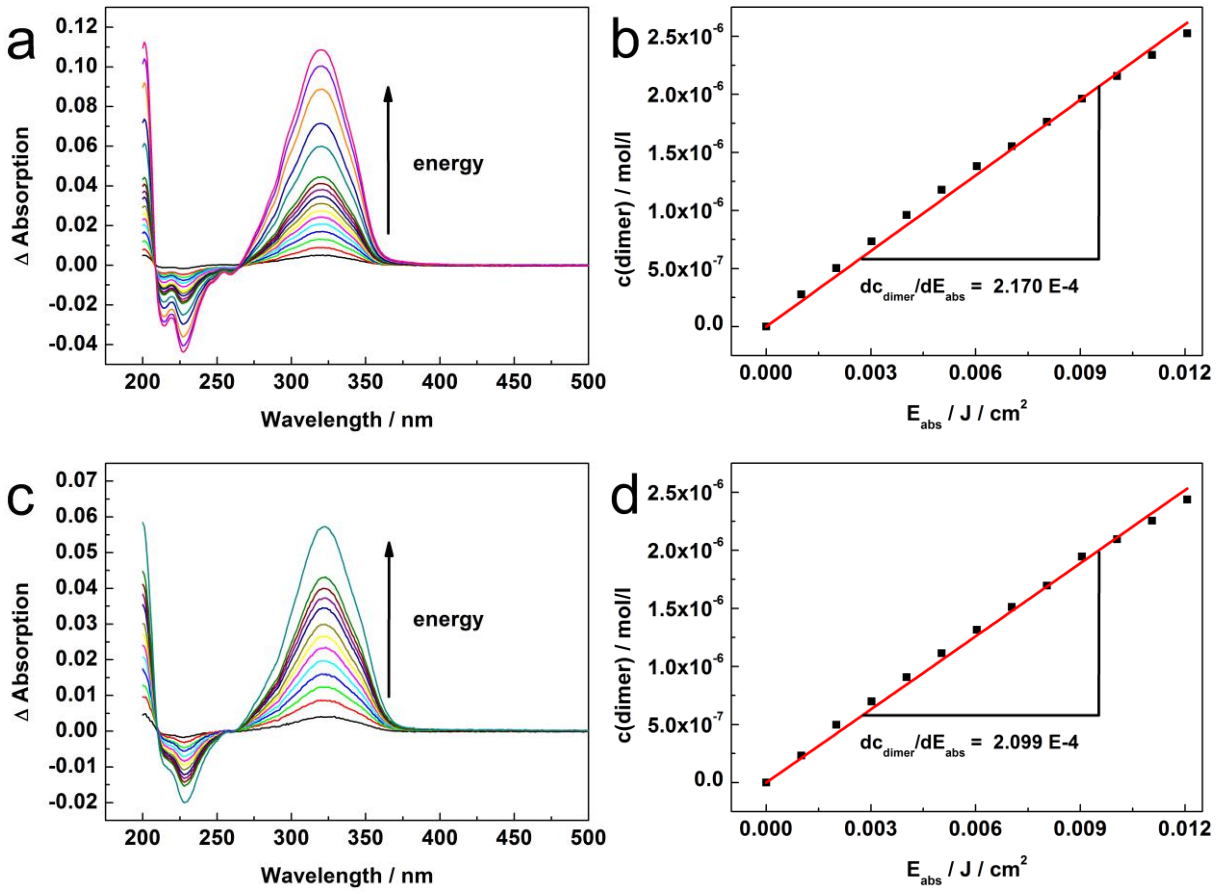

Figure 3.13: Photo-cleavage of coumarin dimers on SiO_2-nanoparticles. a/c: Difference spectra of dimerized TPC-NPs/TPC-Ly-NP-2 dispersed in acetonitrile/water during photo-cleavage with light of 280 nm wavelength. b: (TPC-NPs) /d: (TPC-Ly-NP-2): Determination of quantum efficiency from the change in concentration versus the absorbed energy.

With Equation 3.3 $n_{dimer} \cdot E_{abs}^{-1}$ is calculated to be $2.61 \cdot 10^{17}\ J^{-1} \cdot cm^2$ for TPC-NP and $2.52 \cdot 10^{-17}\ J^{-1} \cdot cm^2$ for TPC-Ly-NP-2 respectively. According to Equation 3.4 the number of photons per energy unit results in $9.07 \cdot 10^{17}\ J^{-1} \cdot cm^2$

$$\frac{n_{photon}}{E_{abs}} = \frac{\lambda}{c \cdot h \cdot A} \tag{3.4}$$

Equation 3.4: λ: irradiated wavelength; c: speed of light; h: Planck constant; A: irradiated area.

Using Equation 3.1 the quantum yield of the dimer cleavage is determined to be 0.288 for TPC-NP and 0.279 for TPC-Ly-NP. Since absorption is size independent, it is not surprising that the quantum yield of the photo cleavage is size independent as well. The difference of 3% between the differently sized nanoparticles is within the error of the measurement. Compared to quantum yields of similar coumarin derivatives measured in solution this is an average value.[162, 163]

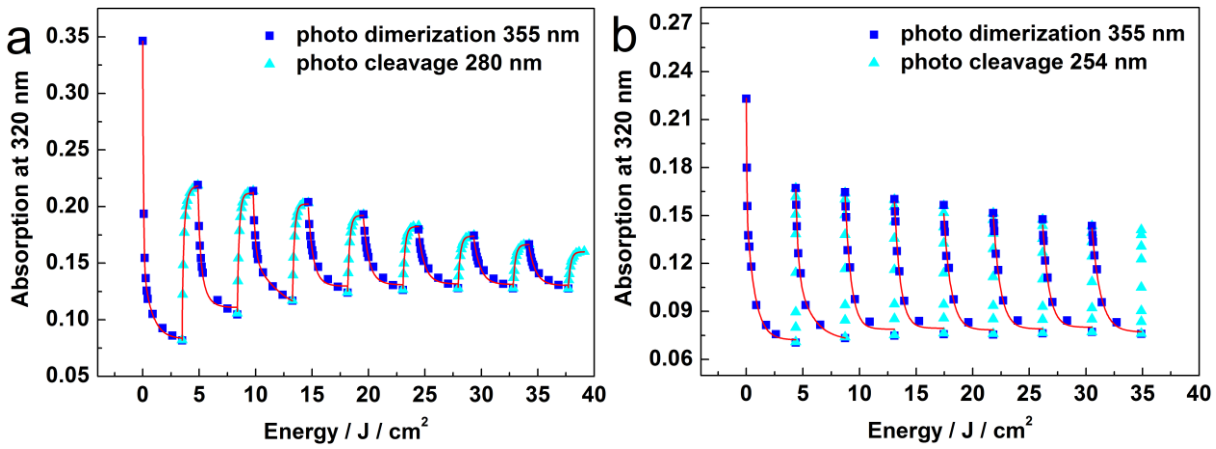

Figure 3.14: Reversibility of the photo-dimerization / photo-cleavage process. Depicted are the absorption at 320 nm/321 nm versus the irradiated energy at 355 nm (dimerization, squares) and 280 nm/254 nm (cleavage, triangles), respectively. Solid red lines show 2nd order numerical fits. (a: TPC-NP; b: TPC-Ly-NP-2).

Figure 3.14 a shows the absorption at 320 nm versus the irradiated energy at 355 nm and 280 nm respectively over 8 cycles of irradiation for a dispersion of 0.1 mg·ml^{-1} of TPC-NP in acetonitrile. Figure 3.14 b shows the same for a dispersion of 0.1 mg·ml^{-1} of TPC-Ly-NP-2 in water, irradiated with 355 nm and 254 nm. Surprisingly the photo reaction is not completely reversible as observed for SAM's with coumarin head groups on silicon oxide surfaces[43]. After dimerization of 81% of the coumarin attached to the particle, cleavage with 280 nm in case of TPC-NP results in a recovery of 55% of the starting absorption of the coumarin groups only. Photo cleavage at 254 nm for TPC-Ly-NP-2 increases reversibility up to 77% of the absorption at the beginning of the irradiation cycle, still far from the expected complete reversibility known from experiments in solution or on SAMs. To ensure no loss of coumarin groups due to the high energy laser pulses occurred, dimerized TPC-NPs were centrifuged, dried and analyzed by TGA, but neither increase nor any decrease in weight loss was measured. This strongly suggests that all coumarin groups are still attached to the nanoparticles and did not undergo any chemical side reactions which would have caused a change in molecular weight.

To further investigate those surprising results, the photo cleavage of both particle types was conducted at three different wavelengths below 300 nm (254 nm, 266 nm, 280), and compared to the photo cleavage behavior of unfunctionalized dicoumarin in an isomeric mixture.

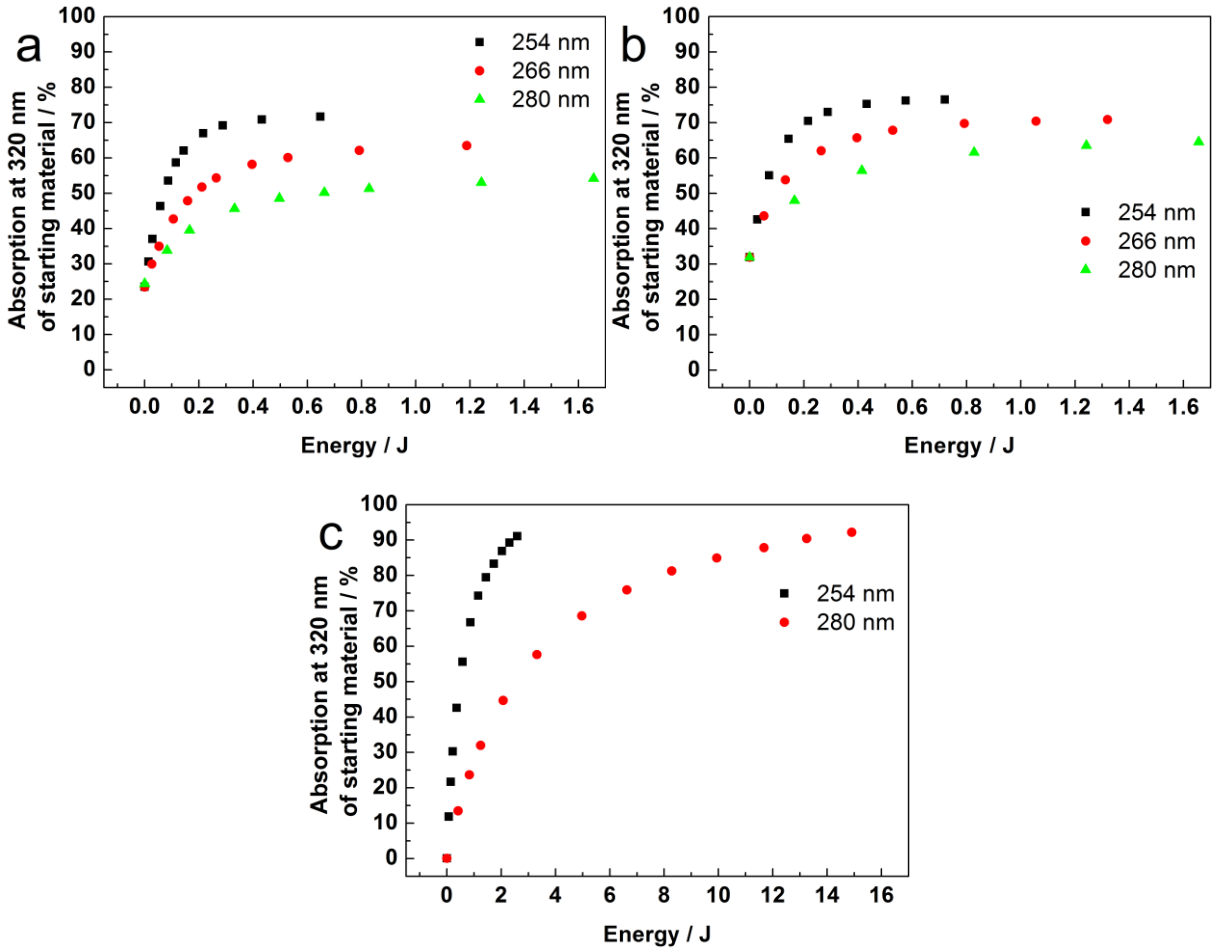

Figure 3.15: Wavelength dependency of photo-cleavage of a: TPC-NPs b: TPC-Ly-NP-2 c: solution of an isomeric mixture of non-functionalized dicoumarin.

Figure 3.15 a-c show the quite different behavior in wavelength dependent photo cleavage experiments of coumarin groups attached to a nanoparticle surface and unfunctionalized dicoumarin in solution. Whereas in an isomeric mixture of unfunctionalized dicoumarin cleavage is complete under UV-irradiation, independent of the irradiated wavelength (Figure 3.15 c), the coumarin moieties on the silica nanoparticle surfaces show lower wavelength dependent equilibrium levels. In case of TPC-NPs (Figure 3.15 a) the initial absorption before dimerization was 0.48 resulting in 55% cleavage for 280 nm, 64% for 266 nm and 72% for 254 nm. The initial absorption of TPC-Ly-NP-2 (Figure 3.15 b) was 0.22 resulting in 65% cleavage for 280 nm, 71% cleavage for 266 nm and 77% cleavage for 254 nm. This wavelength dependency of photo-cleavage is not observed on the flat surface of a SAM, where dimerization has an aligning effect on the absorbed coumarin groups resulting in an even higher absorption at 320 nm after photo-cleavage.[43]

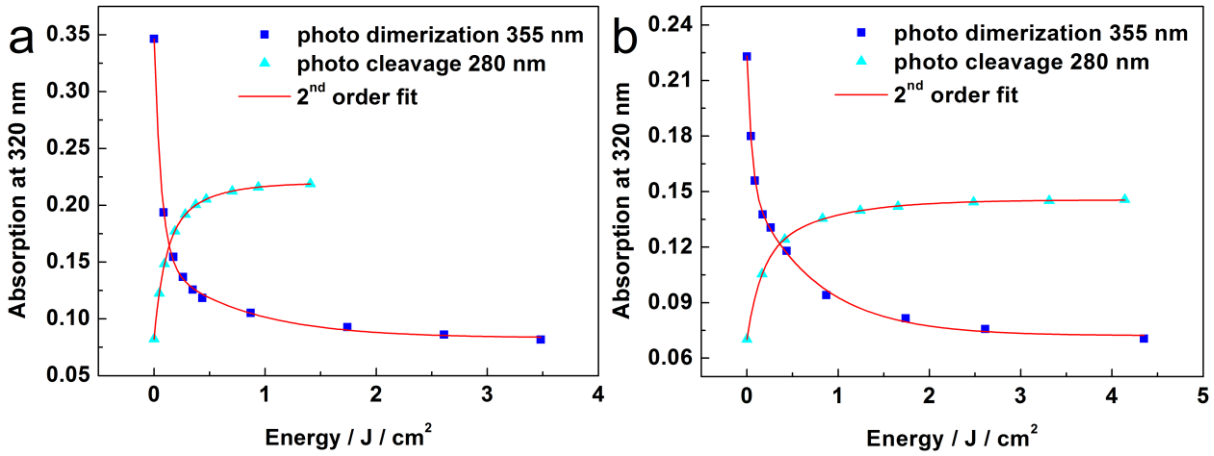

Figure 3.16: Numerical analysis of the photo-dimerization and the photo-cleavage of a: TPC-NP, b: TPC-Ly-NP-2. The data points are best fitted with two second order fits.

Those findings can be explained by the formation of equilibrium between photo-dimerization and photo-cleavage. In solution the short lifetime of the excited state in the photo cleavage process induced by UV-light, makes reformation of dimers in a stirred diluted solution very unlikely, i.e. the photo-dimerization is kinetically hindered. On the nanoparticle surface the covalently anchored coumarin moieties are in closer proximity and reformation of dimers occurs effectively and the wavelength-dependent equilibrium state is observed. The order of magnitude for the forward and the backward reaction rate become the same. The different equilibrium states at the same wavelength for TPC-NP and TPC-Ly-NP-2 can be explained by the different solvents of the particle dispersions. The protic and more polar solvent water in case of TPC-Ly-NP-2 seems to shorten the lifetime of the excited state and therefore increases the percentage of cleaved coumarin dimers, compared to the aprotic less polar ACN in case of TPC-NPs. Figure 3.16 shows the absorption change at 320 nm during photo dimerization and photo cleavage respectively, of TPC-NP (a) and TPC-Ly-NP (b) versus the applied energy. Both sets of data points accurately match a second order exponential fit. This is surprising taking into account that photo cleavage reactions are known as classical first order reactions. The change in the reaction order, indicated by the higher quality of a second order over a first order fit, can be explained by the wavelength dependent equilibrium, which is caused by the superposition of photo-dimerization and photo-cleavage.

In this case both reaction rates, that of the forward and that of the backward reaction are of the same order of magnitude.[159]

Besides the wavelength dependent equilibrium, further irradiation of the same sample with the same amount of energy over seven additional cycles (Figure 3.14) reveals another interesting effect. Every cycle shows a further loss of absorption after photo-cleavage as well as a higher remaining absorption after photo-dimerization, which is related to an apparent loss of monomeric coumarin groups. One possible explanation for the decreasing photo cleavage efficiency is photo induced formation of nanoparticle clusters like in Figure 3.1 c. In these dimerized clusters, coumarin crosslinks between nanoparticles are shielded from irradiation, resulting in an increasingly inefficient photo cleavage as described in literature.[58] DLS-measurements after 8 cycles of photo dimerization and photo cleavage yield an average diameter of 65 nm for TPC-NP and of 25 nm for TPC-Ly-NP respectively, about 50% more than after preparation, further substantiating this explanation. Another possible explanation are irreversible side reactions for example due to decarboxylation as discussed in literature.[164] The loss of CO_2 in such little amounts is beyond the detection limit of TGA measurements, therefore this explanation should be considered as a possible contribution, when the observed loss in reversibility is discussed.

After these promising results with regards to the photochemistry of coumarin moieties on the nanoparticle surface, investigations concerning the possibility of utilizing the particles for drug load were attempted. As mentioned before, coumarin can be used for drug delivery approaches, by hetero dimerization with a drug bearing a C-C double bond, that is able to undergo [2π+2π] cycloaddition. In solution two major problems occur, utilizing 5-FU as model drug for potential ophthalmologic applications. First, homo dimerization of two coumarins is much more likely than hetero dimerization between 5FU and coumarin, resulting in low yields of the hetero dimer desired for drug delivery. To overcome this drawback 5FU is used in excess resulting in increased hetero dimerization yields, which can be enhanced further by utilizing high energy laser light, generating an excess of excited coumarins in a flow cell approach. Purification of the resulting product is the second major problem, because multiple extensive steps including preparative HPLC are necessary.[151] Here, coumarin functionalized silica nanoparticles could be a great simplification. If it is possible to generate hetero dimers on the particle surface in high 5FU excess, the resulting drug loaded particles can be easily purified by simple centrifugation.

Unfortunately all attempts of hetero dimerization between 5FU and TPC-NP or TPC-Ly-NP-2 respectively were ineffective. Neither TGA measurements nor drug release experiments showed any drug load.

The reason for this is the close proximity of the coumarin groups on the nanoparticle surface, favoring homo dimerization with such overwhelming majority, that even in a saturated 5FU solution no hetero dimerization is observed. To prove this, quantum yield of photo dimerization for TPC-NP and TPC-Ly-NP-2 is derived and compared with the quantum yield of 7-*tert*-butyldimethylsiliyloxycoumarin (TBS-C) as model substance in solution. The direct comparison to the functionalization agent TPC was not possible due to its instability in solution, therefore the common model substance TBS-C was used.[146]

The quantum yield of the photochemical dimerization ϕ_{dim} can be calculated analog to the photo cleavage quantum yield by:

$$\Phi_{dim} = \frac{n_{mono}}{n_{photon}} = \frac{n_{mono}}{E} \cdot \frac{E}{n_{photon}} \tag{3.5}$$

Equation 3.5: n_{mono}: number of dimerized coumarin monomers; n_{photon}: number of photons absorbed by coumarin monomers.

The number of dimerized coumarins per absorbed energy can be calculated by

$$\frac{n_{mono}}{E} = \frac{c_{mono}}{E} \cdot V \cdot N_A \tag{3.6}$$

Equation 3.6: c_{mono}: concentration of dimerized monomers.

It is necessary to take into account that every excited coumarin can only react with an unexcited coumarin. Therefore only half of the monitored change in concentration by absorption spectroscopy is due to dimerization of an excited coumarin contributing to the quantum yield of the dimerization process. According to Equation 3.4 the number of photons per energy unit at 355 nm results in $8.94 \cdot 10^{17}$ $J^{-1} \cdot cm^2$. Plotting the concentration of dimerized coumarins versus the irradiated energy results in a linear increase with $c_{mono} \cdot E^{-1}$ as the slope of the linear regression of the data. The coefficient of determination for the linear fittings was 0.998 in all cases. (Figure 3.17 a and b).

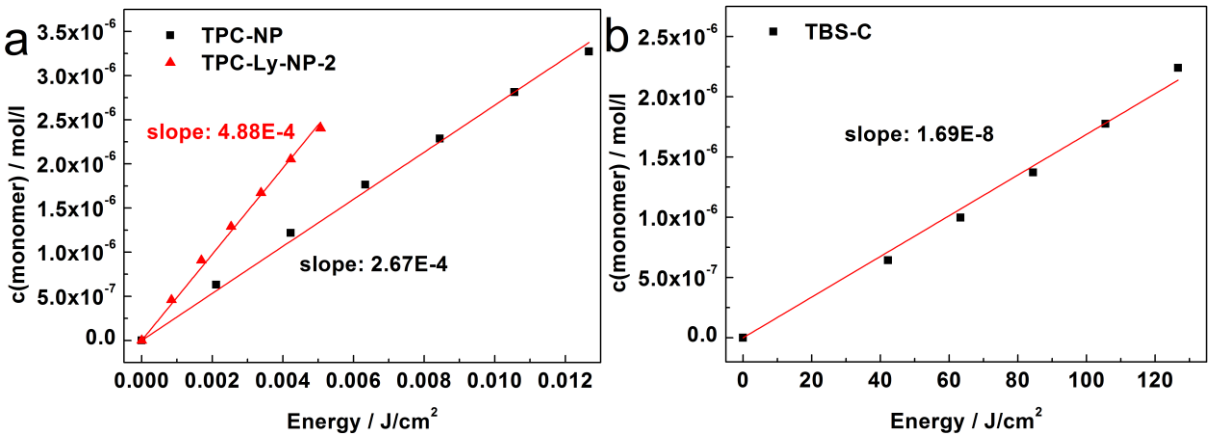

Figure 3.17: Concentration of dimerized coumarin over the irradiated energy. a: TPC-NP and TPC-Ly-NP b: TPC.

With Equation 3.5 and Equation 3.6 the quantum yields for photochemical dimerization can be calculated to:

	Quantum yield / %
TPC-NP	36
TPC-Ly-NP	65
TBS-C	0.0022

Table 3.2: Quantum yields of photochemical dimerization of TPC-NP, TPC-Ly-NP-2 and TBS-C.

The difference in quantum yield between the different coumarin functionalized silica nanoparticles can be attributed to the difference in absorption at 355 nm of the irradiated dispersions.

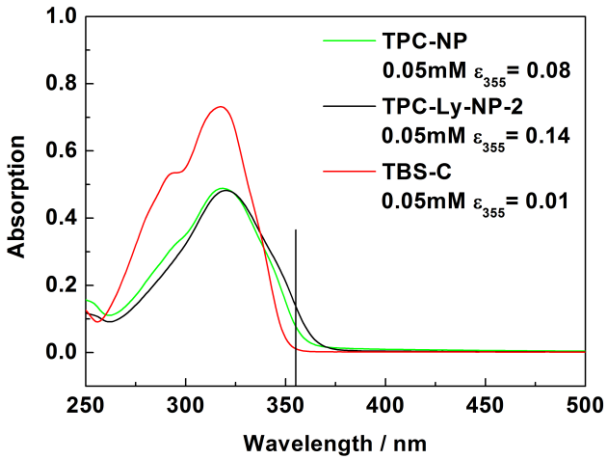

Figure 3.18: Absorption of Dispersions/Solution of TPC-NP, TPC-Ly-NP-2 and TBS-C prior to dimerization.

Due to a slight solvatochromic effect, the absorption of TPC-NP at 355 nm is only 57% of the absorption of TPC-Ly-NP-2 at 355 nm, corresponding exactly to the calculated quantum yield. Under the same assumption a quantum yield of 4.5% is expected for TBS-C, but the actually measured quantum yield is almost 2000 times lower than that. This shows how tremendous the reaction rate of coumarin dimerization depends on the proximity of the coumarin groups and it also explains why photochemical hetero dimerization with a drug molecule is not possible.

3.2 *o*-NBnCs for photochemical drug delivery.

3.2.1 Synthesis of *o*-NBnCs

In this thesis two different precursors for *o*-NBnCs were synthesized. The design of the photoactive compound includes two nitro groups in *ortho*-position to the benzyl alcohol which can be used for drug load (compound **2** Scheme 3.1). A methoxy group in *para*-position resulting from the starting material directs the selective nitration. The hydroxyl group in 3-postion was used for further functionalization with either a polymerizable group or a triethoxy functionality for silica nanoparticle attachment.

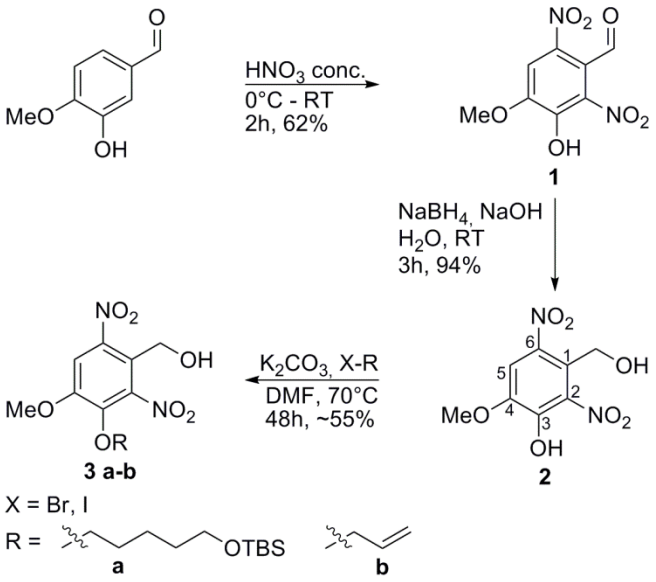

Scheme 3.1: Synthesis of *o*-NBnC precursors.

The first three steps of the synthesis follow a protocol by Agasti et al., starting from Isovanilin.[84] The describe nitration in concentrated nitric acid could be improved by suspending the isovanilin in a few milliliter of water prior to the addition of the acid,

increasing the yield from 35% to 62%. After reduction of the aldehyde to the benzyl alcohol with sodium borohydride, two different side chains for further functionalization were introduced as an ether via the hydroxyl group in 3-postion. 5-Iodo-1-*tert*-butyldimethylsilyloxypentane is introduced as flexible linker to a polymerizable group, which can be implemented via the protected hydroxyl group (compound **3a** Scheme 3.1). Usage of the more reactive iodine instead of the bromine increased the yield by about 15%. In case of allylbromide the received ether enables hydrosilylation with triethoxysilane, resulting in a potential functionalization agent for silica nanoparticles (compound **8** Scheme 3.1).

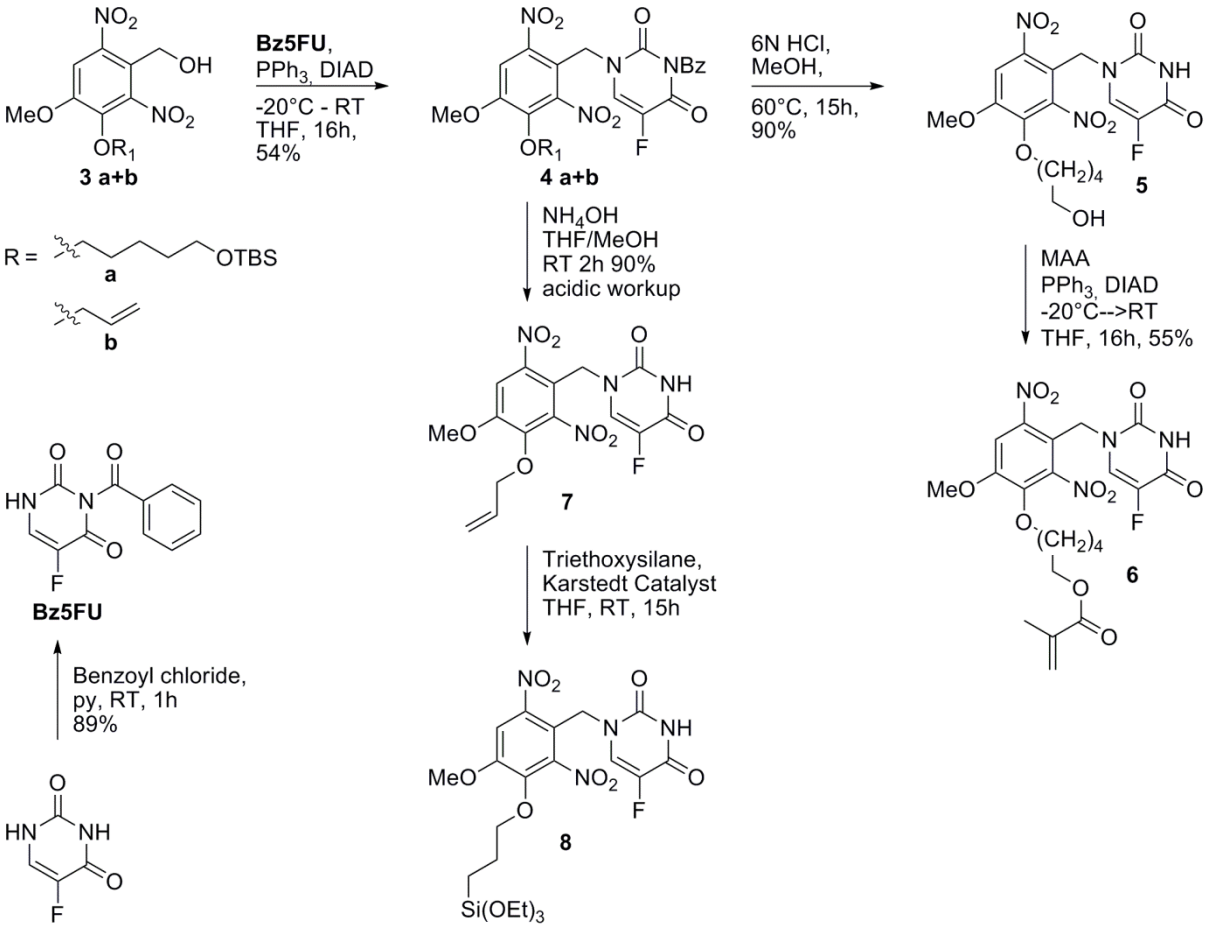

Scheme 3.2: Synthesis of drug loaded *o*-NBnCs for nanoparticle functionalization (**8**) or copolymerization with methacrylic polymers (**6**).

As model drug 5-fluoro uracil (5FU) was chosen. This well-known cytostatic drug might be a potential, already FDA approved, active substance for functional IOLs with integrated drug delivery system. Drug load of the *o*-NBnC precursors with 5FU was enabled by the Mitsunobu reaction. (Scheme 3.2) Therefore 5FU was protected with benzoyl chloride in the 1-N-position as described by Kametani et al.[156] Following the protocol of Ludek and Meier,

who described the selective 2-N-alkylation of 1-N-benzyl protected thymine with benzyl alcohol[165] by Mitsunobu reaction, it was possible to generate the desired drug loaded *o*-NBnC. (compounds **4a/b**) Deprotection of the active agent could be achieved selectively either in strongly acidic or alkaline media. Utilizing the Mitsunobu reaction improved the yield from 7% over three steps in 48 hours, as described by Agasti et al., to 70% over two steps within a reaction time of 17 hours. The resulting drug loaded precursors were now functionalized either with methacrylic acid or triethoxysilane to receive the desired functional molecules.

3.2.2 Photochemistry of *o*-NBnCs in Solution

Prior to the development of the synthesized functional molecules in their potential applications as drug delivery polymers and drug loaded silica nanoparticles, it is necessary to investigate their photochemical properties in detail in solution. Therefore compound **4a** was used as model substance because of it good solubility and the fact that undesired side reactions of the secondary amine and the primary alcohol are minimized by their protecting groups.

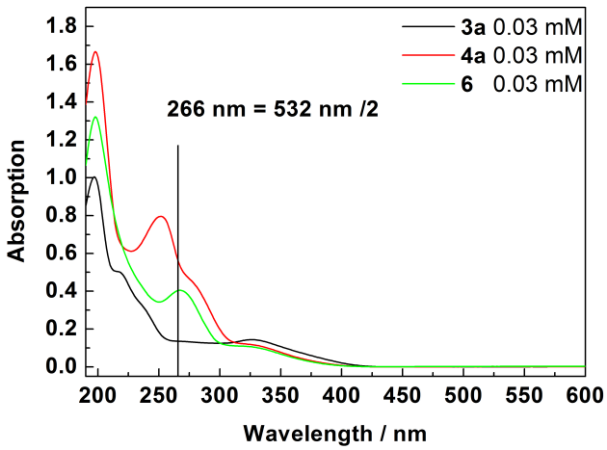

Figure 3.19: Absorption spectra of *o*-NBnC **3a**, **4a**, and **6**.

Figure 3.19 shows the absorption spectra of **3a**, **4a** and **6**. The *o*-NBnC precursor **3a** has a weak broad absorption between 260 nm and 400 nm with a maximum at 324 nm. The *o*-NBnC drug conjugate (**4a**) shows a stronger absorption band with a maximum at 252 nm corresponding to the Bz-protecting group. The shoulder of this absorption band at 268 nm corresponds to the absorption maximum of 5FU and is revealed as main absorption after deprotection and esterification with MAA. (**6**)

To investigate SPA induced drug release a 1 mM solution of **4a** is irradiated at 266 nm with increasing energy doses. The photochemical release process could be monitored by HPLC.

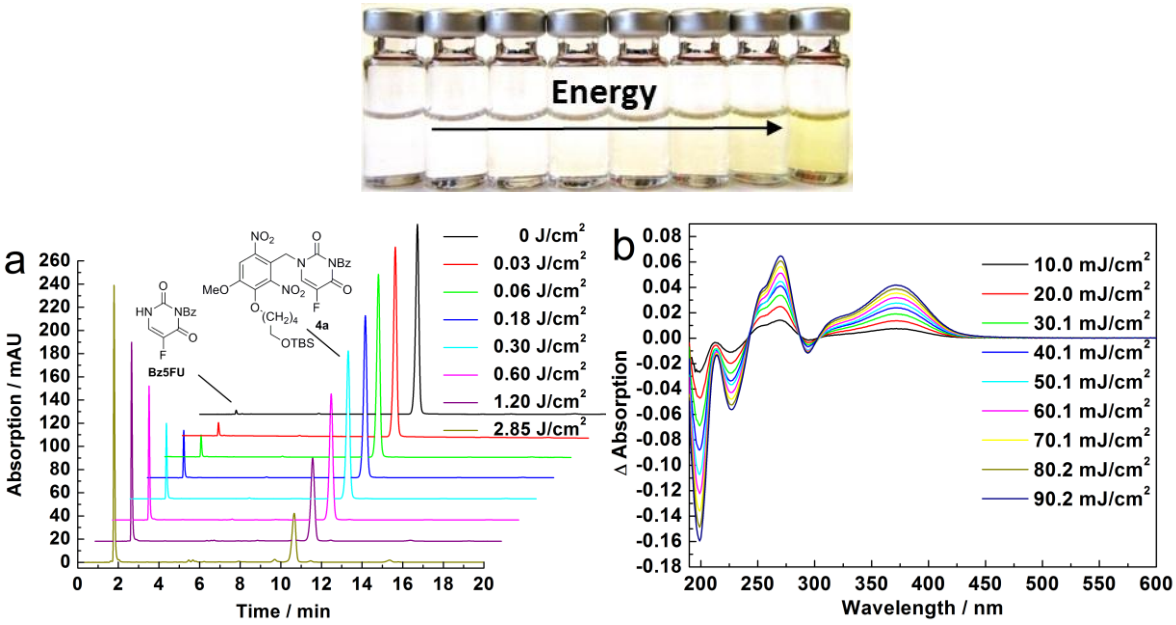

Figure 3.20: a) Samples and HPLC Chromatograms of 1 mM solution of **4a** after consecutive irradiations with 266 nm light with total energies given. b) Change in absorption after irradiation with 266 nm (total energies given) of a 25 µM solution of **4a** in ACN.

Figure 3.20 shows HPLC chromatograms of a 1 mM solution of **4a**. The increasing signal at a retention time of 1.8 min corresponds to the released Bz5FU, the decreasing signal at 10.7 min to cleaved **4a** and the nitroso aldehyde generated during the photo induced release process. Although both compounds have the same retention time they can be identified, due to their different absorption spectra.

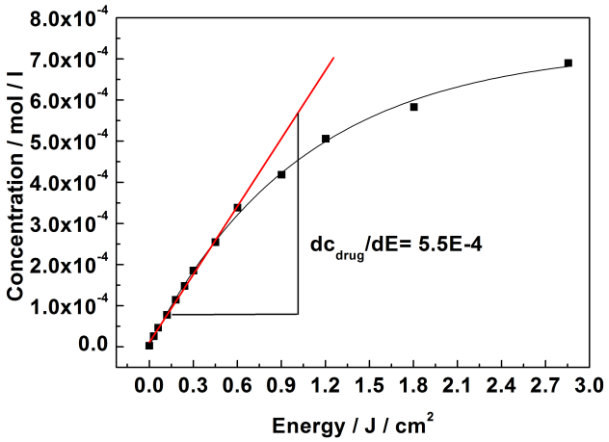

Figure 3.21: Determination of quantum efficiency from the concentration of released Bz5FU versus the absorbed energy for **4a.**

To quantify the degree of cleavage the peak area of the Bz5FU signals was measured and correlated to prior measured Bz5FU standards of known concentration. Thereby it is possible to calculate SPA quantum yield ϕ_{SPA} of the drug release similar to the photo cleavage of the coumarin compounds.

$$\Phi_{SPA} = \frac{n_{drug}}{n_{photon}} = \frac{n_{drug}}{E} \cdot \frac{E}{n_{photon}} \tag{3.7}$$

Equation 3.7: n_{drug}: number of released Bz5FU; n_{photon}: number of photons absorbed by **4a**.

Plotting the concentration of released Bz5FU versus the absorbed energy in the beginning of the photochemical reaction, results in a linear increase with $c_{drug} \cdot E^{-1}$ as the slope of the linear fit of the data points. (Figure 3.21)

$$\frac{n_{drug}}{E} = \frac{c_{drug}}{E} \cdot V \cdot N_A \tag{3.8}$$

Equation 3.8: c_{drug}: concentration of released Bz5FU; V: volume (1 ml).

With Equation 3.8 $n_{drug} \cdot E^{-1}$ is calculated to be $3.64 \cdot 10^{17}$ $J^{-1} \cdot cm^2$. The number of photons per energy unit at 266 nm results in $1.34 \cdot 10^{18}$ $J^{-1} \cdot cm^2$ according to Equation 3.4. Using Equation 3.7 the quantum yield of the photochemical drug release is determined to be 27 % corresponding well with the literature[166]

However, SPA mediated drug release by UV-light is useless for potential application in IOLs, due to the UV-absorbing properties of the cornea. Therefore, the second step in photochemical characterization is to explore the two-photon activity of the designed *o*-NBnC. In general o-NBnC compounds are cleaved by irradiation with UV-light with a wavelength of about 310 nm to 360 nm, due to their use in biochemical application or as photochemical protecting group in organic chemistry, where irradiation with UV-light of wavelengths shorter than 300 nm might damage the biological specimen/sample or the protected organic compounds. The usually low absorption in the range between 310 nm and 360 nm as shown in Figure 3.19 for compound **3a**, results in quantum yields for SPA cleavage of only about 1%. Nevertheless, most investigations concerning TPA mediated cleavage of o-NBnCs use laser light around 700 nm, resulting in very low TPA cross sections for the induced photochemical cleavage reactions.[167, 168]

In this thesis laser light of a wavelength of 532 nm was used for TPA experiments. This wavelength coincides well with the absorption maximum of the designed *o*-NBnCs, is easily generated even at high intensities by a pulsed Nd:YAG laser, does not affect the caged drug according to prior TPA experiments with hetero dimers of tetralone or coumarin with 5FU[145, 151] and passes the cornea easily, which is prerequisite for the potential application.

To prove that TPA mediated drug release is possible a 6.05 mM solution of **4a** in ACN was irradiated at 532 nm with increasing energy doses. The photochemical release process could be monitored by HPLC.

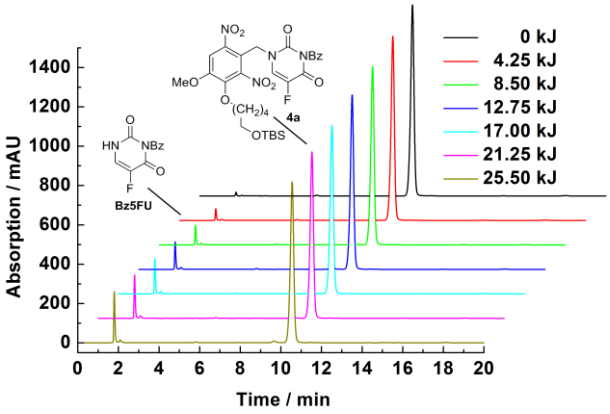

Figure 3.22: HPLC Chromatograms of 6.05 mM solution of **4a** after consecutive irradiations with 532 nm light with total energies given.

Again the increasing signal at a retention time of 1.8 minutes corresponds to the released Bz5FU, the decreasing signal at 10.7 minutes corresponds to cleaved **4a** and the nitroso aldehyde generated during the photo-induced release process (Figure 3.22).

As described in 1.1.4 a TPA process is dependent on the intensity squared. This can be verified by measuring the reaction rate of the photo cleavage at different pulse intensities. Based on this a 0.5 mM solution of 4a in ACN was irradiated at different pulse intensities over a certain period of time. The photo cleavage was monitored by the absorption change at 370 nm in the differential UV-Vis spectra. Figure 3.23 a shows the absorption change over the course of irradiation at different pulse energies. The reaction rates can be calculated from the slope of the linear regression.

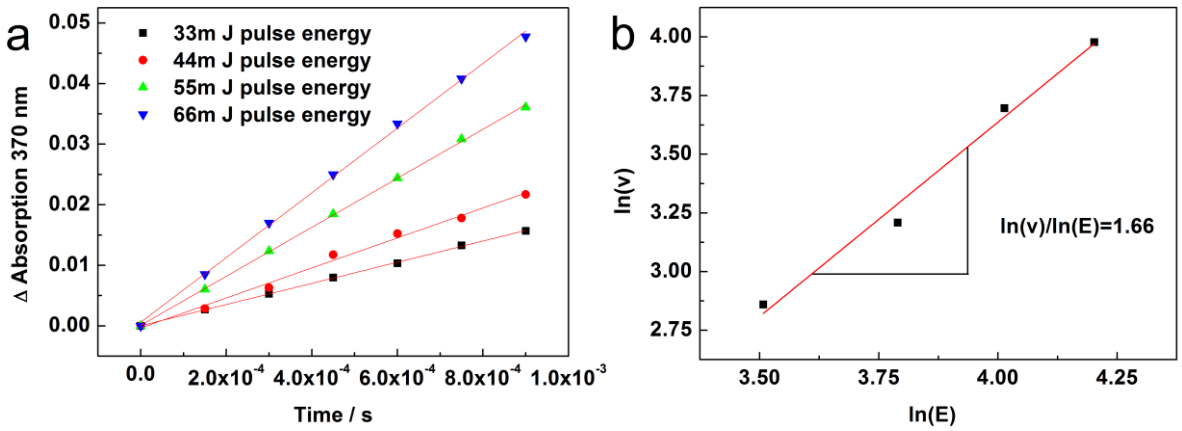

Figure 3.23: a: Absorption at 375 nm versus time of irradiation at different pulse energies b: double logarithmic plot of reaction rate over pulse energy.

Figure 3.23 b shows a double logarithmic plot of the reaction rate over the different pulse energies. Linear regression of the data points reveals a slope of 1.66 indicating a TPA process. To quantify the TPA process it is possible to derive the TPA cross section σ_{TPA} from Equation 1.2:

$$\frac{dn}{dt} = \sigma_{TPA} \cdot N \cdot F^2$$

Considering:

$$N = \Phi_{TPA} \cdot c_0 \cdot V_{ir} \tag{3.9}$$

Equation 3.9: N: number of absorbing molecules; Φ_{TPA}= TPA quantum yield; c_0: starting concentration of the irradiation solution; V_{ir}: irradiated Volume (0.196 cm^3).

And:

$$F = \frac{E \cdot \lambda}{h \cdot c \cdot A \cdot t} \tag{3.10}$$

Equation 3.10: F: Photon density; E: Pulse energy; λ: wavelength of irradiate light (532 nm); A: irradiated area (0.196 cm^2); t: pulse length (3 ns).

And:

$$\frac{dn}{dt} = \frac{dc}{dt} \cdot V_{total} \tag{3.11}$$

Equation 3.11: dn/dt: change in amount of substance over time; dc/dt: change in concentration of released Bz5FU over time; V_{total}: total sample volume (1.5 ml)

This results in:

$$\sigma_{TPA} = \frac{dc}{dt} \cdot V_{total} \cdot \left(\frac{h \cdot c \cdot A \cdot t}{E \cdot \lambda} \right)^2 \cdot \frac{1}{\Phi_{TPA} \cdot c_0 \cdot V_{ir}} \tag{3.12}$$

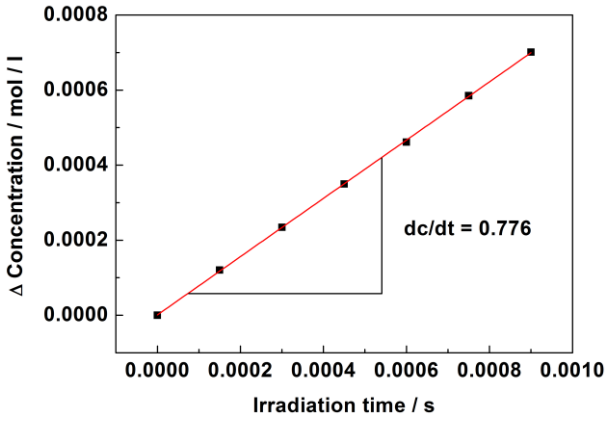

Figure 3.24: Change in concentration of released Bz5FU over irradiation time.

Figure 3.24 shows the concentration of released Bz5FU, derived from the peak area of the Bz5FU signals in Figure 3.22 by correlating them to prior measured Bz5FU standards of known concentration, over the actual irradiation time derived from the pulse length and the number of irradiated pulses. Under the assumption that the TPA quantum yield is equal to the SPA quantum yield a TPA cross section of $2.41 \cdot 10^{-50}$ cm^4s or 2.41 GM is calculated respectively. This value exceeds the measured values of other *o*-NBnCs in the range of 0.01 GM to 0.1 GM by more than one order of magnitude. Compared to the TPA cross sections of photochemical drug delivery approaches, utilizing coumarin or tetralone homo or hetero dimers, this value is within the same range and therefore competitive.

So far it could be shown that the synthesized *o*-NBnC is a suitable photochemically induced drug delivery system. Compared to known *o*-NBnCs its high SPA quantum yield as well as its high TPA cross section makes it an adequate option for the potential application in IOLs.

With respect to this particular application it should be noted that the standard IOL materials contain up to 1 wt% of an UV-absorbing agent like 2(4-Benzoyl-3-hydroxy phenoxy) ethyl acrylate (UV-Abs). Consequently, the next step in exploring the photochemical properties of the synthesized o-NBnC is to investigate if the TPA induced drug release is still possible in the presence of an UV-absorbing agent. The main absorption of UV-Abs, as expected by its purpose, is between 270 nm and 350 nm efficiently blocking the UV-portion of the sun light.

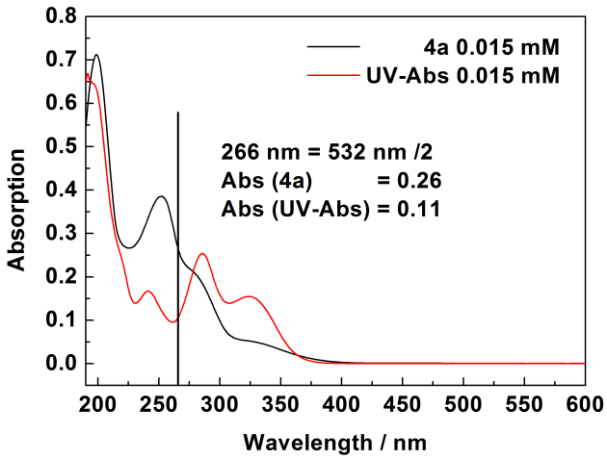

Figure 3.25: Absorption spectra of **4a** and UV-Abs.

Regarding the complete absorption spectrum of UV-Abs, a minium at 266 nm is observed, preserving the possiblity of TPA of **4a**, assuming that UV-Abs is not effected by the irradiated pulsed laser light enabling the TPA process. (Figure 3.25) This was verified by irradiation of 3 mM solution of the UV-Abs with 25.5 kJ of laser light at 532 nm. Neither in the HPLC chromatogramm nor in the UV-Vis spectrum of the irraditated solution any change in structure or absorbance intensity was observed. Convinced that the UV-Abs does not undergo any undesirable side reactions, a mixture of 0.4 wt% (6.05 mM) of **4a** and 0.1 wt% (3.2 mM) of UV-Abs corresponding to a 1 mm thick IOL with the common amount of 1 wt% of UV-absorber and an active drug load of 1 wt%, was irradiated in a 10 mm cuvette with pulsed laser light at 532 nm.

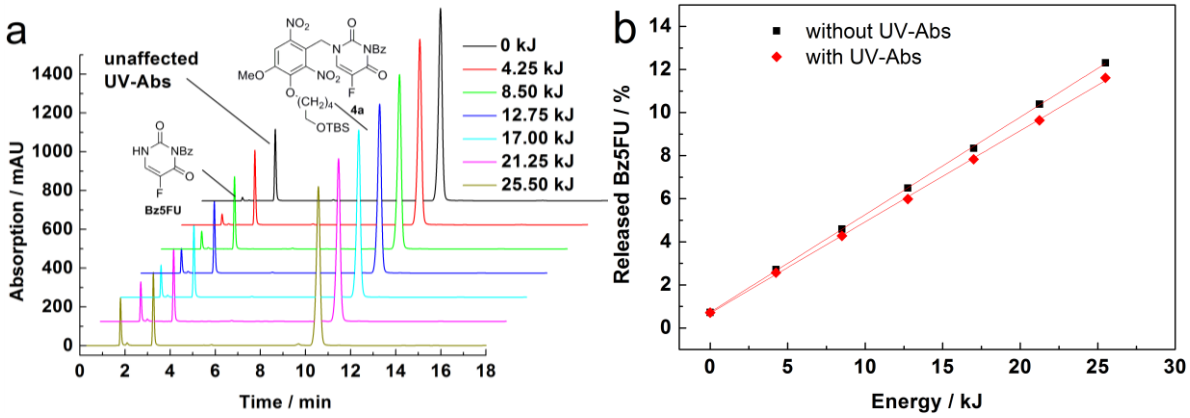

Figure 3.26: a: HPLC Chromatograms of 6.05 mM solution of **4a** in the presence of UV-Abs at a concentration of 3.2 mM, after consecutive irradiations with 532 nm light with total energies given. b: Amount of Bz5FU released with and without UV-Abs.

Figure 3.26 shows the HPLC chormatogramms of the irradiated solution as well as the amount of released Bz5FU over the irradiated energy compared to the achieved release without UV-Abs. As shown in Figure 3.20 a and Figure 3.22., the increasing signal at a retention time of 1.8 min corresponds to the released Bz5FU, the decreasing signal at 10.7 min to cleaved **4a** and the nitroso aldehyde generated during the photo induced release process. The constant signal, at a retention time of 2.5 min, results from the unaffected UV-Abs.

The TPA cross section of *o*-NBnC seems to be reduced by 6% in the presence of UV-Abs. This reduction in drug release efficency indicates that UV-Abs is not completely TPA inactive, but taking the concentration ration into account, its TPA cross section is only 11% of the TPA cross section of *o*-NBnC and therefore still allows for an efficent TPA induced drug release. This is the first experimental prove that a TPA induced drug release in the presence of a UV absorbing agent is possible.

3.2.3 Photochemistry of *o*-NBnCs in Polymer Matrix

After these promising results in solution the synthesized methacrylic *o*-NBnC monomer **6** was copolymerized in bulk. A mixture of 86.5 wt% HEMA , 12 wt% MMA, 1 wt% EGDMA as cross linker and a combination of 0.25 wt% of campherquinone and 0.25 wt% of ethyl-4-aminobenzoate as photo initiator at 465 nm served as basic monomer solution. The amount of **6** in the polymerization mixture was 4 wt% corresponding to a final drug load of 1 wt% of 5FU. To be able to verify the results of SPA as well as TPA induced drug release in the presence of UV-Abs, the polymerization was conducted once with and once without 1 wt% of UV-Abs. The basic polymer components are typically used in standard hydrophilic methacrylic IOLs. The photo initiator was chosen due to its fast initiation rate. The utilized free radical polymerization normally initiated with the slower thermal initiator AIBN is suboptimal for *o*-NBnC which can act as polymerization inhibitors and thereby lose its functionality due to uncontrolled drug release during the polymerization process. The fast polymerization by photo initiation minimized this problem but could not avoid it completely. Therefore the polymer plates were extracted with deionized water prior to photochemical drug release. HPLC analysis of the water used for extraction revealed 4.25% of remaining monomer due to the inhibiting effect on polymerization of the used *o*-NBnC. Fortunately, the amount of extracted 5FU that was released during polymerization was less than 1% of

the total drug load. The final water uptake of the polymer plates was between 21.5% and 22.8%.

Drug delivery could be analyzed by irradiation of a 9 mm x 9 mm x 1 mm polymer plate surrounded by water. Drug concentration in the water immediately after the irradiation and at different times of diffusion could be quantified by absorption spectroscopy. To ensure a homogeneous irradiation of the whole polymer plate, the 254 nm line of a low-pressure mercury-vapor lamp was used as light source.

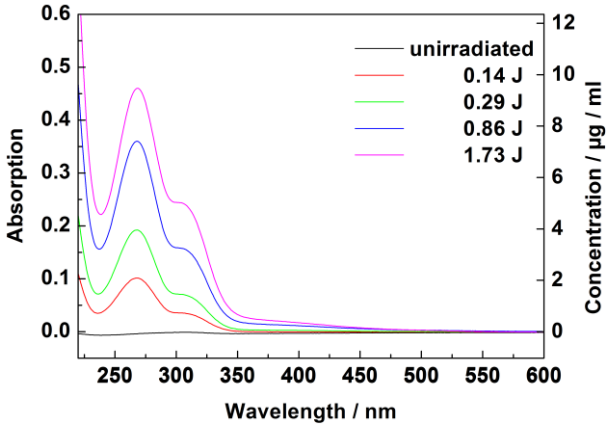

Figure 3.27: UV-Vis spectra of polymer surrounding water after 5 doses of irradiation at 254 nm with total energies given.

Figure 3.27 shows the SPA induced drug delivery from a polymer plate without UV-Abs. The increasing absorption band at 268 nm corresponds to the released 5FU. After irradiation with 1.73 J, a 5FU concentration of 9.5 µg/ml could be achieved.

Figure 3.28: Drug loaded polymer plate before (left) and after irradiation (right) at 254 nm (6.34 J).

The drug release results in an increasing absorption at 370 nm as already seen in the differential spectra characterizing SPA in solution. This absorption band, corresponding to

the generated nitroso functionality, unfortunately causes further increase in yellow color of the polymer plate. (Figure 3.28)

TPA induced drug delivery was realized by irradiation of another 9 mm x 9 mm x 1 mm polymer plate containing besides 4 wt% of the synthesized o-NBnC 1 wt% of UV-Abs.

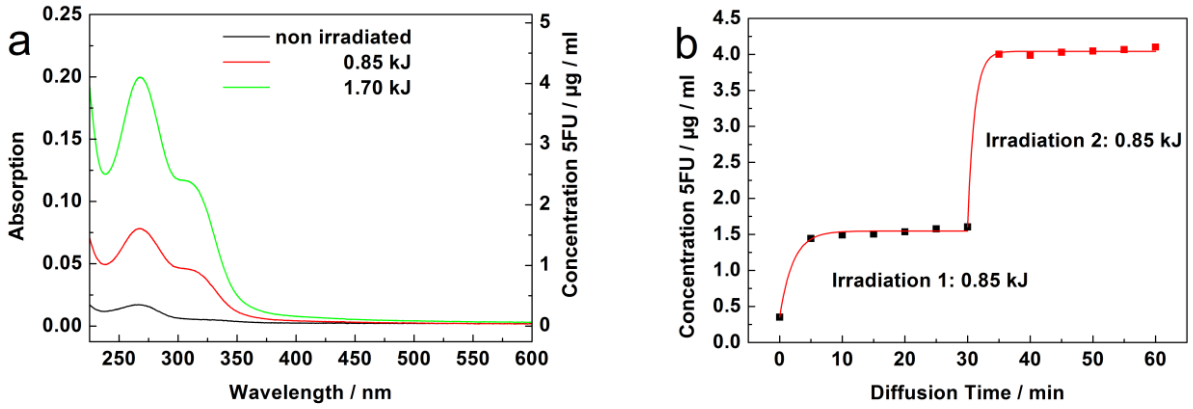

Figure 3.29: TPA induced drug release from polymer plate containing 1 wt% UV-Abs.

Analog to the SPA induced drug release irradiation at 532 nm enables energy dependent photo cleavage. As expected from the results in solution the presence of the UV absorbing agent does not prevent TPA induced drug release. Multi dose drug delivery is possible with fast drug diffusion into the surrounding medium. (Figure 3.29)

Figure 3.30: Drug loaded polymer plate before (left) and after irradiation at 532 nm with 0.85 kJ (middle) and 1.7 kJ (right) respectively.

As for irradiation with 254 nm drug release results in increasing yellow to orange discoloration of the polymer plate. This effect has to be taken into account during irradiation, due to the fact that the increasing absorption also increases the absorption of

laser light that does not induce a TPA process, but may lead to thermal effects that induce undesired side reactions or even damage the polymeric material. To avoid this effect the samples should be scanned with a focused laser beam, so that no overexposure of already irradiated areas occurs. This also enhances the intensity of laser light, making a TPA process more probable.

As further prove of principle a thermal polymerized polymer plate utilizing AIBN as initiator, containing 4 wt% of **6** and 0.5 wt% UV-Abs was used by Dr. Schmidt Intraocularlinsen to fabricate three model IOLs.

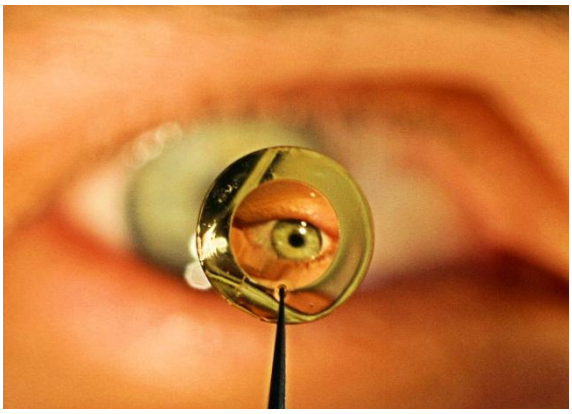

Figure 3.31: Model IOL manufactured from *o*-NBnC containing polymer.

The model IOLs were of a basic design with a 'Saturn ring' haptic. The diameter of the entire IOL was 7.5 mm the diameter of the lens was 5.0 mm at a thickness of 0.9 mm. The optical power was 22.5 dpt. To prove the possibility of TPA induced drug delivery in presence of UV-Abs, the lens was irradiated two times with 0.65 kJ at 532 nm surrounded by 1.5 ml of a 0.9% NaCl solution (physiological saline solution).

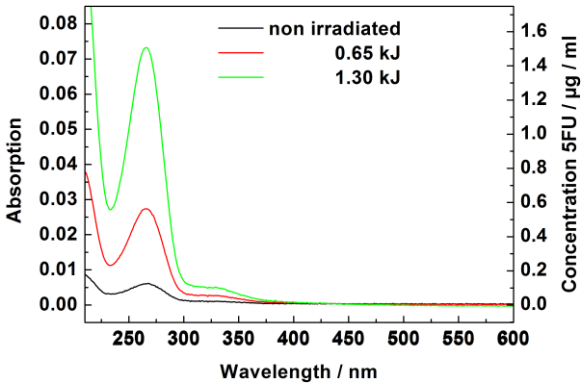

Figure 3.32: TPA induced drug release from model IOL into 1.5 ml of a 0.9% NaCl solution.

Again the absorption at 268 nm in Figure 3.32 corresponds to the released 5FU. After irradiation with 1.3 kJ the concentration of released 5FU reached 1.5 µg·ml^{-1} 35 minutes after the irradiation started, proving that the estimated therapeutic dosage of 1.0 µg·ml^{-1} could be reached.

3.2.4 Functionlization of Silica Nanoparticles with *o*-NBnC.

In a second attempt to generate photo active silica nanoparticles for drug delivery, the synthesized *o*-NBnC was utilized. Similar to the functionalization with coumarin, Stöber particles with an average diameter of 44.6 nm ±15.9 nm, according to DLS measurements, were functionalized with **8**. Unfortunately functionalization enhanced particle agglomeration resulting in an average diameter of 159.6 nm ±86.5 nm derived from DLS measurements.

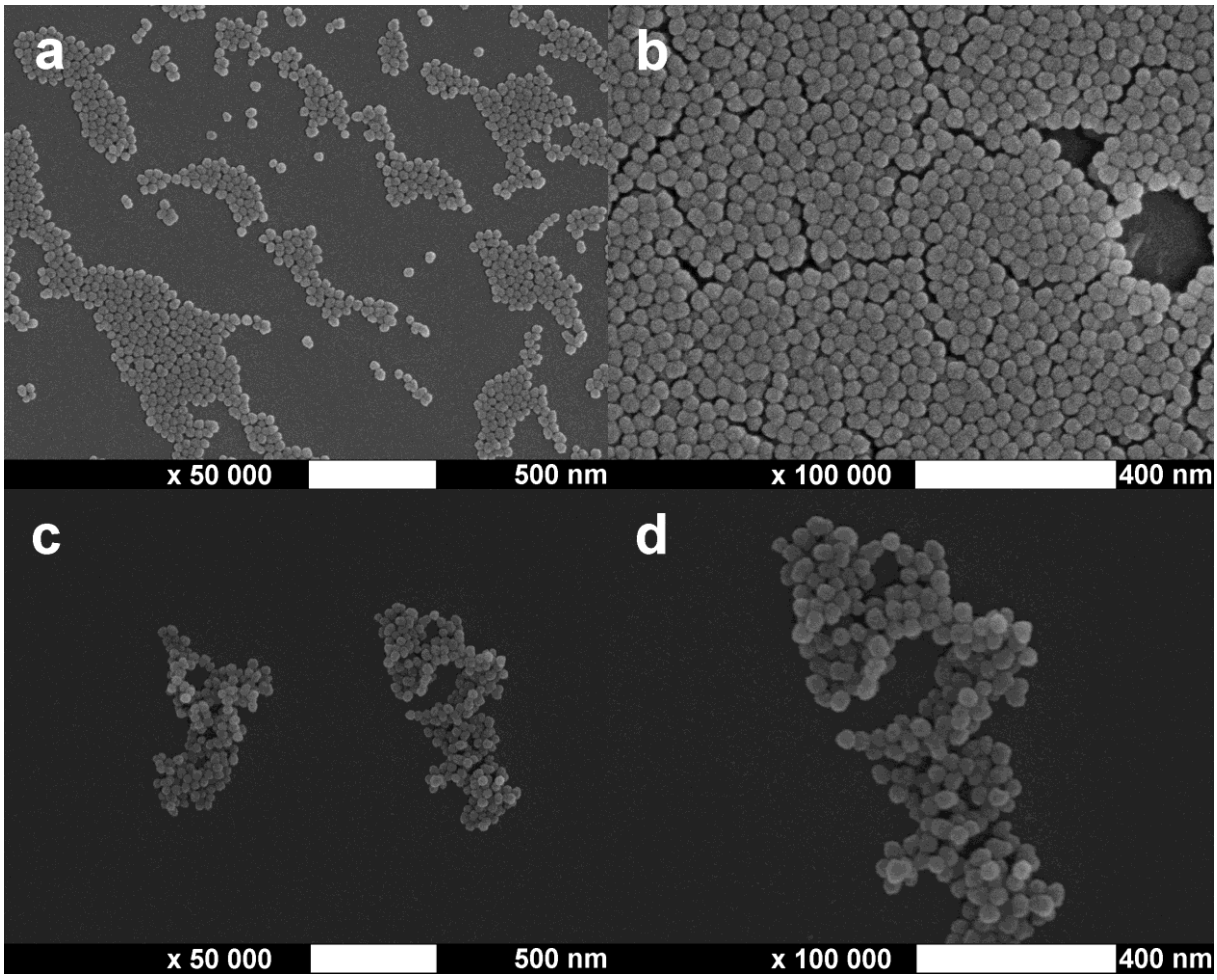

Figure 3.33: a, b: SEM pictures of unfunctionalized Stöber particles. c, d: SEM images of *o*-NBnC functionalized Silica nanoparticles

However SEM images of functionalized and unfunctionalized particles were taken and besides the tendency to agglomerate, no significant change in particle size or morphology could be found. (Figure 3.33)

To quantify the degree of functionalization, TGA measurements were performed. Between 100 °C and 800 °C, the sample showed a weight loss of 10.6%. Assuming that at these temperatures only the organic functionalization is effected and the amorphous silica core is not, it is possible to determine the molar concentration of *o*-NBnC per particle mass to 0.27 µmol·mg^{-1} or 14,450 functional molecules per particle. This value corresponds quite nicely with the formation of a mono layer, under the assumption that only 1.5 out of 3 triethoxy-functionalities react with the 27,370 surface hydroxyl groups per particle.

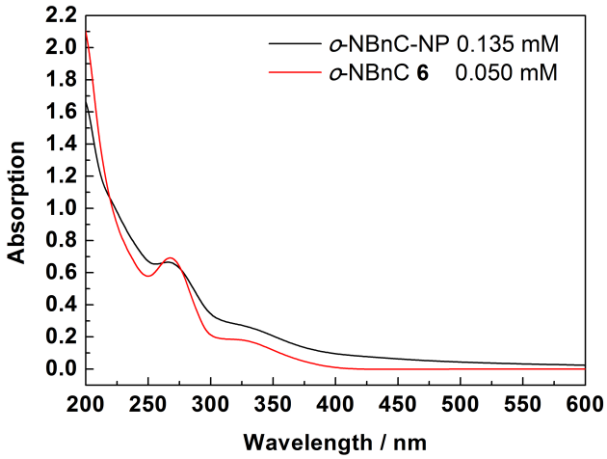

Figure 3.34: Absorption spectra of *o*-NBnC-NP and *o*-NBnC based methacrylic monomer **6.**

Figure 3.34 shows the absorption spectrum of silica nanoparticles with functionalized *o*-NBnC **8** (*o*-NBnC-NP). The spectrum shows the typical absorption band at 268 nm corresponding to 5FU and the broader absorption band between 310 nm - 360 nm characteristic for *o*-NBnCs. Compared to the absorption spectrum of **6,** *o*-NBnC-NP cause a broader spectrum, which can be explained by the agglomerates formed. Formation of agglomerates results in a higher diffusion within the sample resulting in a broader signal. Besides this agglomerates are the reason for the low absorption of *o*-NBnC-NP compared to **6** in solution. As seen for TPC-NP an absorption of 50% compared to the corresponding chromophore in solution would be expected. However, *o*-NBnC groups within the agglomerates are shielded from irradiation and therefore from detection, resulting in an even lower absorption.

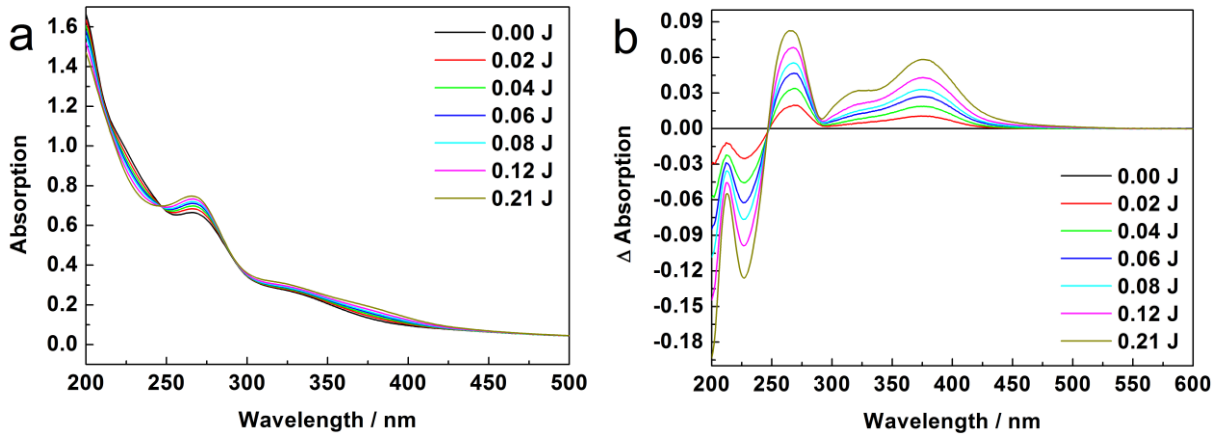

Figure 3.35: Change in absorption after irradiation with 266 nm (total energies given) of *o*-NBnC-NP dispersed in ACN. a: raw absorption; b: differential spectra.

To check the photochemical activity of *o*-NBnC-NP, a dispersion containing 0.5 mg·ml^{-1} (0.135 mM) was irradiated with light of 266 nm. (Figure 3.35) The monitored absorption change is almost identical to the observed change for **4a** in Figure 3.20 b, indicating the same photochemical properties. To finally prove drug delivery from the synthesized nanoparticles, different samples, each containing two milliliters of the same dispersions, were irradiated with different energy doses. Drug release was probed for in the supernatant of the dispersion after centrifugation at 13,000 rpm for two hours.

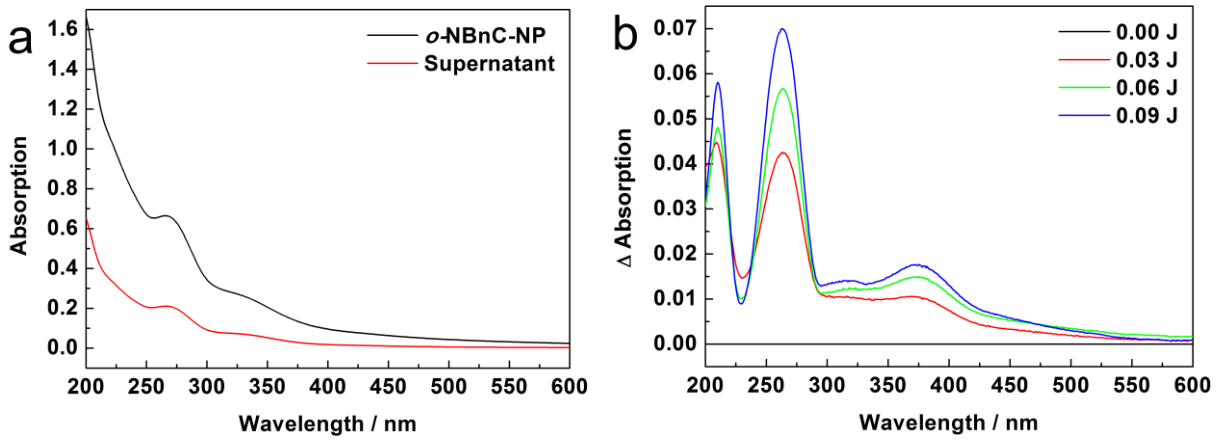

Figure 3.36: a: Absorption spectra of a non-irradiated *o*-NBnC-NP dispersion before and after centrifugation. b: differential spectra between supernatants of *o*-NBnC-NP irradiated with increasing energy and the supernatant of non-irradiated *o*-NBnC-NP.

Unfortunately, the resulting supernatants were not completely particle free as shown in Figure 3.36 a for a non-irradiated sample. However, the differential spectra between the supernatants of a non-irradiated sample and samples irradiated at 266 nm with increasing

energy show the typical spectrum of 5FU with a strong absorbance at 268 nm, besides only minor absorbance at 370 nm resulting from not sedimented particles in the supernatant. The achieved drug release was 8% of the total amount of 5FU bound to the particle surface. The access of 5FU to not sedimented particles proves the possibility of photochemical drug delivery from o-NBnC-NP. The *ortho*-nitrobenzyl moiety remains covalently bound to the particle surface while the active free drug is released into the solution. This first proof of principle shows how the concept of o-NBnC can be easily transferred from solution and polymer matrix into nanotechnology. Further improvement of the functionalization agent enhancing dispersal will result in a powerful nano-composite material that can be combined with different other e.g. polymeric materials, to develop new photoactive drug delivery systems.

4 Summary and Outlook

Within this work two different approaches to synthesize new composite materials for photochemical drug delivery and their potential application in IOLs were investigated.

In the first part of this thesis the photochemical properties of coumarin functionalized silica nanoparticles were examined. Employing two different synthetic methods particles of 45 nm and 16 nm were produced. The larger ones synthesized utilizing the Stöber synthesis, bear a Coumarin double layer on the surface and form stable dispersions in ACN. The smaller particles were synthesized by modifying the recently developed protocol of Yokoi et al.,[108] resulting in particles functionalized with a coumarin monolayer, which form stable dispersions in water. The following photochemical investigations revealed that, analog to the photochemistry in solution, the coumarin groups on the particle surface undergo [2π+2π]-cycloaddition as well as [2π+2π]-cycloreversion. The quantum yield for the cycloreversion at 280 nm was determined to be Φ = 0.27 for both particles, confirming the hypothesis that the photochemistry of the coumarin groups on the surface is independent from particle size. Investigations on the reversibility of the reaction revealed an astonishing wavelength dependency. On the nanoparticle surface the covalently anchored coumarin moieties are in close proximity and a simultaneous dimerization and photo cleavage is observed. This coincides with a wavelength-dependent equilibrium state. The forward and the backward reaction rate become of the same order of magnitude, resulting in a change in the reaction order. The closer proximity of the coumarin moieties increased the photo dimerization rate about 2000-fold. This fast reaction on the nanoparticle surface was found to be the reason for the fact that hetero dimerization of the coumarin groups with the model drug 5FU in solution was ineffective and only negligible drug loads were obtained. To achieve a suitable amount of drug load a different approach had to be investigated, utilizing an already drug loaded functionalization agent.

Taking those considerations into account, in the second part of this thesis a four step synthesis, which was improved in yield and reaction time compared to the literature, was utilized to create an *ortho*-nitrobenzyl compound (*o*-NBnC) for photochemical drug delivery. Photochemical investigations in solution revealed a single photon quantum yield of Φ = 0.27 and a two-photon cross section of σ = 2.41 GM. Those values exceeded the results reported

in literature for similar compounds and are competitive to other photochemical drug delivery systems. Furthermore it was proven that two-photon induced drug delivery is possible in presence of an UV-absorbing agent. For the investigated molar ratio, only a decrease in drug delivery of 6% was observed, concluding that the UV-absorbing agent is not completely two-photon inactive, but its two-photon cross section is at least one order of magnitude lower than for the *o*-NBnC. Within the experimental framework no structural changes due to two-photon absorption of the UV-absorbing agent were noticed, being indispensable for a drug delivery approach. Functionalization of the *o*-NBnC with a methacrylic moiety enabled investigations on the drug delivery behavior from a polymeric matrix, by copolymerization with a polymer common for the potential application in IOLs, as well as the actual fabrication of model IOLs, from which the two-photon absorption induced drug delivery in presence of an UV-absorbing agent has been successfully proven.

In conclusion the photochemistry of silica nanoparticles was investigated in detail, revealing interesting new properties of the [2π+2π]-cycloreversion reaction of coumarin moieties bound to a surface which could not be observed in solution, polymer matrix or SAM before.
Utilizing the synthesized *o*-NBnC it was proven that those photoactive compounds are a suitable platform for drug delivery with potential application in IOLs. The photochemical properties are comparable to those of prior studies utilizing coumarin or tetralone hetero dimers for drug delivery, while the synthetic effort could be simplified and reduced. The problem of the *o*-NBnC being incompatible with free radical polymerization could be easily overcome in future investigations by transferring these promising results onto a silicon based monomer, which could be easily copolymerized without any undesired side reactions by polycondensation.
Finally both approaches were successfully combined by functionalization of silica nanoparticles with *o*-NBnC, overcoming the limitation resulting from photochemical drug load. Further the resulting particles may be dispersed within a silicon based polymer for IOLs increasing their lower refractive index, one of the disadvantages of silicon based IOLs over methacrylic IOLs, while still preserving their drug release properties. Owing to this reason those particles are the most promising composite material, aiming at photo active IOLs for drug delivery and are well worth future research.

5 Zusammenfassung

Im Rahmen der vorliegenden Arbeit wurden zwei unterschiedliche Ansätze für die Herstellung neuer Composite Materialien zur photochemischen Wirkstofffreisetzung, sowie deren mögliche Anwendung in IOLs untersucht.

Der erste Teil der Arbeit beschäftigte sich mit den photochemischen Eigenschaften Coumarin funktionalisierter SiO_2-Nanopartikel. Es wurden zwei unterschiedliche Methoden zur Synthese verwendet. Zum einen wurden unter Anwendung der Stöber Synthese 45 nm große Partikel hergestellt, welche eine Coumarin Doppelschicht auf der Oberfläche aufwiesen und in ACN stabile Dispersionen bildeten. Zum anderen wurde das erst kürzlich von Yokoi et al. vorgestellte Protokoll[108] so modifiziert, dass mit einer Coumarin Monolage funktionalisierte SiO_2-Nanopartikel mit einem Durchmesser von 16 nm hergestellt werden konnten, die in Wasser stabile Dispersionen ausbilden. Anschließenden photochemischen Untersuchungen zeigten, dass analog zur Photochemie in Lösung, [2π+2π] Cycloadditionen sowie [2π+2π] Cycloreversionen der Coumaringruppen auf der Oberfläche beobachtete werden können. Zunächst wurden zur weiteren Charakterisierung die Quantenausbeuten für die Cycloreversion bei 280 nm beider Partikelarten mit 0.27 bestimmt, die Hypothese bestätigend das die Photochemie auf der Oberfläche Partikelgrößen unabhängig ist. Untersuchungen zur Reversibilität der Reaktion förderten eine ungewöhnliche Wellenlängenabhängigkeit der Cycloreversionsreaktion zu Tage. Auf Grund der großen räumlichen Nähe der Coumaringruppen auf der Partikel Oberfläche ist es möglich das gespaltene noch photochemisch angeregte Moleküle sofort zurückreagieren, was eine Änderung der Reaktionsordnung zur Folge hat. Das entstehende Gleichgewicht zwischen Hin und Rückreaktion ist wellenlängenabhängig. Die große räumliche Nähe der Coumaringruppen hat auch eine um das zweitausendfache schnellere Dimersierung auf der Oberfläche zur Folge. Aufgrund dessen war die ursprünglich beabsichtigte Heterodimersierung mit dem Modell Wirkstoff 5FU vernachlässigbar gegenüber der Homodimerisierung der Coumarin auf der Oberfläche. Um eine ausreichende Wirkstoffbeladung zu realisieren wurde daher ein neuer Ansatz basierend auf einem bereits Wirkstoffbeladenen Funktionalisierungsreagenz entwickelt.

Im zweiten Teil der vorliegenden Arbeit wurde in einer vierstufigen Synthese, die in Ausbeute und Reaktionsdauer gegenüber der Literatur verbessert werden konnte, eine *ortho*-Nitrobenzyl basierende Verbindung zur photochemischen Wirkstofffreisetzung hergestellt. Untersuchungen der photochemischen Eigenschaften in Lösung ergaben eine Ein-Photon-Quantenausbeuten bei 266 nm von $\Phi = 0.27$ sowie einen Zwei-Photonen-Querschnitt bei 532 nm von $\sigma = 2.41$ GM. Die erhaltenen Werte übertrafen die in der Literatur bekannten Ergebnisse für ähnliche Verbindungen und waren mit denen anderer photochemischer Systeme zur Wirkstofffreisetzung vergleichbar. Zudem wurde Nachgewiesen, dass eine Zwei-Photonen induzierte Wirkstofffreisetzung auch in Anwesenheit eines UV-Absorbers möglich ist. Es konnte bei dem untersuchten molaren Verhältnis lediglich eine Verringerung der Wirkstofffreisetzung um 6% beobachtet werden, was den Schluss nahe legt, dass der UV-Absorber nicht vollkommen Zwei-Photonen inaktiv ist, jedoch sein Zwei-Photonen-Querschnitt um eine Größenordnung geringer ist, als der der *ortho*-Nitrobenzyl Verbindung. Im Rahmen der durchgeführten Untersuchungen wies der UV-Absorber keinerlei strukturelle Veränderungen aufgrund der Zwei-Photonen-Absorption auf, eine unabdingbare Voraussetzung für den Einsatz in einem Drug Delivery System. Funktionalisierung der Verbindung mit einem Methacrylatrest ermöglichte die Untersuchung der Wirkstofffreisetzung aus einer Polymermatrix durch Copolymerisation mit einem für die potentielle Anwendung in IOLs üblichen Polymer, sowie die Herstellung erster Model IOLs, aus denen ebenfalls eine erfolgreiche Zwei-Photonen induzierte Wirkstofffreisetzung in Anwesenheit eines UV-Blockers gezeigt werden konnte.

Abschließend konnten durch die erfolgreiche Kombination beider Ansätze wirkstoffbeladene SiO_2-Nanopartikel synthetisiert werden, deren Funktionalisierung auf einer *ortho*-Nitrobenzyl Verbindung basierte, die mit einem Triethoxysilylrest versehen wurde. Erste photochemische Untersuchungen konnten zeigen, dass eine lichtinduzierte Wirkstofffreisetzung möglich ist. Dies macht diese Partikel zu einem vielversprechenden Composite Material für den Einsatz in IOLs, welches noch weitere Untersuchungen wert ist.

6 References

[1] J. Priestley, in *Experiments and Observations on Diffrent Kinds of Air, Vol. 3*, Thomas Pearson, Birmingham, **1790**, pp. 126-128.

[2] J. Priestley, in *Experiments and Observations on Diffrent Kinds of Air, Vol. 3*, Thomas Pearson, Birmingham, **1790**, pp. 293-305.

[3] H. D. Roth, *Angew. Chem.* **1989**, *101*, 1220-1234.

[4] J. F. Döbereiner, *Pharm. Centralbl.* **1831**, *2*, 383-385.

[5] C. G. Hatchard, C. A. Parker, *Proc. R. Soc. London, A* **1956**, *235*, 518-536.

[6] C. A. Parker, *Proc. R. Soc. London, A* **1953**, *220*, 104-116.

[7] H. Trommsdorff, *Ann. Pharm.* **1834**, *11*, 190-207.

[8] F. Sestini, *Bull. Soc. Chim. Fr.* **1866**, *5*, 202.

[9] S. Cannizzaro, G. Fabris, *Ber. Dtsch. Chem. Ges.* **1886**, *19*, 2260-2265.

[10] S. Cannizzaro, F. Sestini, *Gazz. Chim. Ital.* **1873**, *3*, 241-251.

[11] N. D. Heindel, M. A. Pfau, *J. Chem. Educ.* **1965**, *42*, 383-null.

[12] G. Ciamician, *Gazz. Chim. Ital.* **1886**, *16*, 111-112.

[13] G. Ciamician, P. Silber, *Ber. Dtsch. Chem. Ges.* **1886**, *19*, 2899-2900.

[14] H. Klinger, *Ber. Dtsch. Chem. Ges.* **1886**, *19*, 1862-1870.

[15] G. Ciamician, P. Silber, *Ber. Dtsch. Chem. Ges.* **1902**, *35*, 4128-4131.

[16] G. Ciamician, P. Silber, *Ber. Dtsch. Chem. Ges.* **1901**, *34*, 2040-2046.

[17] G. Ciamician, *Science* **1912**, *36*, 385-394.

[18] T. H. Maiman, *Nature* **1960**, *187*, 493-494.

[19] H. D. Roth, *Pure Appl. Chem.* **2001**, *73*, 395-403.

[20] G. Porter, *Journal of the Chemical Society, Faraday Transactions 2: Molecular and Chemical Physics* **1986**, *82*, 2445-2451.

[21] O. Diels, K. Alder, *Ber. Dtsch. Chem. Ges.* **1929**, *62*, 554-562.

[22] O. Diels, K. Alder, *Ber. Dtsch. Chem. Ges.* **1929**, *62*, 2081-2087.

[23] O. Diels, K. Alder, *Liebigs Ann. Chem.* **1928**, *460*, 98-122.

[24] O. Diels, K. Alder, *Liebigs Ann. Chem.* **1929**, *470*, 62-103.

[25] S. Laschat, *Angew. Chem., Int. Ed.* **1996**, *35*, 289-291.

[26] S. Kotha, M. Meshram, A. Tiwari, *Chem. Soc. Rev.* **2009**, *38*, 2065-2092.

[27] R. Hoffmann, R. B. Woodward, *J. Am. Chem. Soc.* **1965**, *87*, 2046-2048.

[28] R. Hoffmann, R. B. Woodward, *J. Am. Chem. Soc.* **1965**, *87*, 4389-4390.

[29] J. T. Woodward, A. Ulman, D. K. Schwartz, *Langmuir* **1996**, *12*, 3626-3629.

[30] K. Fukui, T. Yonezawa, H. Shingu, *The Journal of Chemical Physics* **1952**, *20*, 722-725.

[31] K. Fukui, *Science* **1982**, *218*, 747-754.

[32] G. O. Schenck, I. von Wilucki, C. H. Krauch, *Chem. Ber.* **1962**, *95*, 1409-1412.

[33] C. H. Krauch, S. Farid, G. O. Schenck, *Chem. Ber.* **1966**, *99*, 625-633.

[34] T. Wolff, H. Görner, *Phys. Chem. Chem. Phys.* **2004**, *6*, 368-376.

[35] J. Fritzsche, *Liebigs Ann. Chem.* **1859**, *109*, 247-250.

[36] C. Liebermann, *Liebigs Ann. Chem.* **1871**, *158*, 299-315.

[37] G. S. Hammond, C. A. Stout, A. A. Lamola, *J. Am. Chem. Soc.* **1964**, *86*, 3103-3106.

[38] M. D'Auria, R. Racioppi, *J. Photochem. Photobiol., A* **2004**, *163*, 557-559.

[39] F. D. Lewis, S. V. Barancyk, *Journal of American Chemical Society* **1989**, *111*, 8653-8661.

[40] N. Yonezawa, M. Hasegawa, *Bull. Chem. Soc. Jpn.* **1983**, *56*, 367-368.

[41] N. Yonezawa, M. Kubo, K. Saigo, M. Hasegawa, *Bull. Chem. Soc. Jpn.* **1988**, *61*, 1005-1007.

[42] N. Yonezawa, T. Yoshida, M. Hasegawa, *J. Chem. Soc., Perkin Trans. 1* **1983**, 1083-1086.

[43] D. Kehrloesser, J. Traeger, H.-C. Kim, N. Hampp, *Langmuir* **2009**, *26*, 3878-3882.

[44] R. S. Becker, S. Chakravorti, C. A. Gartner, M. d. G. Miguel, *J. Chem. Soc., Faraday Trans.* **1993**, *89*, 1007.

[45] T. A. Moore, M. L. Harter, P.-S. Song, *J. Mol. Spectrosc.* **1971**, *40*, 144-157.

[46] J. Seixas de Melo, P. F. Fernandes, *J. Mol. Struct.* **2001**, *565-566*, 69-78.

[47] Y. Chen, C. F. Chou, *J. Polym. Sci., Part A: Polym. Chem.* **1995**, *33*, 2705-2714.

[48] Y. Chen, J. D. Wu, *J. Polym. Sci., Part A: Polym. Chem.* **1994**, *32*, 1867-1875.

[49] T. Ngai, C. Wu, *Macromolecules* **2003**, *36*, 848-854.

[50] Y. Chujo, K. Sada, T. Saegusa, *Macromolecules* **1990**, *23*, 2693-2697.

[51] J. Träger, J. Heinzer, H.-C. Kim, N. Hampp, *Macromoleculer Biosience* **2008**, *in press*.

[52] J. Trager, H.-C. Kim, N. Hampp*, Vol. 6138* (Eds.: M. Fabrice, G. S. Per, H. Arthur), SPIE, **2006**, p. 61381D.

[53] J. Trager, H.-C. Kim, N. Hampp, *Nat. Photonics* **2007**, *1*, 509-511.

[54] Y. Chen, C.-S. Jean, *J. Appl. Polym. Sci.* **1997**, *64*, 1749-1758.

[55] Y. Chen, C.-S. Jean, *J. Appl. Polym. Sci.* **1997**, *64*, 1759-1768.

[56] W. Li, V. Lynch, H. Thompson, M. A. Fox, *J. Am. Chem. Soc.* **1997**, *119*, 7211-7217.

[57] J. Fang, C. Whitaker, B. Weslowski, M.-S. Chen, J. Naciri, R. Shashidhar, *J. Mater. Chem.* **2001**, *11*, 2992-2995.

[58] C. Graf, W. Schärtl, N. Hugenberg, *Adv. Mater. (Weinheim, Ger.)* **2000**, *12*, 1353-1356.

[59] N. K. Mal, M. Fujiwara, Y. Tanaka, *Nature* **2003**, *421*, 350-353.

[60] M. Fujiwara, K. Shiokawa, N. Kawasaki, Y. Tanaka, *Adv. Funct. Mater.* **2003**, *13*, 371-376.

[61] L. Zhao, D. A. Loy, K. J. Shea, *J. Am. Chem. Soc.* **2006**, *128*, 14250-14251.

[62] S.-W. Ha, C. E. Camalier, G. R. B. Jr, J.-K. Lee, *Chem. Commun.* **2009**, 2881-2883.

[63] J. A. Barltrop, P. Schofield, *Tetrahedron Lett.* **1962**, *3*, 697-699.

[64] J. A. Barltrop, P. Schofield, *J. Chem. Soc.* **1965**, 4758-4765.

[65] A. Patchornik, B. Amit, R. B. Woodward, *J. Am. Chem. Soc.* **1970**, *92*, 6333-6335.

[66] T. Schmierer, F. Bley, K. Schaper, P. Gilch, *J. Photochem. Photobiol., A* **2011**, *217*, 363-368.

[67] K. Schaper, M. Etinski, T. Fleig, *Photochem. Photobiol.* **2009**, *85*, 1075-1081.

[68] T. Schmierer, S. Laimgruber, K. Haiser, K. Kiewisch, J. Neugebauer, P. Gilch, *Phys. Chem. Chem. Phys.* **2010**, *12*, 15653-15664.

[69] Q. Q. Zhu, W. Schnabel, H. Schupp, *J. Photochem.* **1987**, *39*, 317-332.

[70] F. Bley, K. Schaper, H. Görner, *Photochem. Photobiol.* **2008**, *84*, 162-171.

[71] R. T. Cummings, G. A. Krafft, *Tetrahedron Lett.* **1988**, *29*, 65-68.

[72] S. R. Adams, J. P. Y. Kao, R. Y. Tsien, *J. Am. Chem. Soc.* **1989**, *111*, 7957-7968.

[73] T. Milburn, N. Matsubara, A. P. Billington, J. B. Udgaonkar, J. W. Walker, B. K. Carpenter, W. W. Webb, J. Marque, W. Denk, *Biochemistry* **1989**, *28*, 49-55.

[74] K. Schaper, S. Abdollah M. Mobarekeh, C. Grewer, *Eur. J. Org. Chem.* **2002**, *2002*, 1037-1046.

[75] C. G. Bochet, *J. Chem. Soc., Perkin Trans. 1* **2002**, 125-142.

[76] H. M. D. Bandara, D. P. Kennedy, E. Akin, C. D. Incarvito, S. C. Burdette, *Inorg. Chem.* **2009**, *48*, 8445-8455.

[77] J. Jiang, X. Tong, D. Morris, Y. Zhao, *Macromolecules* **2006**, *39*, 4633-4640.

[78] D. Klinger, K. Landfester, *Soft Matter* **2011**, *7*, 1426-1440.

[79] A. Diaspro, F. Federici, C. Viappiani, S. Krol, M. Pisciotta, G. Chirico, F. Cannone, A. Gliozzi, *J. Phys. Chem. B* **2003**, *107*, 11008-11012.

[80] J. L. Vivero-Escoto, I. I. Slowing, C.-W. Wu, V. S. Y. Lin, *J. Am. Chem. Soc.* **2009**, *131*, 3462-3463.

[81] C. Park, K. Lee, C. Kim, *Angew. Chem., Int. Ed.* **2009**, *48*, 1275-1278.

[82] K. K. Coti, M. E. Belowich, M. Liong, M. W. Ambrogio, Y. A. Lau, H. A. Khatib, J. I. Zink, N. M. Khashab, J. F. Stoddart, *Nanoscale* **2009**, *1*, 16-39.

[83] S. S. Banerjee, D.-H. Chen, *Nanotechnology* **2009**, 185103.

[84] S. S. Agasti, A. Chompoosor, C.-C. You, P. Ghosh, C. K. Kim, V. M. Rotello, *J. Am. Chem. Soc.* **2009**, *131*, 5728-5729.

[85] M. Göppert-Mayer, *Ann. Phys.* **1931**, *401*, 273-294.

[86] W. Kaiser, C. G. B. Garrett, *Phys. Rev. Lett.* **1961**, *7*, 229.

[87] J. D. Bhawalkar, et al., *Reports on Progress in Physics* **1996**, *59*, 1041.

[88] M. D. Cahalan, I. Parker, S. H. Wei, M. J. Miller, *Nat. Rev. Immunol.* **2002**, *2*, 872-880.

[89] Y. Imanishi, K. H. Lodowski, Y. Koutalos, *Biochemistry* **2007**, *46*, 9674-9684.

[90] K.-S. Lee, R. H. Kim, D.-Y. Yang, S. H. Park, *Prog. Polym. Sci.* **2008**, *33*, 631-681.

[91] D.-Y. Y. Kwang-Sup Lee, Sang Hu Park, Ran Hee Kim,, *Polym. Adv. Technol.* **2006**, *17*, 72-82.

[92] A. Ovsianikov, A. Ostendorf, B. N. Chichkov, *Appl. Surf. Sci.* **2007**, *253*, 6599-6602.

[93] K. E. Borbas, D. Lahaye, *Photodynamic Therapy of Cancer*, John Wiley & Sons, Ltd, **2008**.

[94] P. K. Frederiksen, M. Jørgensen, P. R. Ogilby, *J. Am. Chem. Soc.* **2001**, *123*, 1215-1221.

[95] C. T. Kresge, M. E. Leonowicz, W. J. Roth, J. C. Vartuli, J. S. Beck, *Nature* **1992**, *359*, 710-712.

[96] S. Inagaki, Y. Fukushima, K. Kuroda, *J. Chem. Soc., Chem. Commun.* **1993**, 680-682.

[97] I. I. Slowing, J. L. Vivero-Escoto, B. G. Trewyn, V. S. Y. Lin, *J. Mater. Chem.* **2010**, *20*, 7924-7937.

[98] I. I. Slowing, J. L. Vivero-Escoto, C.-W. Wu, V. S. Y. Lin, *Adv. Drug Delivery Rev.* **2008**, *60*, 1278-1288.

[99] J. L. Vivero-Escoto, I. I. Slowing, B. G. Trewyn, V. S. Y. Lin, *Small* **2010**, *6*, 1952-1967.

[100] Y. Klichko, M. Liong, E. Choi, S. Angelos, A. E. Nel, J. F. Stoddart, F. Tamanoi, J. I. Zink, *J. Am. Ceram. Soc.* **2009**, *92*, S2-S10.

[101] B. G. Trewyn, I. I. Slowing, S. Giri, H.-T. Chen, V. S. Y. Lin, *Acc. Chem. Res.* **2007**, *40*, 846-853.

[102] R. Lucena, B. M. Simonet, S. Cárdenas, M. Valcárcel, *Journal of Chromatography A* **2011**, *1218*, 620-637.

[103] W. Stöber, A. Fink, E. Bohn, *J. Colloid Interface Sci.* **1968**, *26*, 62.

[104] L. L. Hench, J. K. West, *Chem. Rev. (Washington, DC, U. S.)* **1990**, *90*, 33-72.

[105] H. K. Schmidt, E. Geiter, M. Mennig, H. Krug, C. Becker, R. P. Winkler, *J. Sol-Gel Sci. Technol.* **1998**, *13*, 397-404.

[106] T. Aubert, F. Grasset, S. Mornet, E. Duguet, O. Cador, S. Cordier, Y. Molard, V. Demange, M. Mortier, H. Haneda, *J. Colloid Interface Sci.* **2010**, *341*, 201-208.

[107] R. K. Iler, *The chemistry of silica: solubility, polymerization, colloid and surface properties, and biochemistry* Wiley, New York **1979**.

[108] T. Yokoi, Y. Sakamoto, O. Terasaki, Y. Kubota, T. Okubo, T. Tatsumi, *J. Am. Chem. Soc.* **2006**, *128*, 13664-13665.

[109] S. E. Pratsinis, *Progr. Energy Combust. Sci.* **1998**, *24*, 197.

[110] A. K. Van Helden, J. W. Jansen, A. Vrij, *J. Colloid Interface Sci.* **1981**, *81*, 354-368.

[111] C. G. Tan, B. D. Bowen, N. Epstein, *J. Colloid Interface Sci.* **1987**, *118*, 290-293.

[112] V. K. LaMer, R. H. Dinegar, *J. Am. Chem. Soc.* **1950**, *72*, 4847-4854.

[113] C. Blum, Dissertation, Universtiy of Paderborn (Paderborn), **2004**.

[114] T. Matsoukas, E. Gulari, *J. Colloid Interface Sci.* **1988**, *124*, 252-261.

[115] A. Van Blaaderen, J. Van Geest, A. Vrij, *J. Colloid Interface Sci.* **1992**, *154*, 481-501.

[116] S. G. Stitchell, K. D. M. Harris, A. E. Aliev, *Struct. Chem.* **1994**, *5*, 327-333.

[117] J. K. Bailey, M. L. Mecartney, *Colloids Surf.* **1992**, *63*, 151-161.

[118] H. Boukari, J. S. Lin, M. T. Harris, *J. Colloid Interface Sci.* **1997**, *194*, 311-318.

[119] D. Pontoni, T. Narayanan, A. R. Rennie, *Langmuir* **2002**, *18*, 56-59.

[120] C. D. Geddes, *J. Fluoresc.* **2002**, *12*, 343-367.

[121] D. Tleugabulova, A. M. Duft, Z. Zhang, Y. Chen, M. A. Brook, J. D. Brennan, *Langmuir* **2004**, *20*, 5924-5932.

[122] A. P. Philipse, A. Vrij, *J. Colloid Interface Sci.* **1989**, *128*, 121-136.

[123] A. van Blaaderen, A. Vrij, *J. Colloid Interface Sci.* **1993**, *156*, 1-18.

[124] T. Yokoi, J. Wakabayashi, Y. Otsuka, W. Fan, M. Iwama, R. Watanabe, K. Aramaki, A. Shimojima, T. Tatsumi, T. Okubo, *Chem. Mater.* **2009**, *21*, 3719-3729.

[125] K. D. Hartlen, A. P. T. Athanasopoulos, V. Kitaev, *Langmuir* **2008**, *24*, 1714-1720.

[126] J. Wang, A. Sugawara, A. Shimojima, T. Okubo, *Langmuir* **2010**, *26*, 18491-18498.

[127] C. Walter, *Macromol. Rapid Commun.* **2000**, *21*, 705-722.

[128] Z. Zeng, J. Yu, Z.-X. Guo, *Macromol. Chem. Phys.* **2004**, *205*, 2197-2204.

[129] T. Mizutani, K. Arai, M. Miyamoto, Y. Kimura, *J. Appl. Polym. Sci.* **2006**, *99*, 659-669.

[130] B. Radhakrishnan, R. Ranjan, W. J. Brittain, *Soft Matter* **2006**, *2*, 386-396.

[131] J. M. Rodríguez, T. A. o. t. Pulp, P. I. P. A. Committee, *Micro and nanoparticles in papermaking*, TAPPI Press, **2005**.

[132] E. P. K. Currie, M. Tilley, *Journal of the Society for Information Display* **2005**, *13*, 773-780.

[133] J. M. Rosenholm, C. Sahlgren, M. Linden, *Nanoscale* **2010**, *2*, 1870-1883.

[134] Y. Piao, A. Burns, J. Kim, U. Wiesner, T. Hyeon, *Adv. Funct. Mater.* **2008**, *18*, 3745-3758.

[135] G. Yao, L. Wang, Y. Wu, J. Smith, J. Xu, W. Zhao, E. Lee, W. Tan, *Anal. Bioanal. Chem.* **2006**, *385*, 518-524.

[136] L. Wang, K. Wang, S. Santra, X. Zhao, L. R. Hilliard, J. E. Smith, Y. Wu, W. Tan, *Anal. Chem.* **2006**, *78*, 646-654.

[137] X. M. Qian, S. M. Nie, *Chem. Soc. Rev.* **2008**, *37*, 912-920.

[138] C. Nilsson, S. Nilsson, *Electrophoresis* **2006**, *27*, 76-83.

[139] C. Nilsson, S. Birnbaum, S. Nilsson, *Journal of Chromatography A* **2007**, *1168*, 212-224.

[140] I. U. Vakarelski, S. C. Brown, B. M. Moudgil, K. Higashitani, *Advanced Powder Technology* **2007**, *18*, 605-614.

[141] W. Tan, K. Wang, X. He, X. J. Zhao, T. Drake, L. Wang, R. P. Bagwe, *Med. Res. Rev.* **2004**, *24*, 621-638.

[142] A.-H. Lu, E. L. Salabas, F. Schüth, *Angew. Chem., Int. Ed.* **2007**, *46*, 1222-1244.

[143] A. Fleming, *British Journal of Experimental Pathology* **1929**, *10*, 226-236.

[144] http://www.who.int/blindness/causes/priority/en/index1.html, 27.05.2011

[145] H.-C. Kim, S. Hartner, M. Behe, T. M. Behr, N. A. Hampp, *J. Biomed. Opt.* **2006**, *11*, 34024-34029.

[146] H. C. Kim, S. Härtner, N. Hampp, *J. Photochem. Photobiol., A* **2008**, *197*, 239-244.

[147] J. Liese, N. A. Hampp, *J. Photochem. Photobiol., A* **2010**, *209*, 128-134.

[148] S. Härtner, H.-C. Kim, N. Hampp, *J. Polym. Sci., Part A: Polym. Chem.* **2007**, *45*, 2443-2452.

[149] T. Buckup, J. Möhring, V. Settels, J. Träger, H.-C. Kim, N. Hampp, M. Motzkus, in *Ultrafast Phenomena XVI, Vol. 92* (Eds.: P. Corkum, S. Silvestri, K. A. Nelson, E. Riedle, R. W. Schoenlein), Springer Berlin Heidelberg, **2009**, pp. 574-576.

[150] C. Sinkel, A. Greiner, S. Agarwal, *Macromolecules* **2008**, *41*, 3460-3467.

[151] J. Liese, N. A. Hampp, *J. Photochem. Photobiol., A* **2011**, *219*, 228-234.

[152] A. Einstein, *Ann. Phys.* **1905**, *322*, 549-560.

[153] M. von Smoluchowski, *Ann. Phys.* **1906**, *326*, 756-780.

[154] G. Gauglitz, S. Hubig, *J. Photochem.* **1981**, *15*, 255-257.

[155] Y. Kita, T. Toma, T. Kan, T. Fukuyama, *Org. Lett.* **2008**, *10*, 3251-3253.

[156] T. Kametani, K. Kigasawa, M. Hiiragi, K. Wakisaka, S. Haga, Y. Nagamatsu, H. Sugi, K. Fukawa, O. Irino, *J. Med. Chem.* **1980**, *23*, 1324-1329.

[157] R. C. Esse, B. E. Christensen, *J. Org. Chem* **1960**, *25*, 1565-1569.

[158] D. J. Clarke, R. S. Robinson, *Tetrahedron* **2002**, *58*, 2831-2837.

[159] D. Kehrloesser, R.-P. Baumann, H.-C. Kim, N. Hampp, *Langmuir* **2011**, *27*, 4149-4155.

[160] T. Melin, H. Diesinger, S. Barbet, D. Deresmes, T. Baron, D. Stievenard, *Mater. Res. Soc. Symp. Proc.* **2004**, *832*, 179-188.

[161] J. Pacifico, et al., *Nanotechnology* **2009**, *20*, 095708.

[162] H.-C. Kim, S. Kreiling, A. Greiner, N. Hampp, *Chem. Phys. Lett.* **2003**, *372*, 899-903.

[163] S. Härtner, H.-C. Kim, N. Hampp, *J. Photochem. Photobiol., A* **2007**, *187*, 242-246.

[164] T. Wolff, H. Görner, *J. Photochem. Photobiol., A* **2010**, *209*, 219-223.

[165] O. R. Ludek, C. Meier, *Synlett* **2005**, *2005*, 3145,3147.

[166] E. Reichmanis, R. Gooden, C. W. Wilkins, H. Schonhorn, *J. Polym. Sci., Polym. Chem. Ed.* **1983**, *21*, 1075-1083.

[167] E. B. Brown, J. B. Shear, S. R. Adams, R. Y. Tsien, W. W. Webb, *Biophys. J.* **1999**, *76*, 489-499.

[168] I. Aujard, C. Benbrahim, M. Gouget, O. Ruel, J.-B. Baudin, P. Neveu, L. Jullien, *Chem. Eur. J.* **2006**, *12*, 6865-6879.

7 List of Abbreviations

ACN ..... Acetonitrile
AFM/EFM ..... Atomic Force and Electrostatic Force Microscopy
$CDCl_3$ ..... Deuterochloroform
DAD ..... Diode Array Detector
DCM ..... Dichloromethane
DIAD ..... Diisopropyl Azodicarboxylate
DLS ..... Dynamic Light Scattering
DMF ..... N,N-Dimethylformamide
DMSO ..... Dimethylsulfoxid d_6
EGDMA ..... Ethylene Glycoal Dimethacrylate
EI… ..... Electron Impact Ionization
eq ..... Equivalent
ESI ..... Electrospray Ionization
HEMA ..... Hydroxyethyl Methacrylate
HOMO ..... Highest Occupied Molecular Orbital
HPLC ..... High Performance Liquid Chromatography
HRMS ..... High Resolution Mass Spectrometry
LUMO ..... Lowest Unoccupied Molecular Orbital
MMA ..... Methyl Methacrylate
MS ..... Mass Spectra
Nd:YAG ..... Neodymium Dope Yttrium Aluminium Garnet
NMR ..... Nuclear Magnetic Resonance Spectroscopy
o-NBnC-NP ..... 3-N-(3(3-Triethoxy)-propyloxy-4-methoxy-2,6-dinitrobenzyl)-5-fluorouracil functionalized silica nanoparticles
o-NBnCs ..... *ortho*-Nitrobenzyl Compounds
ppm ..... Parts Per Million
RT ..... Room Temperature
SEM ..... Single Electron Scanning Microscopy
SOMO ..... Single Occupied Molecular Orbital
TBSCl ..... *tert*-Butyldimethylsilily Chloride
TEOS ..... Tetraethyl Orthosilicate
TGA ..... Thermo Gravimetric Analysis
THF ..... Tetrahydrofuran, Tetrahydrofuran
TLC ..... Thin Layer Chromatography
TPA ..... Two-Photon Absorption
TPC ..... 7-(3-triethoxysilylpropyloxy)coumarin
TPC-Ly-NP ..... 7-(3-Triethoxysilylpropyloxy)coumarin functionalized silica nanoparticles according to Yokoi
TPC-NP ..... 7-(3-Triethoxysilylpropyloxy)coumarin functionalized silica nanoparticles according to Stöber
UV-Vis ..... Ultra Violet-Visible Spektroscopy
δ ..... Chemical Shifts

Danksagung

An dieser Stelle möchte ich all denen danken die zum Gelingen dieser Arbeit beigetragen haben und mich in den acht Jahren meines Studiums unterstützt, gefördert und manchmal auch abgelenkt haben. Mein besonderer Dank gilt:

- Herrn Prof. Dr. Hampp für die freundliche Aufnahme in seiner Arbeitsgruppe, die interessante Aufgabenstellung und die stete Diskussionsbereitschaft und Hilfe bei allen Problemen die die Durchführung einer solchen Arbeit mit sich bringt.
- Herrn Prof. Dr. Parak für die freundliche Übernahme der Zweitkorrektur.
- meiner Freundin Helen für ihre Unterstützung und Geduld während der gesamten Zeit meiner Promotion.
- meinen Eltern, die mir jeder Zeit ein sorgenfreies Studium ermöglicht haben und mich in all meinen Ideen unterstützt haben.
- meinem Bruder, der von Zeit zu Zeit für den richtigen Ansporn gesorgt hat.
- Inge Dingler für die schnelle und hervorragende Prüfung dieser Arbeit auf sprachliche Schwächen und Korrektur eben dieser.
- der gesamten Arbeitsgruppe Hampp für die angenehme Arbeitsatmosphäre insbesondere:
    - Peter Baumann für die vielen interessanten Diskussionen, die Aufnahme der tollen AFM/EFM Aufnahmen sowie für die schnelle Durchsicht dieser Arbeit.
    - Dr. Hee-Cheol Kim der jeder Zeit bereit war Hilfestellung in technischen und theoretischen Fragestellung zu geben.
    - Der Gesamten ActIOL Abteilung für die problemlose und konstruktive Zusammenarbeit.
    - Natascha Galka und Philipp Kahler für die Hilfe bei Synthese und Analytik.
    - Meiner lieben Bürokollegin Nina Schromczyk für die immer lustige und entspannte Atmosphäre.
- der Feinmechanik für das immer schnelle Anfertigen diverser ausgefallener Halterungen und Spezialanfertigungen.
- Michael Hellwig und Hendrik Reinhardt für die Aufnahme der vielen SEM-Bilder.

Curriculum Vitae

April 2008 – Juli 2011:	Doktorarbeit zum Thema: „Photochemistry of Coumarin Functionalized Silica Nanoparticles and Photochemically Induced Drug Delivery Utilizing *o*-Nitrobenzyl Compounds“ in der Arbeitsgruppe von Herrn Prof. Dr. Norbert Hampp an der Philipps Universität Marburg.
März 2008:	Diplom in Chemie
Juni 2007 – März 2008:	Diplomarbeit zum Thema „Darstellung photoaktiver selbstorganisierender Monoschichten auf glatten und gekrümmten Oxidschichten von Silizium“ in der Arbeitsgruppe von Herrn Prof. Dr. Norbert Hampp an der Philipps Universität Marburg.
April 2005 – Juni 2007	Hauptstudium der Chemie an der Philipps Universität Marburg.
April 2005:	Vordiplom in Chemie
April 2003 – März 2005:	Grundstudium der Chemie an der Philipps Universität Marburg.
März 2002:	Abitur
August 1993 – März 2002:	Martin Butzer Gymnasium, Dierdorf, Westerwald.